DOKUZ EYLÜL UNIVERSITY

GRADUATE SCHOOL OF NATURAL AND APPLIED SCIENCES

EXPERIMENTAL FAILURE ANALYSIS OF THRUST BEARINGS

by

Hasan Oğuz EMİR

July, 2019

İZMİR

EXPERIMENTAL FAILURE ANALYSIS OF THRUST BEARINGS

A Thesis Submitted to the
Graduate School of Natural and Applied Sciences of Dokuz Eylül University
In Partial Fulfillment of the Requirements for the Degree of Master of Science in Mechanical Engineering, Machine Theory and Dynamics Program

by

Hasan Oğuz EMİR

July, 2019

İZMİR

M.Sc THESIS EXAMINATON RESULT FORM

We have read the thesis entitled **"EXPERIMENTAL FAILURE ANALYSIS OF THRUST BEARINGS"** completed by **HASAN OĞUZ EMİR** under supervision of **PROF.DR. ZEKİ KIRAL** and we certify that in our opinion it is fully adequate, in scope and in quality, as a thesis for the degree of Master of Science.

Prof.Dr. Zeki KIRAL

Supervisor

Dr.Öğr.Üyesi Murat AKDAĞ

(Jury Member)

Dr.Öğr.Üyesi Barış Oğuz GÜRSES

(Jury Member)

Prof. Dr. Kadriye ERTEKİN

Director

Graduate School of Natural and Applied Sciences

ACKNOWLEDGMENTS

I would like to present my profound thanks to my professor, Prof. Dr. Zeki KIRAL, who guided me by sharing his knowledge, experience, and valuable ideas on every step of this study.

I would also like to thank owners of the works that I used and names of which I mentioned in the references section, for their valuable efforts.

In the last place, I would like to my family and my wife who never deny their support to me during this work.

Hasan Oğuz EMİR

EXPERIMENTAL FAILURE ANALYSIS OF THRUST BEARINGS

ABSTRACT

Ball bearings are the most commonly used bearing elements in machines. For the healthy and long term operations of the machine, it is closely related to conditions of the ball bearings. Therefore, early detection of the failures in ball bearings is very crucial for machine health. In this study, analysis of failure in thrust ball bearings is discussed by using experimental vibration signals. In the experimental setup, various defects have been created on the raceway of thrust ball bearing ring. Vibration measurements have been taken in the horizontal, vertical and axial directions from the close points in the test setup, in order to see defected and healthy situations under different rotate speeds and two different axial load. Time waveform and frequency spectrum graphs were generated from the data of vibration measurements. Defect analyzes have been performed for raw and filtered signals by using statistical indicators as peak to peak, root mean square, crest factor and kurtosis which are calculated for vibration data. It has been shown that the defects on the thrust ball bearing ring can be determined by analyzing the vibration data in time and frequency domains.

Keywords: Thrust ball bearing, vibration analysis, condition monitoring, bearing defect

EKSENEL RULMANLARIN DENEYSEL HATA ANALİZİ

ÖZ

Rulmanlar makinelerde en çok kullanılan yataklama elemanlarıdır. Makinelerin sağlıklı ve uzun süreli çalışması rulmanların durumu ile yakından ilişkilidir. Bu nedenle rulmanlarda oluşabilecek arızaların önceden tespiti makine sağlığı açısından oldukça önemlidir. Bu çalışmada eksenel rulman hatalarının deneysel titreşim sinyalleri kullanılarak analizi ele alınmıştır. Oluşturulan deney düzeneğinde kullanılan eksenel rulman bileziğinin yuvarlanma yolu üzerinde çeşitli hatalar oluşturulmuştur. Arızasız ve arızalı durumlar için farklı dönüş hızları ve iki farklı eksenel yük altında, deney düzeneği üzerinde rulmana yakın noktalardan; yatay, düşey ve eksenel doğrultularda titreşim ölçümleri alınmıştır. Titreşim ölçümlerine ait verilerden zaman dalgaformu ve frekans spektrumu grafikleri oluşturulmuştur. Titreşim verileri için hesaplanan tepeden tepeye, kare ortalamalarının karekökü, crest faktör ve kurtosis gibi istatistiksel göstergelerden faydalanılarak ham ve filtrelenmiş sinyaller için hata analizleri gerçekleştirilmiştir. Zaman ve frekans ortamı için titreşim verilerinin analizi ile eksenel rulman bileziği üzerindeki hataların tespit edilebileceği gösterilmiştir.

Anahtar kelimeler: Eksenel rulman, titreşim analizi, durum izleme, rulman arızası

CONTENTS

Page

M.Sc THESIS EXAMINATION RESULT FORM……..…...ii

ACKNOWLEDGEMENTS…….…..iii

ABSTRACT……....iv

ÖZ……...v

LIST OF FIGURES……x

LIST OF TABLES…….……...…xv

CHAPTER ONE - INTRODUCTION 1

CHAPTER TWO - BEARINGS 8

2.1 Brief History of Bearings 8

2.2 Bearing Theory 9

2.2.1 Sliding Bearing 9

2.2.2 Rolling Bearings 10

2.2.2.1 Bearing Components 10

2.2.2.1.1 Inner Ring 11

2.2.2.1.2 Outer Ring 11

2.2.2.1.3 Rolling Elements 11

2.2.2.1.4 Cage 12

2.2.2.2 Bearings According to Load Direction 12

2.2.2.2.1 Radial Bearings 13

2.2.2.2.2 Thrust or Axial Bearings 14

CHAPTER THREE - THEORY OF VIBRATION 15

3.1 Introduction 15

3.2 Vibration Basics 15

3.2.1 Mass (m) 17
3.2.2 Stiffness (k) 17
3.2.3 Damping (c) 17
3.3 Vibration Terms and Definitions 17
3.3.1 Cycle 17
3.3.2 Amplitude 17
3.3.3 Period of Oscillation (T) 18
3.3.4 Frequency of Oscillation (f) 18
3.3.5 Phase (ø) 19
3.3.6 Angular Frequency (ω) 19
3.3.7 Natural Frequency 19
3.3.8 Resonance 20
3.4 Harmonic Motion, Displacement, Velocity and Acceleration 20
3.5 Classification of Vibration 22
3.5.1 Free Vibration 22
3.5.2 Forced Vibration 22
3.5.3 Undamped Vibration 23
3.5.4 Damped Vibration 23
3.5.5 Linear and Nonlinear Vibration 24
3.5.6 Deterministic and Random Vibration 25
3.6 Quantifying the Vibration Level 25
3.6.1 Peak to Peak 26
3.6.2 Zero to Peak 26
3.6.3 Root Mean Square (RMS) 26
3.6.4 Average 26
3.7 Vibration Analysis Techniques 27
3.7.1 Time Domain Analysis 27
3.7.1.1 Time Waveform 27
3.7.1.2 Orbit 28
3.7.1.3 Statistical Methods 29
3.7.2 Frequency-Domain Analysis 29
3.7.3 Quefrency-Domain Analysis 31

CHAPTER FOUR - BEARING FAILURES 32

4.1 Introduction 32

4.2 Types of the Bearing Failures and the Causes 33

4.2.1 Normal Fatigue Failure (flaking, pitting) 33
4.2.2 Peeling 33
4.2.3 Wear and Fretting 34
4.2.4 Cracks and Chips 34
4.2.5 Brinelling and Nicks 35
4.2.6 Misalignment 36
4.2.7 Rust and Corrosion 36
4.2.8 Seizure 37
4.2.9 Electrical Pitting 38
4.2.10 Damage of Cages 39
4.2.11. Reverse Loading 39
4.2.12. Creeping 40

CHAPTER FIVE - EXPERIMENTAL SETUP 41

5.1 Test Rig 41
5.2 Instrumentation 44
5.3 Creation of Defect 46
5.4 Measurement Conditions 47

CHAPTER SIX - THRUST BEARINGS FAILURE DETECTION WITH VIBRATION ANALYSIS METHODS 48

6.1 Time Waveform Analysis 48
6.1.1 Characteristics Time Waveform 48
6.1.2 Analysis of Experimental Time Waveform Graphs 51
6.2 Comparison of Raw Statistical Indicators 73
6.2.1 For Axial Measurement Point (P1) 73

6.2.2 For Horizontal Measurement Point (P2) 77
6.2.3 For Vertical Measurement Point (P3) 80
6.3 Filtering of Vibration Signals 83
6.4 Frequency Spectrum Analysis 86
6.4.1 Bearing Characteristic Frequencies 86
6.4.2 The Fast Fourier Transform 87
6.4.3 Analysis of Experimental Frequency Spectrum Graphs 87

CHAPTER SEVEN - CONCLUSIONS 108

REFERENCES 111

APPENDICES 117

LIST OF FIGURES

Page

Figure 2.1 Set of ball bearings, sketched by Leonardo da Vinci in Codex Madrid I, 500 years before the modern set of ball bearings 8
Figure 2.2 Linear bearing 9
Figure 2.3 Journal bearing 10
Figure 2.4 Bearing components 11
Figure 2.5 Types of rolling elements 12
Figure 2.6 Force directions on the shaft 12
Figure 2.7 Radial bearings a) deep groove b) angular contact..... 13
Figure 2.8 Thrust ball bearings a) single direction b) double direction 14
Figure 2.9 Double direction angular contact thrust ball bearing..... 14
Figure 3.1 Spring-mass system 16
Figure 3.2 Comparison of waves with different amplitudes 18
Figure 3.3 Phase relationship between two similar waves 19
Figure 3.4 Harmonic motion 20
Figure 3.5 A simple pendulum 22
Figure 3.6 Forced vibration (mass,, spring and damper system) 23
Figure 3.7 Undamped Vibration (mass-spring system) 23
Figure 3.8 Damped vibration (mass, spring and damper system)..... 24
Figure 3.9 Two seperate oscillations with a damping ratio of 0.1 and 0.3 24
Figure 3.10 Vibration amplitudes for sinusoidal wave 25
Figure 3.11 Guide to vibration severity per ISO 10816..... 27
Figure 3.12 Example of time waveform 28
Figure 3.13 Orbit Construction 28
Figure 3.14 LMV 311 Gearbox signature frequencies 30
Figure 4.1 Causes of failure in rolling bearings 32
Figure 4.2 Inner ring, outer ring and balls are flaked 33
Figure 4.3 Peeling on rolling contact surfaces..... 33
Figure 4.4 Wear and fretting failures..... 34

Figure 4.5 Cracks and chips failures 35
Figure 4.6 Brinelling on outer and inner ring raceway surface of ball bearing 35
Figure 4.7 Effect of misalignment on the inner and outer ring raceways 36
Figure 4.8 Corrosion of bearing rings 37
Figure 4.9 Inner ring of double row tapered roller bearing 37
Figure 4.10 Effect of electrical pitting on inner and outer ring 38
Figure 4.11 Examples of cage damages 39
Figure 4.12 Ball damage of angular contact ball bearing 40
Figure 4.13 Creeping of inner rings 40
Figure 5.1 Overview of the experimental setup 42
Figure 5.2 Bearing housing 43
Figure 5.3 Sectional drawing of bearing housing 43
Figure 5.4 Thrust ball bearing components 44
Figure 5.5 Thrust ball bearing geometry (FEB, 51113 44
Figure 5.6 Vibration analysis flow chart 45
Figure 5.7 Minimo brand electro erosion machine 46
Figure 5.8 Housing washers of thrust bearings that defect generated 46
Figure 5.9 Measurement points on the experimental setup 47
Figure 6.1 Experimental waveform for bearings of different conditions a) healthy bearing b)defect bearing 49
Figure 6.2 Experimental waveform for bearings of different conditions a) healthy bearing b) bearing with inner race defect 49
Figure 6.3 Unbalance characteristic waveform for acceleration response 50
Figure 6.4 Misalignment characteristic waveform 50
Figure 6.5 Misalignment characteristic waveform phase was changed 90 degrees 51
Figure 6.6 Time waveform for load-1 at point P1, 500 RPM a) healthy bearing b) one defect bearing c) two defects bearing d) four defects bearing 52
Figure 6.7 Time waveform for load-1 at point P2, 500 RPM a) healthy bearing b) one defect bearing c) two defects bearing d) four defects bearing 53
Figure 6.8 Time waveform for load-1 at point P3, 500 RPM a) healthy bearing b) one defect bearing c) two defects bearing d) four defects bearing 54

Figure 6.9 Time waveform for load-1 at point P1, 1000 RPM a) healthy bearing b) one defect bearing c) two defects bearing d) four defects bearing..... 56
Figure 6.10 Time waveform for load-1 at point P2, 1000 RPM a) healthy bearing b) one defect bearing c) two defects bearing d) four defects bearing..... 57
Figure 6.11 Time waveform for load-1 at point P3, 1000 RPM a) healthy bearing b) one defect bearing c) two defects bearing d) four defects bearing..... 58
Figure 6.12 Time waveform for load-1 at point P1, 1500 RPM a) healthy bearing b) one defect bearing c) two defects bearing d) four defects bearing..... 59
Figure 6.13 Time waveform for load-1 at point P2, 1500 RPM a) healthy bearing b) one defect bearing c) two defects bearing d) four defects bearing..... 60
Figure 6.14 Time waveform for load-1 at point P3, 1500 RPM a) healthy bearing b) one defect bearing c) two defects bearing d) four defects bearing..... 61
Figure 6.15 Time waveform for load-2 at point P1, 1500 RPM a) healthy bearing b) one defect bearing c) two defects bearing d) four defects bearing..... 64
Figure 6.16 Time waveform for load-2 at point P2, 1500 RPM a) healthy bearing b) one defect bearing c) two defects bearing d) four defects bearing..... 65
Figure 6.17 Time waveform for load-2 at point P3, 1500 RPM a) healthy bearing b) one defect bearing c) two defects bearing d) four defects bearing..... 66
Figure 6.18 Time waveform for load-2 at point P1, 2000 RPM a) healthy bearing b) one defect bearing c) two defects bearing d) four defects bearing..... 67
Figure 6.19 Time waveform for load-2 at point P2, 2000 RPM a) healthy bearing b) one defect bearing c) two defects bearing d) four defects bearing..... 68
Figure 6.20 Time waveform for load-2 at point P3, 2000 RPM a) healthy bearing b) one defect bearing c) two defects bearing d) four defects bearing..... 69
Figure 6.21 Time waveform for load-2 at point P1, 2500 RPM a) healthy bearing b) one defect bearing c) two defects bearing d) four defects bearing..... 70
Figure 6.22 Time waveform for load-2 at point P2, 2500 RPM a) healthy bearing b) one defect bearing c) two defects bearing d) four defects bearing..... 71
Figure 6.23 Time waveform for load-2 at point P3, 2500 RPM a) healthy bearing b) one defect bearing c) two defects bearing d) four defects bearing..... 72
Figure 6.24 Statistical parameters for load-1 a) peak to peak b) RMS c) crest factor d) kurtosis..... 74

Figure 6.25 Statistical parameters for load-2 a) peak to peak b) RMS c) crest factor d) kurtosis 76
Figure 6.26 Statistical parameters for load-1 a) peak to peak b) RMS c) crest factor d) kurtosis 78
Figure 6.27 Statistical parameters for load-2 a) peak to peak b) RMS c) crest factor d) kurtosis 79
Figure 6.28 Statistical parameters for load-1 a) peak to peak b) RMS c) crest factor d) kurtosis 81
Figure 6.29 Statistical parameters for load-2 a) peak to peak b) RMS c) crest factor d) kurtosis 82
Figure 6.30 Load-2 case, at P1 point, 7.75 Hz a) healthy bearing b) one defect bearing 89
Figure 6.31 Load-2 case, at P2 point, 7.75 Hz a) healthy bearing b) one defect bearing 90
Figure 6.32 Load-2 case, at P3 point, 7.75 Hz a) healthy bearing b) one defect bearing 91
Figure 6.33 Load-2 case, at P1 point, 24.93 Hz a) healthy bearing b) one defect bearing 92
Figure 6.34 Load-2 case, at P2 point, 24.93 Hz a) healthy bearing b) one defect bearing 93
Figure 6.35 Load-2 case, at P3 point, 24.93 Hz a) healthy bearing b) one defect bearing 94
Figure 6.36 Load-1 case, at P1 point a) 16.9 Hz, healthy bearing b) 17.06 Hz, two defects bearing 96
Figure 6.37 Load-1 case, at P2 point a) 16.9 Hz, healthy bearing b) 17.06 Hz, two defects bearing 97
Figure 6.38 Load-1 case, at P3 point a) 16.9 Hz, healthy bearing b) 17.06 Hz, two defects bearing 98
Figure 6.39 Load-2 case, at P1 point a) 16.05 Hz, healthy bearing b) 16.05 Hz, two defects bearing 99
Figure 6.40 Load-2 case, at P2 point a) 16.05 Hz, healthy bearing b) 16.05 Hz, two defects bearing 100

Figure 6.41 Load-2 case, at P3 point a) 16.05 Hz, healthy bearing b) 17.5 Hz, two defects bearing..... 101
Figure 6.42 Load-1 case, at P1 point, 32.83 Hz a) healthy bearing b) four defects bearing..... 102
Figure 6.43 Load-1 case, at P2 point, 32.83 Hz a) healthy bearing b) four defects bearing..... 103
Figure 6.44 Load-1 case, at P3 point, 32.83 Hz a) healthy bearing b) four defects bearing..... 104
Figure 6.45 Load-2 case, at P1 point, 42.78 Hz a) healthy bearing b) two defects bearing..... 105
Figure 6.46 Load-2 case, at P2 point, 42.78 Hz a) healthy bearing b) two defects bearing..... 106
Figure 6.47 Load-2 case, at P3 point, 42.78 Hz a) healthy bearing b) two defects bearing..... 107

LIST OF TABLES

Page

Table 3.1 Natural frequency of test rig 20
Table 6.1 Raw and filtered statistical parameters for load-1 at the speed 2500 RPM a) P1 b) P2 c) P3 84
Table 6.2 Raw and filtered statistical parameters for load-2 at the speed 2500 RPM a) P1 b) P2 c) P3 85
Table 6.3 Characteristic defect frequencies and harmonics of 51113 thrust ball bearing..... 87

CHAPTER ONE
INTRODUCTION

Bearings are widely used in the machinery industry which has rotating elements. They are manufactured in various types and sizes as standardized due to the high number of working conditions. The operation of the bearings without any damage is very important for the running conditions of the machine for a long term and healthy period. However, there may be damages due to manufacturing faults on the surfaces during manufacturing, wrong bearing assemblies, improper working conditions (dirt, dust, improper lubrication, oil-free, overload etc.). These damages are not detected in advance and if it has not taken any prevention, the machine health will be adversely affected and will cause breakdowns. Various status monitoring techniques have been developed in order to detect the damage that may occur in the machines. These could be described; vibration analysis, acoustic emission measurements, motor current signature analysis (MCSA), noise monitoring, temperature monitoring, wear debris analysis, shock pulse method (SPM).

The method of vibration analysis can be considered the best method of determining the condition of a machine (Jensen, Brown, n.d.:4). This method prevents unplanned production losses, especially in production factories and with this method, planned maintenance activities are done more effectively, unnecessary material exchange and stock costs are eliminated. Finally, the reliability of production is ensured.

Many researchers have done various studies on vibration analysis from past to present and have discussed this issue from different perspectives. Research has generally been done in three different ways. The first is to operate the bearing for the entire life span and to observe changes in vibration until a fault occurs in the bearing. The second is to create an artificial error in the bearing and compare the vibration data with the values of the vibrations in the healthy bearing. The third was to create bearing models with computer aided programs and to compare the vibration data obtained with the simulation of healthy and damaged bearings.

Williams, Ribadeneira, Billington & Kurfess (2001) have used new undamaged ball and roller bearings to determine bearing life in the test setup. They have taken vibration measurements until the damage occurred at the fixed and variable speeds. They received vibration measurements until the damage occurred at the fixed and variable speeds. During this process, they have studied changes in the rotational speed of the oil temperature in undamaged bearings. They observed vibration changes by using vibration analysis techniques such as frequency spectrum, time waveform, square root mean square (RMS), kurtosis and crest factor. In this direction, they have evaluated the results obtained for the healthy and defect conditions of ball and roller bearings.

Mathew & Alfredson (1984) aimed to detect fault for bearings which had been newly getting damaged. In this respect, they tracked vibration signals of several rolling element bearings. Following this, they analysed them and evaluated various parameters. They expressed that the frequency domain parameters yield better results than time domain parameters in fault detection. However, as a result, they, by providing evidences, they showed that a single technique should not be trusted and depended on in fault detection of bearings.

Tandon & Choudhury (1999) studied vibration and acoustic measurement methods for defect detection of bearings. They stated that the sound density technique which is the one of acoustic measurement methods gives better results than the sound pressure measurements. The vibration of time domain; RMS, crest factor, probability density and can be measured with values such as kurtosis, but the most effective method among them have stated that kurtosis values.

Dyer & Stewert (1978) stated that the value of kurtosis is close to 3 for an undamaged bearing with Gaussian distribution and the value of kurtosis with greater than 3 is a sign of damage in the bearing. However, the Kurtosis value is nearing the value of 3 in the development of the damage, this situation is a disadvantage for the diagnosis of damage. Therefore, they suggested that the value of kurtosis should be measured in selected frequency bands.

McFadden & Smith (1984) created a single point defect on inner ring of a bearing that was under a constant radial load. They generated a mathematical model in order to determine the generated vibration with a single point defect. In the content of the model are the effects of bearing geometry, bearing load distribution, shaft speed, and exponential vibration disturbances. They saw that the theoretical and empirical results obtained are compatible with each other.

Alfredson, Aust & Mathew (1985) created an test rig with the purpose of determining the possible faults that might occur on bearings beforehand. They studied the vibration signals, which they obtained through the test rig, by using frequency and time domain methods. They indicated that time domain parameters yield better results depending on the fault, yet, that they have to be used besides some other methods to determine the damage on bearings, and that RMS values yield good results in fault detection.

Kıral & Karagülle (2002) modeled the dynamic loading of a rolling element bearing structure with a computer program. They obtained the vibration response of the structure using the IDEAS CAE package. The statistical properties of the displacement, velocity and acceleration responses obtained for healthy and defect bearings were compared at different sensor positions and rotational speeds. They have used the method of Envelope (HFRT) in a given point and RPM that they have determined. Bearing outer ring fault frequencies have emerged, so they have shown that source of the damage could be used to determine by using the envelope method.

Tandon & Choudhury (2006) modelled a rotor bearing mechanism under a radial load as a three degrees of freedom system by using a mass-spring-damper model. They obtained vibration reactions by generating defects on the elements of bearing, which was under the effect of the load. They compared theoretical and empirical vibration values at different load, defect and speeds. Bearing fault frequencies and amplitude values of its harmonics returned to be very close for theoretical and empirical conditions. It was concluded that the defect frequency amplitude obtained for the

defect that they created on the outer race of the roller bearing is higher than the ones obtained for inner race and rolling element under similar load and speed conditions.

Kim, Tan, Mathew & Yang (2006) have experimentally compared the vibration measurement results with ultrasound technique at low RPM (between 30 and 1200 RPM) by creating a defect in the ball bearing inner ring. They concluded that ultrasound signals; RMS values are the best parameter at all speeds, whereas at rates less than 50 RPM, kurtosis and crest factor are the best parameters.

Nabhan, Nouby, Sami & Mousa (2016) simulated a ball bearing and bearing housing by forming a three-dimensional finite element model. They have formed defects in the outer ring at certain intervals. They compared the errors for experimental and simulation results and obtained positive results.

Patel, Agrawal & Joshi (2012) analyzed the damage generated in an induction motor bearing by using the vibration data obtained from the wavelet and Hilbert transforms. Bearing elements have shown that the defect frequencies can be used for damage detection as recommended.

Orhan, Aktürk & Çelik (2006) carried out studies on detecting defects of cylindrical roller bearings and of ball bearings through vibration based monitoring and spectral analysis. They carried out their studies on three real systems. They showed the creation of ball bearing looseness, ball bearing outer race defect and cylindrical bearing outer race defect. By taking various vibration samples, they shared time waveform, frequency spectrum, and vibration level trends in their studies. In the frequency spectrums, they showed bearing defects frequencies and harmonics. They concluded that probable defects can easily be prevented provided that vibration-based monitoring is carried out and vibration analysis is made at certain intervals.

Jayaswal, Wadhwani & Mulchandani (2008) carried out a study on condition monitoring methods applied for rotating equipments. In their study, they refer to

condition monitoring methods such as visual inspection, vibration analysis, temperature monitoring, acoustic emission analysis, noise analysis, wear debris analysis, motor current signature analysis and non-destructive testing. They also explained vibration signature analysis techniques such as time domain, frequency domain, and quefrency domain. They concluded that vibration signature analysis is the most appropriate technique for fault detection.

Segla, S.Wang & F.Wang (2012) created a test rig in order to detect the location of bearing fault precisely by using High Frequency Resonance Technique (HFRT). They generated a local defect on the inner race of the bearing they used. They also studied statistical indicators such as peak (V), root mean square (V), crest and kurtosis in order to review the vibration values they had obtained from three different measure points. They saw that the characteristic defect frequencies of bearing elements also exist in the spectrum they obtained. They concluded that the HFRT technique can precisely detect the source of the fault.

Yiğit (2008) detected the condition of a deep grove ball bearing through vibration measurement on the test rig he created. He created an artificial regional defect on inner or outer race on one of the bearings. The vibration measurements were done by a vibration measuring device at different rotation speeds. The measurements were recorded in terms of accerelation, speed and replacement. Fast Fourier transform (FFT) and short-term Fourier Transform (STFT) were used for detecting the faulty bearing. However, in the main part of the study, Curve Length Transform (CLT), a non-linear time domain transform, was used. Statistical indicators belonging to the curve length transform signals for health and faulty bearings were obtained and compared. Furthermore, he also compared these values with the statistical indicators obtained from raw vibration signals. By using curve length method, he showed that time domain parameters, if enriched, can be beneficial in detecting regional faulty bearings.

Ziebell, Schöppl, Haubner & Konegger (2015) studied on detecting faults of hybrid thrust ball bearings using vibration analysis. Balls of the bearings are ceramic where the washers are metallic. The characteristic vibration frequencies that were obtained

by variety of software-based filter and analysis algorithms were correlated with metallographic reviews of defect bearings. They proved with experimental that even the minor faults on the ball surface (in the range of a few μm) can be detected by FFT derived spectrum.

In this study, vibration data were obtained from different sensor points at different rotational speeds by using healthy and defect thrust bearings in the experimental set up. For the acceleration response of the structure, statistical characteristics such as peak to peak, root mean square (RMS), crest (peak) factor and kurtosis are used, time waveforms are compared and bearing damage frequencies on frequency spectrum are shown in order to examine the applicability of vibration analysis technique in thrust bearings.

Chapter 2 explains basics of bearings as well as the types used in industries and details elements of rolling bearings as well as their load conditions.

Chapter 3 explains what vibration is, what basic concepts can be encountered with respect the vibration, and the classification of vibration. Based on these concepts, vibration levels and vibration analysis methods were detailed.

Chapter 4 explains types, reasons and solutions for faults experienced on bearings used in machines. Effective visuals were shared in order to render and emphasize these faults. Most of the information in this section is made up of information shared by bearing makers.

Chapter 5 provides the details for the test rig used in this study, measuring devices, steps of data processing, creation of fault and vibration measurement conditions.

Chapter 6 is made up of the graphics of vibration signals that were obtained by the vibration measurements. The graphics were created through programs that were generated in parallel to MATLAB context. The vibration analysis for healthy, one defect, two defects, and four defects bearings under different load and speed conditions

was carried out under topics like comparison of statistical indicators, time waveform analysis and frequency spectrum analysis. Vibration values from axial, horizontal, and vertical measure points were shared in aforementioned analysis methods. Generally speaking, all the graphics were tried to be evaluated.

Chapter 7 comprises general and specific results of the empirical study presented in this thesis and presents future recommendations on the fact that fault detection can be performed on thrust bearings through vibration analysis.

CHAPTER TWO
BEARINGS

2.1 Brief History of Bearings

The basics of inventions have the purpose of making human life easier and better. Hundreds of years ago humans used to carry heavy objects from one place to another by pushing them on the ground. Yet, increasing weights and prolonging distances brought about the invention of the wheel. With the advent of the wheel, first plain bearing started to be deployed with wooden blocks, steel shafts, and animal fat in between.

"Early example of a wooden ball bearing supporting a rotating table was retrieved from the remains of a Roman ship in Lake Nemi, Italy" (Bearing Timeline, n.d.).

An illustration of a ball bearing by Leonardo da Vinci from 1500s is shown in Figure 2.1. The first bearing patent was taken by Philip Vaughn in 1794 in Carmarthen, England.

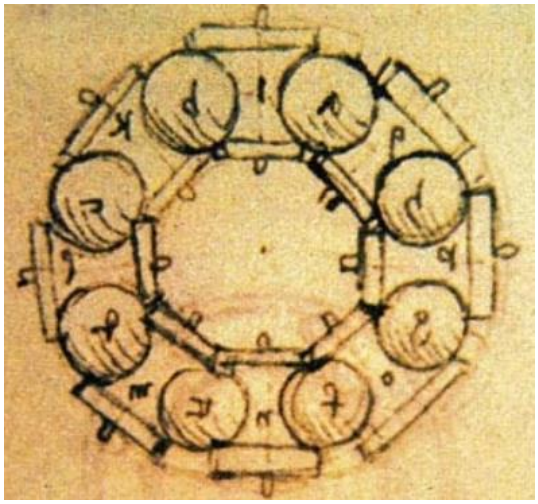

Figure 2.1 Set of ball bearings, sketched by Leonardo da Vinci in Codex Madrid I, 500 years before the modern set of ball bearings (UNESCO, n.d.)

With the advent of the Industrial Evolution, steel became an easier to process material and following these a machine was designed for producing full circular and equal size balls in 1883 by Frederick Fisher (founder of FAG). Thanks to the balls that were produced with higher sensitivity, the amount of friction between the metal surfaces and therefore the energy loss was minimized. Following the emergence of new brands and increasing requirements, bearings of different sizes and types were produced and their use in machines became widespread.

2.2 Bearing Theory

The supporting elements that enable relative movement between two separate objects with minimum friction and energy loss are called bearings. Bearing can be categorized as two types, sliding and rolling bearings.

2.2.1 Sliding Bearing

Sliding bearings are bearings where only sliding friction is generated. There are two different types of sliding bearings; linear bearings and journal bearings.

Linear bearings are produced for linear direction movements. Because of their design, they cannot make their rotation movements. Figure 2.2 shows a linear bearing.

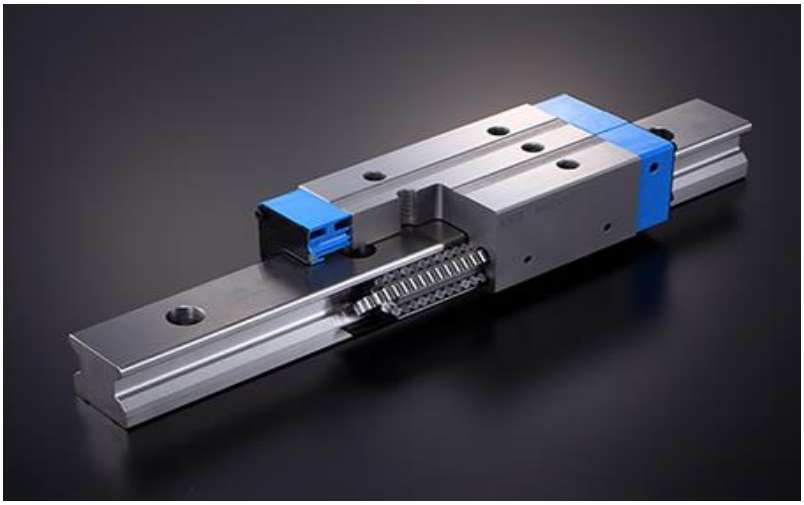

Figure 2.2 Linear bearing (IKO, 2019)

Journal bearings are types of bearings that contain a sliding movement between two surfaces as well as an lubrication film and that enable the rotating movement. They have vibration and noise damping features. They can carry very heavy loads. A journal bearing is shown in Figure 2.3

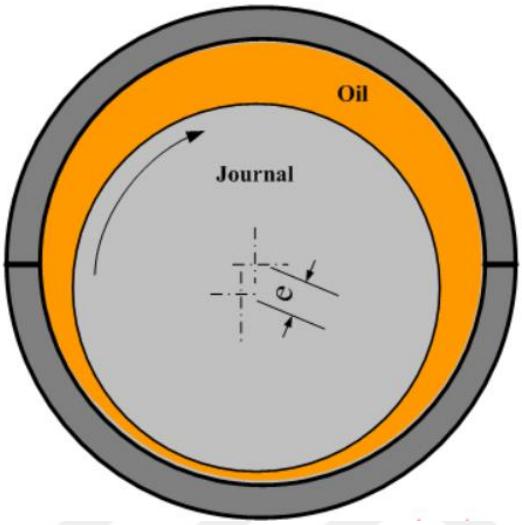

Figure 2.3 Journal bearing (Substech, 2019)

2.2.2 Rolling Bearings

They are bearing elements that allow the relative movement between two machine elements with minimum friction by preventing the movement in the direction of the force.

2.2.2.1 Bearing Components

There are four basic bearing components for each type of bearing. These are inner ring, outer ring, rolling elements and cage. Despite the fact that it does not exist in all types, seal is also a bearing component. Bearing components are shown in Figure 2.4.

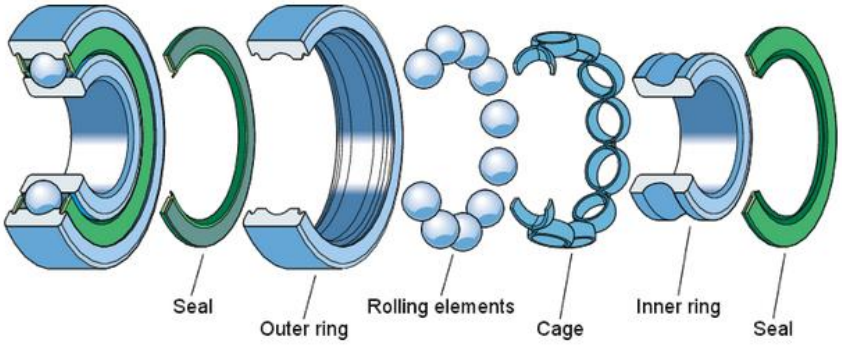

Figure 2.4 Bearing components (SKF, 2013)

2.2.2.1.1 Inner Ring. They can also be defined as the inner race or cup. They are located on the shaft. Mostly, they are the rotating part and have the closest proximity to the shaft. They rotate at the same RPM with the shaft. The mounted part of it can be conical or cylindrical, depending on the type of the bearing. The inner ring raceway can show differences according to the types of the rotating elements.

2.2.2.1.2 Outer Ring. It can be defined as the outer race or cup. They are mounted on the body of the machine. Mostly, they are the non-rotating part of the bearing. The outer ring raceway can show differences according to the types (spherical, cylindirical or tapered) of the rotating elements.

2.2.2.1.3 Rolling Elements. It is the rotating part between the inner ring and the outer ring. According to the type of the bearing, there is some space at a specific tolerance between the rings and the rolling elements. By lubricating it, a thin layer is created in this space. They transfer the loads they carry by this way. Rolling elements have different forms such as balls, cylindrical rollers, symmetrical spherical rollers, asymmetrical spherical rollers, tapered rollers, and needle roller. Rolling element types are shown in Figure 2.5.

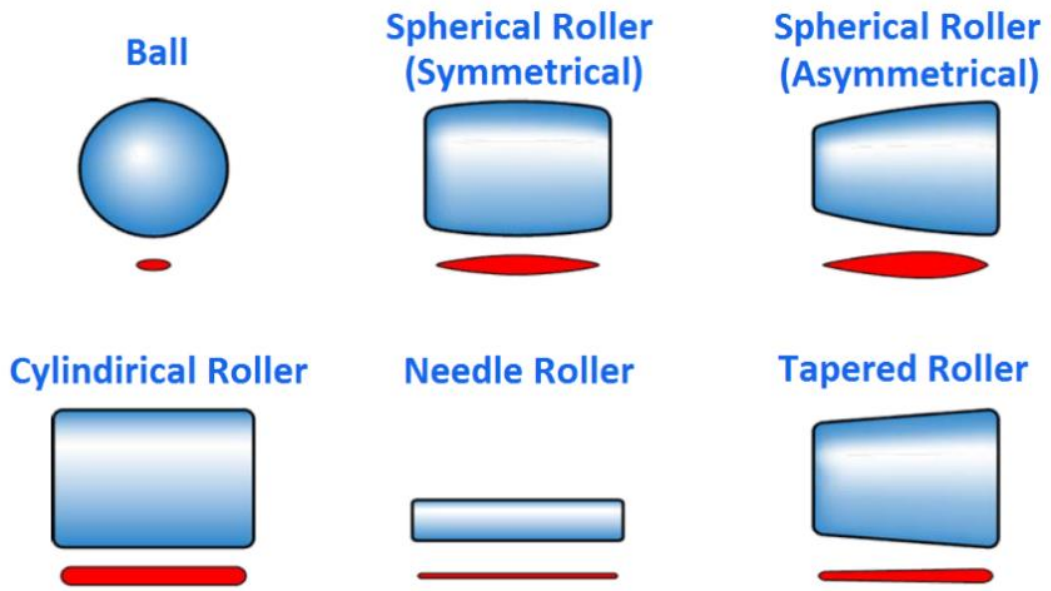

Figure 2.5 Types of rolling elements (SKF, 2013)

2.2.2.1.4 Cage. It can also be defined as seperator or retainer. They hold the rolling elements together and evenly.

2.2.2.2 Bearings According to Load Direction

When the bearings are running, they are subjected to forces in radial and thrust directions. They are divided into two groups, radial and thrust bearings, according to the direction of the force they carry. Directions of the forces that are loaded on the shaft is shown in Figure 2.6.

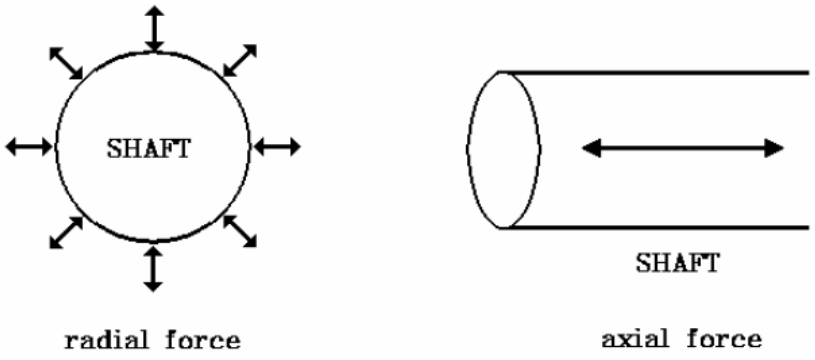

Figure 2.6 Force directions on the shaft (Centec, 2002)

2.2.2.2.1 Radial Bearings. These bearings are the ones that were designed to carry the forces coming from radial direction. Angle of contact, which is created by the contact points of the rolling surfaces and rolling elements, is a significant parameter. While radial bearings are able to carry both radial and axial forces depending on the angle of contact, they can also carry radial forces only when the angle of contact is zero. Radial bearings are shown in Figure 2.7.

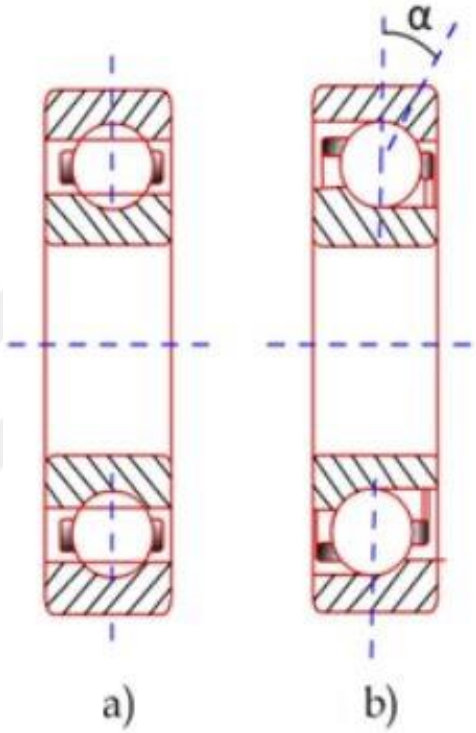

Figure 2.7 Radial bearings a) deep groove b) angular contact (NPTEL, 2019)

2.2.2.2.2 Thrust or Axial Bearings. These bearings are type of bearings designed to carry axial forces. It has types that can carry unilateral and bilateral axial forces. Thrust ball bearing is shown in Figure 2.8. Some types of them can also carry some radial forces. In Figure 2.9, an axial bearing that carries a radial force is shown. During operation, in order for the balls which are under the effect of centrifugal force not to come out of their channels, forces acting on the bearing should not be smaller than a certain value. Therefore, these bearrings are not appropriate for high speed revolutions.

Figure 2.8 Thrust ball bearings a) single direction b) double direction (SKF, 2014)

Figure 2.9 Double direction angular contact thrust ball bearing (SKF, 2012)

CHAPTER THREE
THEORY OF VIBRATION

3.1 Introduction

Vibration can be defined as the small magnitude repetitive movement of any system around the equilibrium position. It has an important place in human life. We hear thanks to the vibration of out eardrums and we speak thanks to the vibration of our vocal cords. While vibration is a desired condition in musical instruments, this phenomenon is an undesired feature in mechanical systems. It can lead to results like energy loss, noise, material fatigue, and material deformation in mechanic systems. Thus, it is an undesired condition for mechanical systems such as jet engines, fans, compressors, turbines and pumps. Moreover, it is also possible for a complete destruction of the machine under a resonance condition. Machines like hammer drills, vibrating strainers, massage tools, electric tooth brushes benefit from vibration (Rao, 2010).

3.2 Vibration Basics

Vibration of a system comprises the energy conversion of kinetic and potential energy in both ways. Therefore, systems making vibrations should have elements that store both potential and kinetic energy. The elements that store kinetic energy are mass and inertia where elements that store potential energy are elastic elements such as springs. There will be a kinetic and potential energy gain if an input is given to a vibration system. Unless there is an damper within the system, the energy conversion goes on forever. However, there is always an damper (such as air resistance). Hence, the system will lose energy and its motion will ceases down mostly in exponential manner.

Below is the explanation of how a spring-mass system reacts against an external force F. Spring-mass system is shown in Figure 3.1.

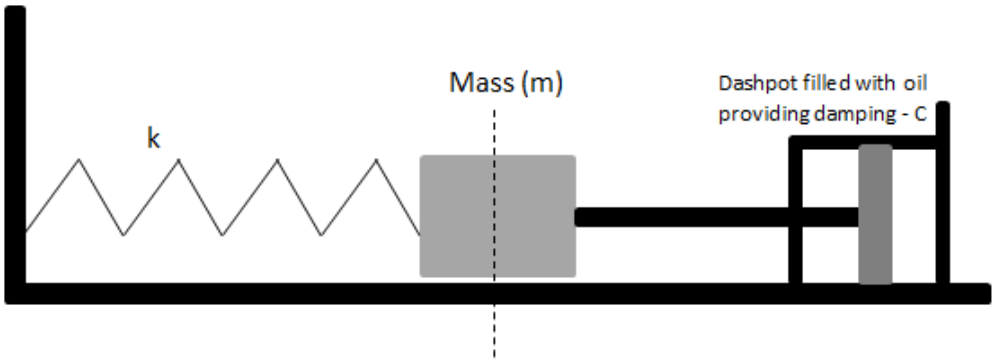

Figure 3.1 Spring-mass system

In the spring-mass system, the m mass is connected both to a spring with stiffness k and to a damper with the damping constant C. When the force F is applied, the spring is tensioned (potential energy is created) and the lubricant flows from the front side towards backwards (tries to damping the system).

The applied force F moves the mass by getting over the inertia of the mass and the reactions of the spring ams damper.

Machines has three main features in order to determine how they react to forces that lead to vibration, as belove.

These are;
Mass (m),
Stiffness (k),
Damping (c).

These features make up the natural characteristics of how machines react to vibration (Scheffer, 2004).

3.2.1 Mass (m)

Mass is the resistance that an object – whether animate or inanimate – shows against an applied force. It is measured in kg.

3.2.2 Stiffness (k)

This can be defined as the level of reacting for elastic elements against the effects of translation and relocation. The higher the stiffness is, the more powerful the force applied becomes in order to relocate. It is measured in N/m.

3.2.3 Damping (c)

Damping is the effect that can slow down the speed of the machine upon launch. It is measured in N/(m/s).

3.3 Vibration Terms and Definitions

3.3.1 Cycle

In Figure 3.2, waves with different amplitudes are shown. A cycle is defined as a vibrating body moves from stable position (point A) to a high level (point B), then to stable position again (point C), then to reverse high position (point D) and then back to stable position (point E) again.

3.3.2 Amplitude

The maximum replacement of a vibrating body is called amplitude. The amplitude value of a vibration is expressed in terms of displacement (mm), velocity (mm/s) or acceleration (g). These are B and D points in Figure 3.2.

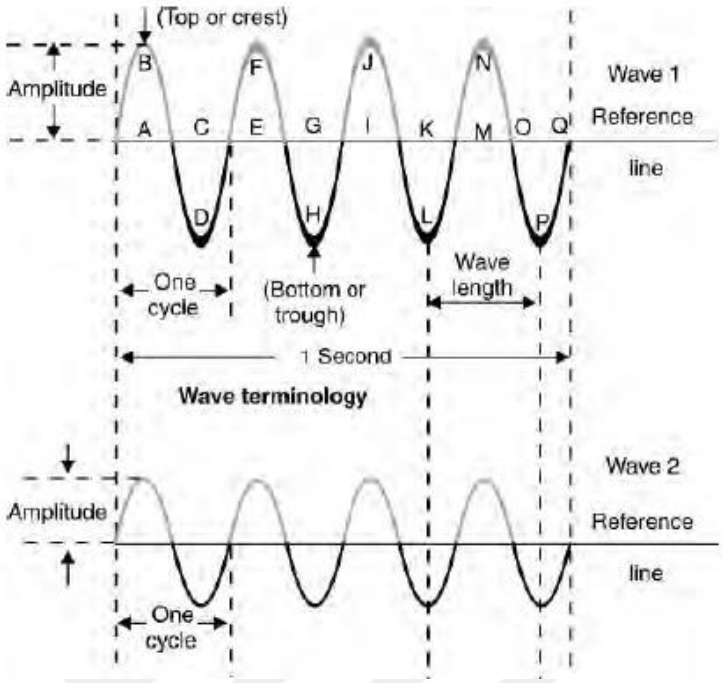

Figure 3.2 Comparison of waves with different amplitudes (Scheffer, 2004)

3.3.3 Period of Oscillation (T)

It is the time it takes for a vibrating body to complete its movement. It is measured second.

$$T = \frac{2\pi}{\omega} \text{ [s]} \tag{3.1}$$

3.3.4 Frequency of Oscillation (f)

Frequency can be expressed as the number of repetations within 1 second and it is measured in Hertz.

$$f = \frac{1}{T} = \frac{\omega}{2\pi} \text{ [Hz]} \tag{3.2}$$

3.3.5 Phase (ø)

Figure 3.3 shows two separate movements. The amplitudes and frequencies of these movements are the same. However there is a difference of T / 4 second between two movements.

"This lag of time is called the phase lag and is measured by the phase angle. A time lag of T is a phase angle of 360°, thus a time lag of T/4 will be a phase angle of 90°. In this case we would normally describe the two waves as out of phase by 90°" (Scheffer, 2004, p.17). It is measured in degree(0-360^0) or in radian(0-2π).

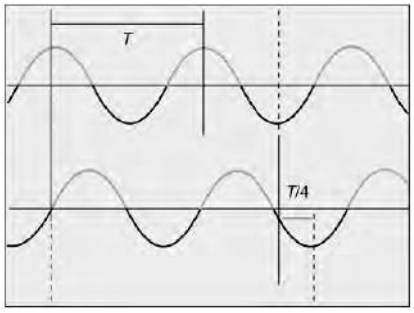

Figure 3.3 Phase relationship between two similar waves (Scheffer, 2004)

3.3.6 Angular Frequency (ω)

Also known as radial or circular frequency, measures angular displacement per unit time. Its units are therefore degrees (or radians) per second.

$$\omega = 2\pi f = \frac{2\pi}{T} \tag{3.3}$$

3.3.7 Natural Frequency

"If a system, after an initial disturbance, is left to vibrate on its own, the frequency with which it oscillates without external forces is known as its natural frequency. The vibratory system having n degrees of freedom will have, in general, n distinct natural frequencies of vibration" (Rao, 2010, p.62).

$$\text{Natural frequency: } \omega_n = \sqrt{\frac{k_{eff}}{m_{eff}}} \text{ [rad/s]} \tag{3.4}$$

In the test rig, natural frequencies were calculated by using resonance frequencies and logarithmic decrement (Table 3.1).

Table 3.1 Natural frequency of test rig

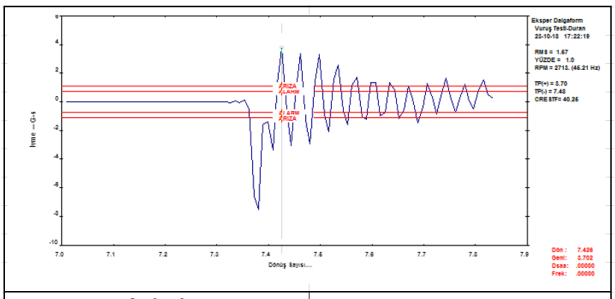

f1 (Hz)	26.5
f2 (Hz)	54.6

3.3.8 Resonance

Vibrations that are under the effect of external forces are called forced vibrations. When the natural frequency of the forced system is equal to the forcing frequency of the forced vibration, resonance occurs. In case of resonance, the amplitude of the system tries to go infinite. High amounts of vibration can occur under resonance conditions and this can lead to excessive damages on the system.

$$\text{Resonance frequency: } \omega_r = \omega_n\sqrt{1-2\zeta^2} \tag{3.5}$$

3.4 Harmonic Motion, Displacement, Velocity and Acceleration

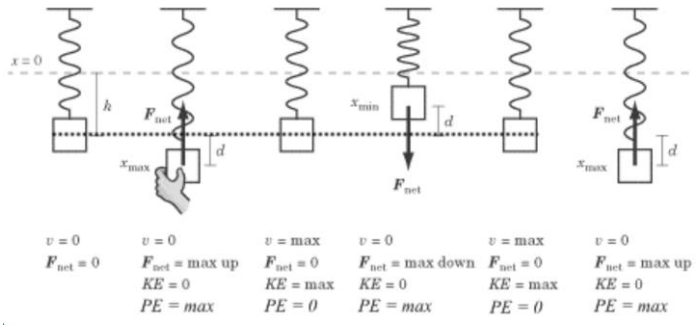

Figure 3.4 Harmonic motion (Augusta Country Public Schools, n.d)

In the harmonic motion shown in Figure 3.4, the mass moves downwards from the stable position following the external force's pull of the spring. Afterwards, it compresses the spring by passing from the stable position and then it comes back to stable position again. Provided that there is no damping element within the system, the system goes on forever like this. This motion is named periodic and harmonic, and the relationship between the displacement of the mass and time is expressed in the form of a sinusoidal equation:

$$x = X_0 sin\omega t \tag{3.6}$$

where

x= displacement at any given instant t; [m];
X_0= maximum displacement [m];
$\omega = 2\pi f$
t=time (seconds)

With to the motion of the mass, the speed changes between zero and the maximum values. For example; while the speed is equal to zero where displacement is at maximum level, the speed gets the maximum value at the point where displacement is zero. The speed of the mass can be obtained by taking the derivative of the displacement equation according to time basis.

$$Velocity = \frac{dX}{dt} = X_0 \omega \cos(\omega t) \tag{3.7}$$

The acceleration of the mass can be obtained by taking the derivative of speed equation according to time basis. The acceleration value is maximum at oscillation points where as at stable position, it is equal to zero.

$$Acceleration = \frac{dV}{dt} = -X_0 \omega^2 sin\omega t \tag{3.8}$$

3.5 Classification of Vibration

3.5.1 Free Vibration

"If a system, after an initial disturbance, is left to vibrate on its own, the ensuing vibration is known as free vibration. No external force acts on the system. The oscillation of a simple pendulum is an example of free vibration" (Rao, 2010, p.17). Figure 3.5 shows the movement of a simple pendulum.

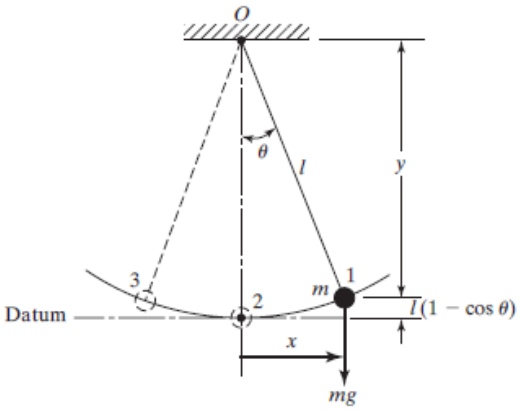

Figure 3.5 A simple pendulum (Rao, 2011)

3.5.2 Forced Vibration

It is the vibration motion of a system that is created under the effect of an external force (often, a repeating type of force). The oscillation that arises in machines such as diesel engines is an example of forced vibration. Also, resonance conditions emerge when the forced external force frequency is the same as the natural frequency of the system. Due to the fact that resonance conditions will damage the system in mechanic structures such as diesel engines, aircraft wings and turbines, the natural frequency of the system and the frequency of forced external frequency are required to be changed following the analysis of system resonance in vibration analyses. Forcing effect on a mass-spring-damper system is shown in Figure 3.6.

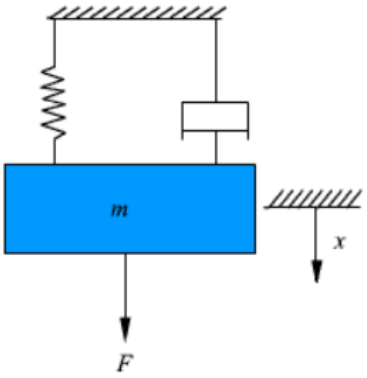

Figure 3.6 Forced vibration (mass, spring and damper system)

3.5.3 Undamped Vibration

"If no energy is lost or dissipated in friction or other resistance during oscillation, the vibration is known as undamped vibration" (Rao, 2010, p.17). In Figure 3.7, an undamped vibration system that was made up of only spring-mass system is shown. The initial force that will be applied to the system will lead to an infinite oscillation since there is no damping element in the system.

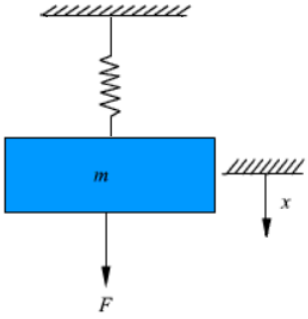

Figure 3.7 Undamped Vibration (mass-spring system)

3.5.4 Damped Vibration

In theory, there is no undamped system. In a spring-mass system, in the worst scenario, air can damp the system. The vibration of systems that have a damping

element aiming at halting the system or diminishing its energy are called damped vibration. In Figure 3.8, a spring-mass-damper system of damped vibration is shown.

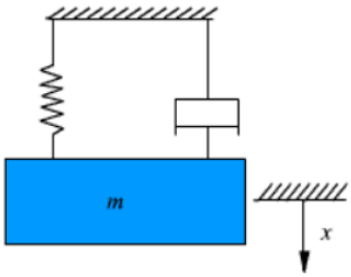

Figure 3.8 Damped vibration (mass, spring and damper system)

Figure 3.9 shows two oscillation graphs with a damping ratio of 0.1 and 0.3.

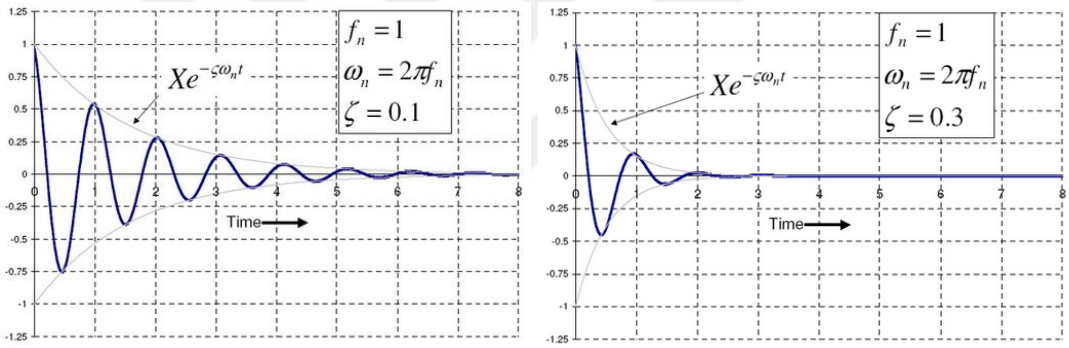

Figure 3.9 Two seperate oscillations with a damping ratio of 0.1 and 0.3 (Wikizero, 2019)

3.5.5 Linear and Nonlinear Vibration

"If all the basic components of a vibratory system the spring, the mass, and the damper behave linearly, the resulting vibration is known as linear vibration. If, however, any of the basic components behaves nonlinearly, the vibration is called nonlinear vibration" (Rao, 2010, p.17).

3.5.6 Deterministic and Random Vibration

Deterministic vibrations are stable. In practice, systems that yield such vibrations do not exist.

Random vibrations are irregular oscillation vibrations. In daily life, we face vibrations as such. As in the case of harmonic oscillation, they do not have a definite frequency and amplitude. Due to the fact that these are irregular vibrations, it cannot be determined which force causes the vibration in the machine. Nevertheless, sinusoidal element of the vibration can be found by using the Fast Fourier Transform (FFT).

3.6 Quantifying the Vibration Level

The amplitude value that defines the magnitude of the vibration can be expressed in four different ways and these are called peak to peak, zero to peak, root mean square (RMS) and average. They are shown in Figure 3.10.

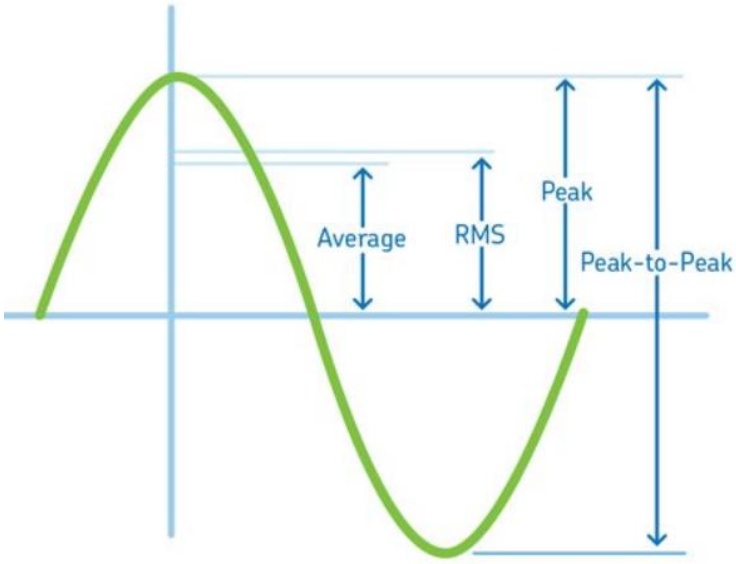

Figure 3.10 Vibration amplitudes for sinusoidal wave (SKF, 2019)

3.6.1 Peak to Peak

It is the difference between (+) high end point and (-) high end point of the oscillation. It is beneficial where mechanic clearance and where the highest amplitudes are very crucial. For example, the manufacturing firms of piston compressors and machines with journal bearings determine a limit value for peak to peak value and by means of this the vibration level can be tracked.

3.6.2 Zero to Peak

It is the distance between the zero (equilibrium) point and the peak value in one direction. It is half the peak to peak value.

3.6.3 Root Mean Square (RMS)

It is the effective value of the vibration. It can be defined as the root mean square of vibration valued measured at a determined time frame. It is the vibration level that we feel when we touch a working machine. It is the most preferred measure for vibration amplitude. At a simple harmonic motion, it is the 0.7071 times of the zero to peak value. For rotating equipment, RMS value is generally used for vibration levels. RMS value is used at ISO 10816 standard.

For a harmonic signal RMS value is calculated as;

$$\tau = \frac{2\pi}{\omega} \tag{3.9}$$

$$RMS = \sqrt{\frac{1}{\tau}\int_0^{\tau} x^2\, dt} = \frac{Peak}{\sqrt{2}} \tag{3.10}$$

3.6.4 Average

It is the arithmetic average of the vibration values measured at certain time intervals. In general, it is not a preferred measure of vibration amplitude.

3.7 Vibration Analysis Techniques

It is the most widespread and most effectively used vibration analysis today for condition monitoring on machines. The health of the machine is monitored by assessing the data collected from appropriate areas of the machines thanks to the vibration measuring sensors. The permitted vibration levels for machines are determined in ISO 10816 standard given im Figure 3.11.

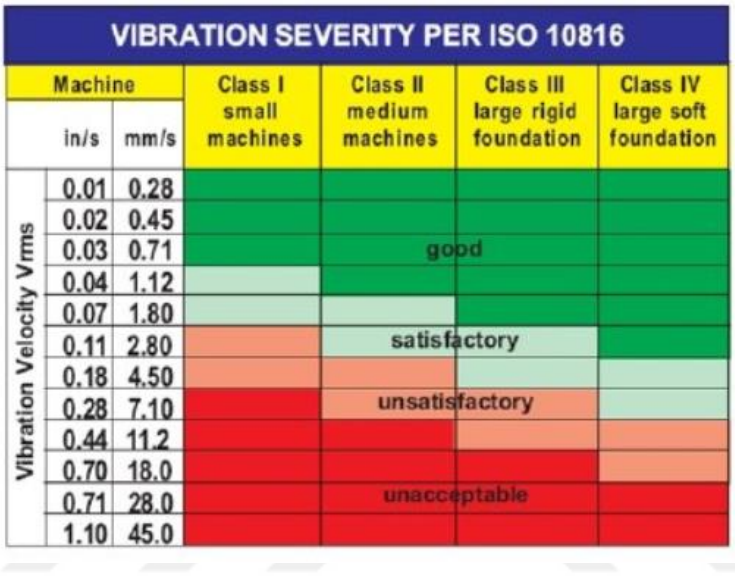

Figure 3.11 Guide to vibration severity as per ISO 10816

3.7.1 Time Domain Analysis

3.7.1.1 Time Waveform

Waveforms signals are generated just like oscilloscope graphics. It is the amplitude-time plot. Waveforms are the raw state of vibration data. Form distortions in the waveforms and amplitude in time can be studied. Defects have characteristic fault graphics (Figure 3.12). An assessment about the health of the machine can be done by comparing the waveforms of machines which have similar faults.

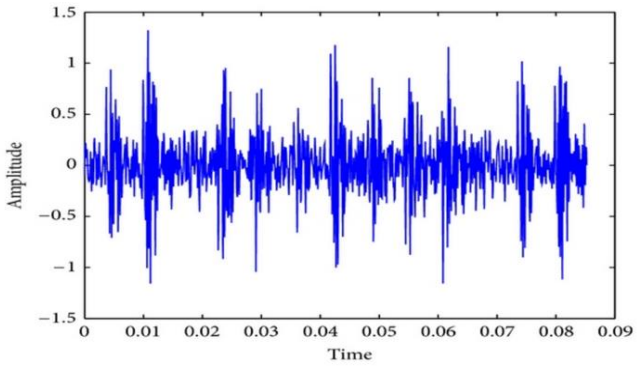

Figure 3.12 Example of time waveform (Liu, 2013)

3.7.1.2 Orbit

"Orbit plots show the path a rotor takes as its vibrates during operation" (Figure 3.13). "Orbits are created from the data from two orthogonal (perpendicular) measurements taken simultaneously" (Vibration Institute, 2018, p.4). These types of measurements are relative vibration readings. Relative readings are considered vibration measurements of the shaft with respect to the bearing housing. "Any change in the pattern of these figures or orbits can be used to identify faults such as misalignment in shafts, unbalance in shafts, shaft rub, wear in journal bearings, and hydrodynamic instability in lubricated bearings" (Rao, 2010, p.910).

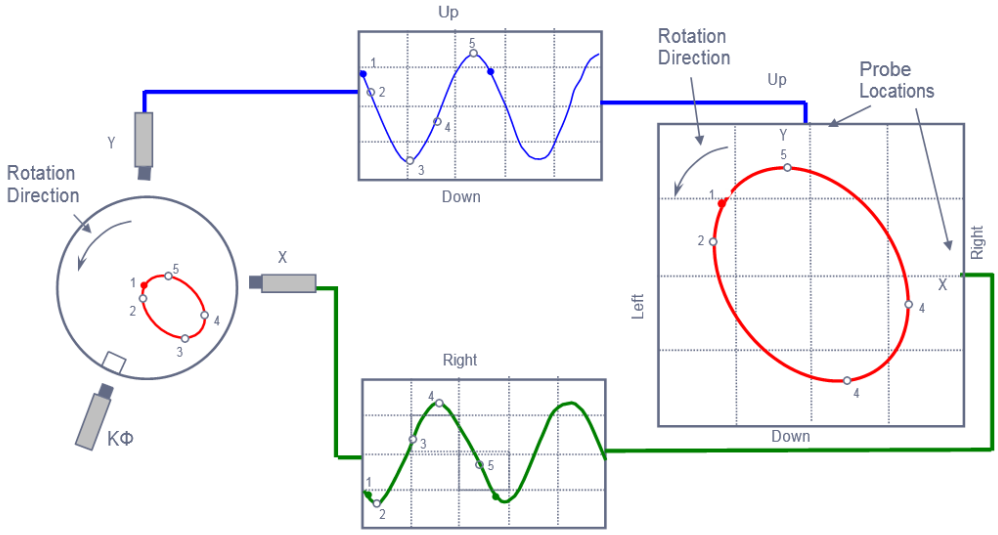

Figure 3.13 Orbit Construction (Vibration Institute, 2018)

3.7.1.3 Statistical Methods

In this method, statistical data such as probability density curve, and moments from other types (mean, standard, deviation, skewness, and kurtosis) are taken advantage. Fault detection can be made by comparing faulty and healthy signals.

$\bar{x}$ is the mean value, σ is the standard deviation, N is the number of sample, x is the vibration sample

$$Mean = \bar{x} = \frac{1}{N}\sum_{i=1}^{N} x_i^2 \tag{3.11}$$

$$Standard\ Deviation = \sigma = \sqrt{\frac{1}{N}\sum_{i=1}^{N}(x_i - \bar{x})^2} \tag{3.12}$$

$$Skewness = \frac{\sum_{i=1}^{N}(x_i - \bar{x})^3}{N\sigma^3} \tag{3.13}$$

$$Kurtosis = \frac{\sum_{i=1}^{N}(x_i - \bar{x})^4}{N\sigma^4} \tag{3.14}$$

A well-known value of the Kurtosis for the normal distribution is 3. It is widely used to detect non periodic shocks (Metravib Technologies, n.d.). Kurtosis is a valid measure of the degradation of a machine, but it does not give any indication of the diagnosis of the problem (Azima DLI, 2009).

Kurtosis is particularly suited to the monitoring of bearings of low speed rotating shafts, where frequency-based techniques are limited.

3.7.2 Frequency-Domain Analysis

The frequency spectrum is the frequency-vibration amplitude graph. It can be derived by using the digital fast Fourier analysis of the time waveform. As long as the driving forces in the machines do not change or change slightly, the frequency spectrums that the machines create will result similar to each other at different times.

Frequency spectrums are the characteristic properties of machines and can be called the signature of the machine.

When damage starts to occur on the machine, the vibration level and the frequency spectrum of the machine will change. By comparing the reference frequency spectrums, the location and the amount of the damage can be determined.

Each rotating element on machines produces an identifiable frequency. An evaluation on the reason of the damage can be made by monitoring these frequency levels. “Since such changes can be detected more easily compared to changes in the overall vibration levels, this characteristic will be very valuable in practice” (Rao, 2010, p. 921). For example, elements in machines like bearings, drums, and gears, have fault frequencies. Figure 3.14 shows fault frequencies that pump elements can generate.

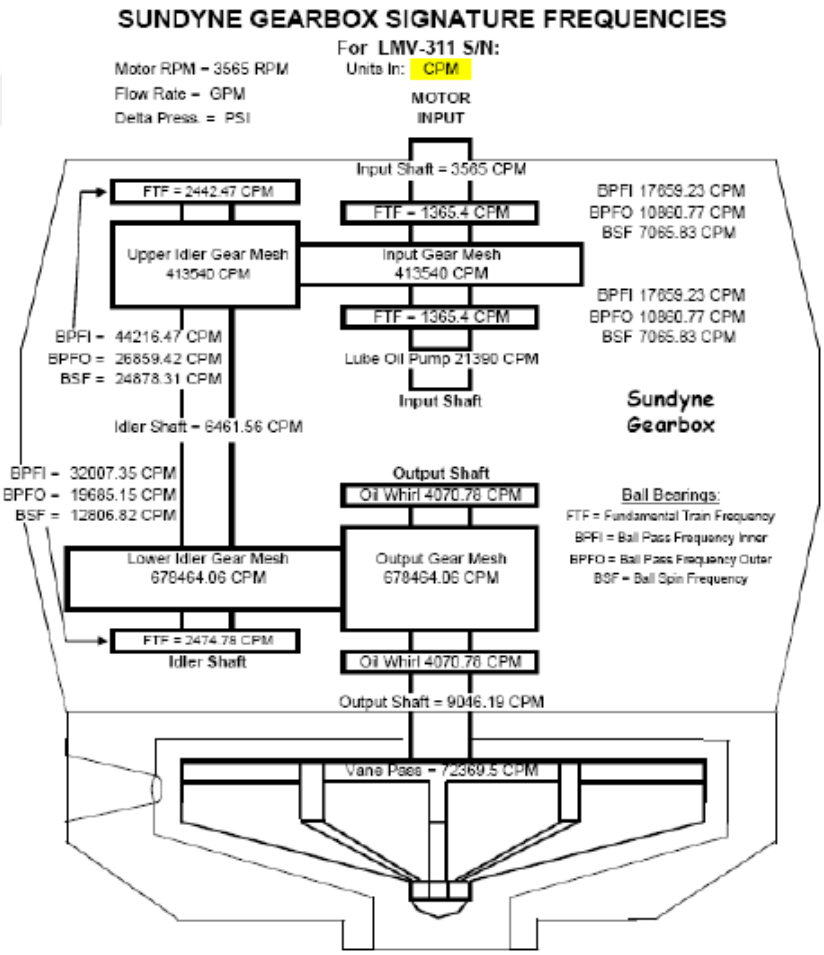

Figure 3.14 LMV 311 Gearbox signature frequencies (Sundyne, 2018)

3.7.3 Quefrency-Domain Analysis

The transformation signals that are obtained by taking the Fourier Transform (cepstrum) of the vibration signal's Fourier Transform one more time are studied. "Many of the terms used in spectrum analysis have been modified for use in cepstrum analysis" (Rao, 2010, p.922).

- Quefrency-Frequency
- Rahmonics-Harmonics
- Gamnitude-Magnitude
- Saphe-Phase

If the Fourier transform of an x(t) signal is F{x(t)},

Power spectrum of this signal; $S_x(\omega) = |F\{x(t)\}|^2$;

Signal of cepstrum; $C(\tau) = |F\{logS_x(\omega)\}|^2$.

CHAPTER FOUR
BEARING FAILURES

4.1 Introduction

Rolling bearings are the most widely used bearings in rotating machines. The fact that the bearings work seamlessly is of great importance for the health of the machine. Damages that can occur on bearings not only have a negative effect on the machine they are used but also can lead to accidental conditions depending on the level of the damage. However, the damage detection of the bearings alone is not sufficient. Determining what causes the damage of the bearing in the long term is of greater importance for the health of the machine. It should not be forgotten that the damage of the bearing does not occur by itself. There are external factors that lead to the emergence of the damage. In machines, early bearing faults may occur due to factors like incorrect bearing positioning, inadequate lubrication, heavy loading, dirt, dust, over lubricating and tight or loose bearing slot. By eliminating these factors, 60% of the early bearing fault can be prevented (SKF, 2008).

Figure 4.1 shows the causes of the failures in rolling elemenst bearings. Only about 0.35% of all rolling bearings do not reach expected life (FAG Antriebstechnik, 1979).

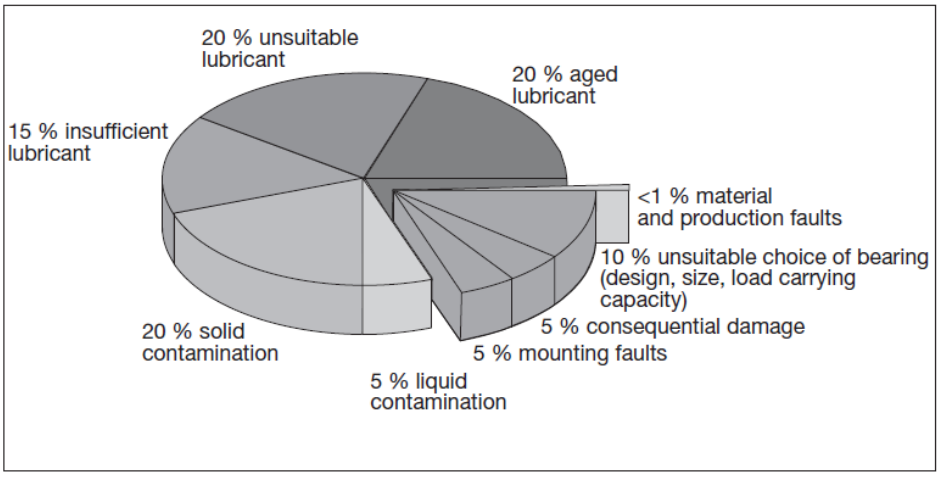

Figure 4.1 Causes of failure in rolling bearings (FAG Antriebstechnik, 1979)

4.2 Types of the Bearing Failures and the Causes

4.2.1 Normal Fatigue Failure (flaking, pitting)

The surfaces of the bearing elements shown in Figure 4.2 became rough after flaking. Flaking, piting may be caused early by overloading, excessive load due to improper handling, poor shaft or housing accuracy, installation error, ingress of dust or dirt, rusting (NTN, 2017). Such damages can be prevented by using a bearing with a heavier nominal load, by searching for the reason of the load, and by using a more viscose grease lubricant.

Figure 4.2 Inner ring, outer ring and balls are flaked (NTN, 2017)

4.2.2 Peeling

Peeling is a cluster of very little spalls (size about 10 micrometer). “Tends to occur if surface of opposite part is rough or lubrication characteristics are poor” (Figure 4.3) (NTN, 2017, p.10). This problem can be solved by preventing the input of the foreign objects and by changing the lubricating material.

Figure 4.3 Peeling on rolling contact surfaces (Action Bearing, n.d)

4.2.3 Wear and Fretting

> "Wear is caused mainly by sliding abrasion on parts including the roller end face and rib, cage pocket surface, cage, and the guide surface of the bearing ring. Wear due to contamination by foreign matter and corrosion occurs not only to the sliding surface but also to the rolling surface. Fretting is a phenomena which occurs when slight sliding is repeatedly caused on the contact surface. On the fitting surface, fretting corrosion occurs, generating a rust like powder" (Koyo, 2015, p.6).

Improvement of lubricant and lubrication type, filtering of oil, improvement of sealing can be solved problem of wear. Inquiry and countermeasures for the source of vibration, enhancement of shaft rigidity can be solved problem of fretting. Figure 4.4 shows wear and fretting damage.

Figure 4.4 Wear and fretting failures (Koyo, 2015)

4.2.4 Cracks and Chips

Cracks include slight cracks, splitting and fracture. "Chips are a type of failure occurring at a certain part of a bearing ring rib or corner of a roller" (Koyo, 2015). Cracks and chips may occur due to excessive impact or load, to jammed solid and big objects. Improvement of interference, reduction of load and removal of thermal impact with can be solved. Cracks and chips damages are shown in Figure 4.5.

Figure 4.5 Cracks and chips failures (Action Bearing, n.d)

4.2.5 Brinelling and Nicks

> "Brinelling is depressions created on the part of the raceway surface which comes into contact with the rolling element, and is due to plastic deformation. Brinelling is also small depressions on the rolling surface caused by contamination by solid foreign matters. Nicks are a flaw caused by the direct impact received when bearings are hit by a hammer or other solid tool" (Koyo, 2015, p.8).

Precautions can be taken by mounting the bearing better, filtering the grease, increasing the impermeability capacity. In Figure 4.6, the brinelling that occurs on the raceway of ball bearing is shown.

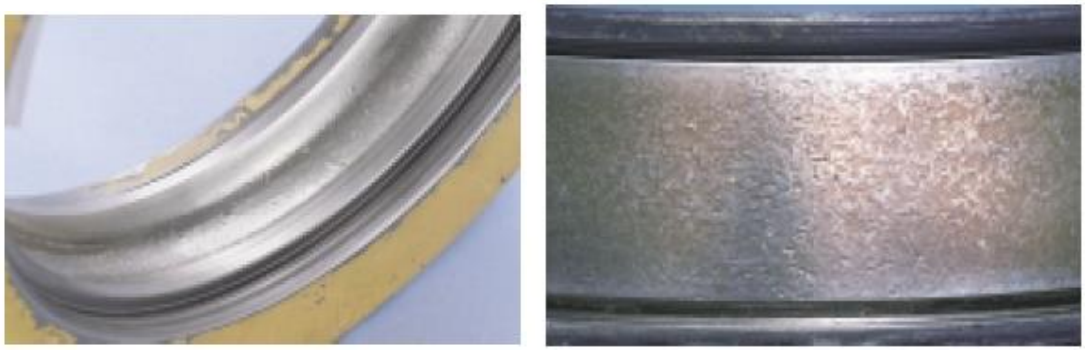

Figure 4.6 Brinelling on outer and inner ring raceway surface of ball bearing (Koyo, 2015)

4.2.6 Misalignment

"Misalignment can be detected on the raceway of the nonrotating ring by a ball wear path that is not parallel to the raceway edges" (Figure 4.7) . "If misalignment exceeds 0.001 inch/inch you can expect an abnormal temperature rise in the bearing and/or housing and heavy wear in the cage ball-pockets" (Barden, n.d., p.13)

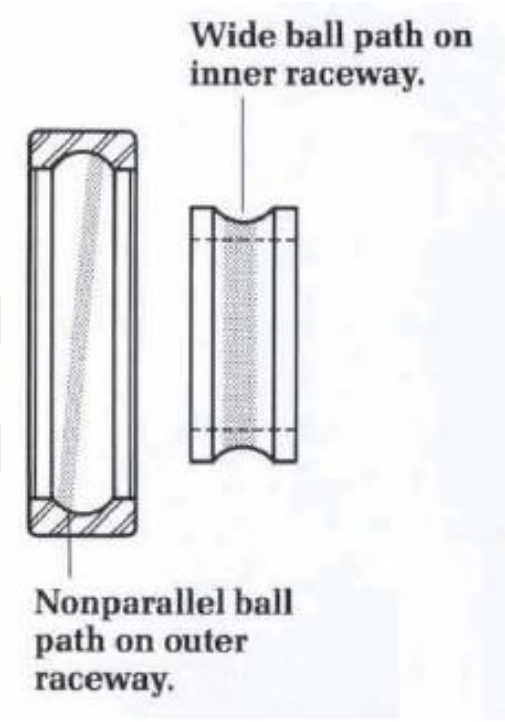

Figure 4.7 Effect of misalignment on the inner and outer ring raceways (Barden, n.d.)

4.2.7 Rust and Corrosion

Corrosion or rusting of bearing rings raceway and rolling element surfaces (Figure 4.8). Rust and corrosion can occur owing to water, corrosive material, concentration of the humidity in the air. The problem by increasing the sealing and periodic inspection of lubricating oil can be solved.

Figure 4.8 Corrosion of bearing rings (NTN, 2017)

4.2.8 Seizure

Bearing generates heat and seizes due to heat, preventing spinning. Discoloration, softening, and welding of raceway surface, rolling contact surfaces. It can happen as a consequence of insufficient dissipation of heat generated by bearing, insufficient lubrication or improper lubricant, clearance excessively small, installation error, excessive load (or preload) (NTN, 2017). This condition can be prevented by eliminating the reasons aforementioned. In Figure 4.9, it can be seen that rollers lead to discolouration in the inner race of the bearing and leave traces at equal intervals. The cause is poor lubrication.

Figure 4.9 Inner ring of double row tapered roller bearing (NTN, 2017)

4.2.9 Electrical Pitting

"Craters in the raceway due to local melting at the contact area of the parts in rolling contact, sometimes several craters in a row or whole chains around the circumference. The surface in the craters shown in Figure 4.10 is partly formed like welding beads" (FAG, 2001, p.38). Avoid flow of electric current by forestall current with a slip ring or insulated bearing (NTN, 2017).

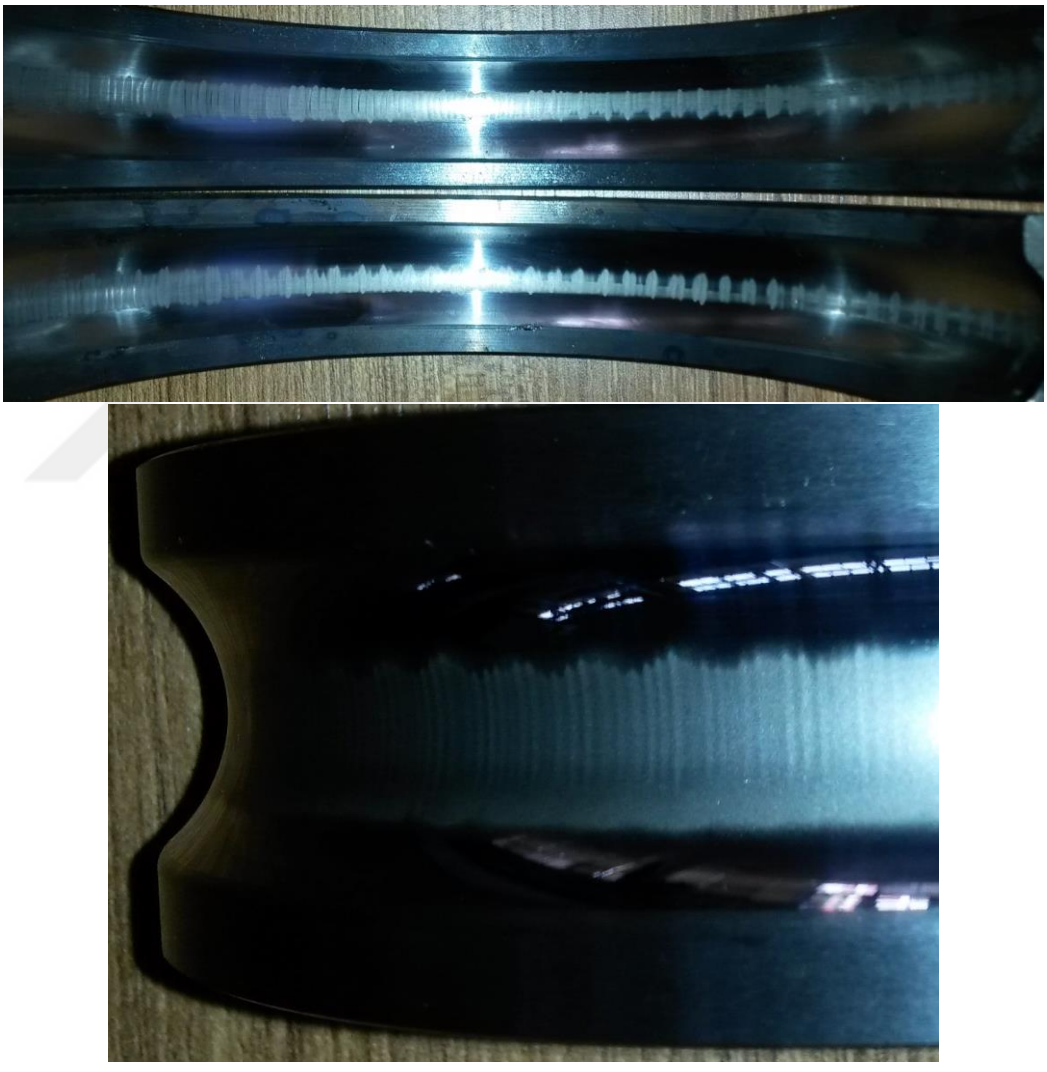

Figure 4.10 Effect of electrical pitting on inner and outer ring (Personal archive, 2015)

4.2.10 Damage of Cages

It is the condition of cage cracking, erosion or relaxed pins under conditions such as excessive moment load, high speed spinning or large fluctuation of speed, poor lubrication, trapping of foreign objects, heavy vibration, poor mounting (crooked bearing), and excessive heat (plastic cage in particular). Should be review of load conditions, cage selection, lubricant and lubrication method, rigidity of shaft and housing and improvement of handling practices (NTN, 2017). Cage damages are shown in Figure 4.11.

Figure 4.11 Examples of cage damages (Koyo, 2015)

4.2.11. Reverse Loading

"Angular contact bearings are designed to accept an axial load in one direction only. When loaded in the opposite direction, the elliptical contact area occurs on the outer ring. The result is excessive stress and an increase in the temperature, followed by increased vibration and early failure. Failure mode is very similar to that of heavy interference (tight) fits. The balls will show a grooved wear band caused by the ball riding over the outer edge of the raceway" (Figure 4.12). "Corrective action is to simply install the bearing correctly. Angular contact bearings must be installed with the resultant thrust on the wide face which is marked "thrust" of the outer ring and the opposite face of the inner ring" (Barden, n.d., p.9).

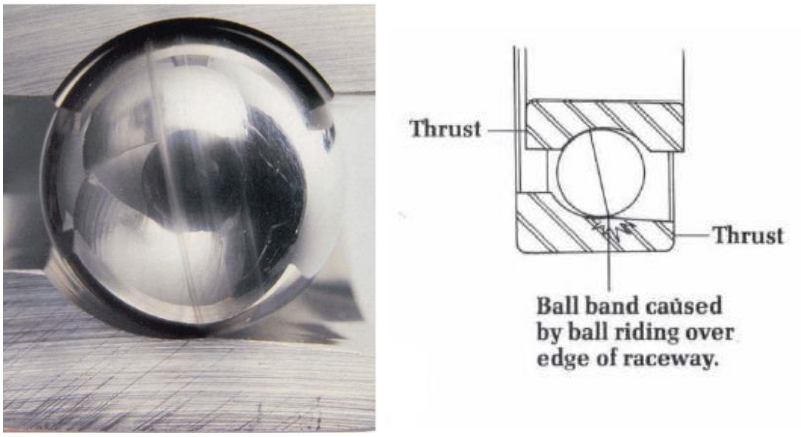

Figure 4.12 Ball damage of angular contact ball bearing. (Barden, n.d.)

4.2.12 Creeping

"Creep is the displacement during operation of a bearing ring, relative to the shaft or housing. Creep occurs when interference is too small in relation to the heat or load generated during operation" (Koyo, 2015, p.13). Should be reviewed interference between inner ring and shaft and between outer ring and housing. In Figure 4.13, creeping that occur on the inner races of deep grove ball bearing and tapered roller ball bearings.

Figure 4.13 Creeping of inner rings (Barden, n.d.)

The most significant parameter that needs to be obeyed so that the bearings can work at a desired lifespan is high quality and appropriate lubrication. The friction on the rolling elements should be minimized by taking the relubrication periods into priority. Thus, it is excessively crucial to determine the possible damages on the bearings in advance.

CHAPTER FIVE
EXPERIMENTAL SETUP

5.1 Test Rig

The rest rig was created with the aim of making the failure analysis on thrust bearings experimentally. The general overview of the test rig is given in Figure 5.1, 5.2 and 5.3. It was decided to use the shaft vertically due to the fact that a thrust bearing with a zero angle of contact in the system. Therefore, the motor was fixed in vertical direction.

The one direction thrust bearing used in the test rig is made up of shaft washer, housing washer, balls and cage, as shown in Figure 5.3. The dimensions of the 51113 type FEB brand thrust bearing used in the rig are given in Figure 5.4. The body where the thrust bearing is mounted is made up of three parts. The first one is the part where the bearing shaft washer is placed. The second one is the part where bearing housing washer is placed. The third one is the part where the radial bearing, which is used to keep the shaft at the centre, is placed. The second and the third parts are screwed together. The first and the third parts hold tight thanks to the firm connection between the radial bearing inner ring and the shaft. This body that is made up of three parts is mounted on a plate by screws. Same methods were deployed during the mounting and unmounting of the bearings for which different defects were created so that conditions did not change. The power transfer between the motor and the body is done by the coupling.

In order to create load on the thrust bearing, a part with 3.1 kg weight is located on the first part by a screw. This is the load-1 condition in vibration measurements. The second 3.1 kg part mounted on the current 3.1 kg part by the screws indicates the load-2 condition. The load-1 and load-2 conditions were generated in order to review the vibration signals under two different load conditions.

The electric motor used in the rig is a 0.37 kW motor and operates on alternative current. A Jaskawa (J1000) speed control device was used in order to adjust the revolution of the electric motor. Thanks to this, vibration measurements at different speeds could be taken by alternating the speed of the shaft.

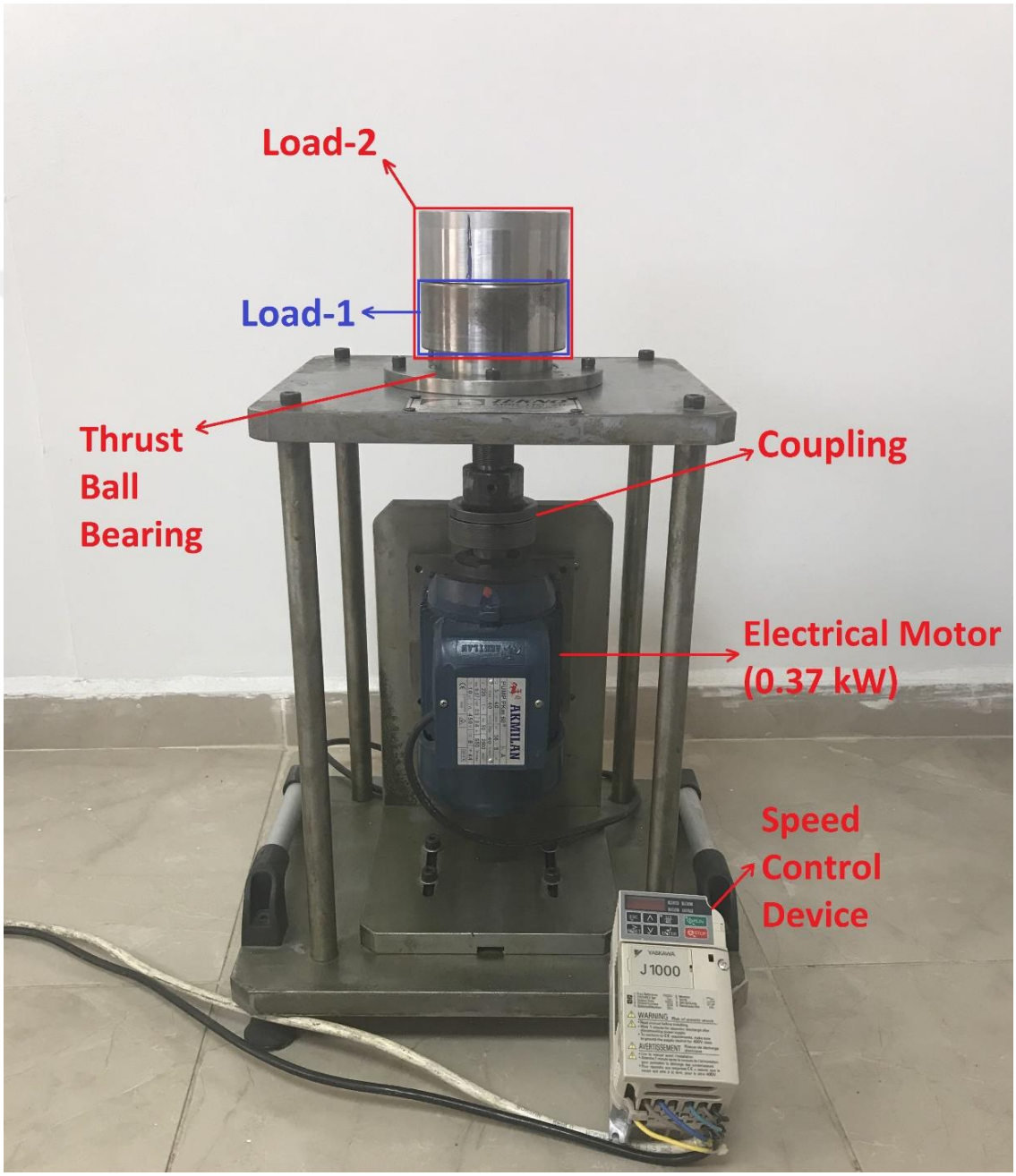

Figure 5.1 Overview of the experimental setup (Personal archive, 2019)

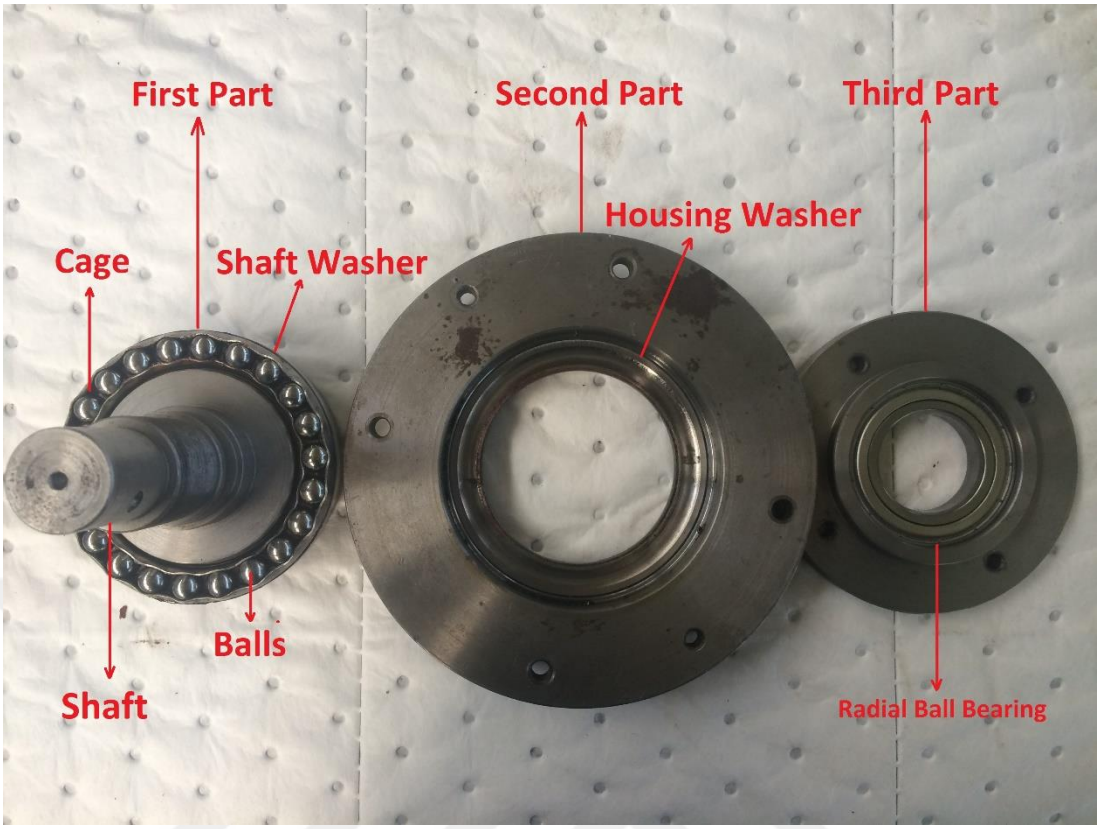

Figure 5.2 Bearing housing (Personal archive, 2019)

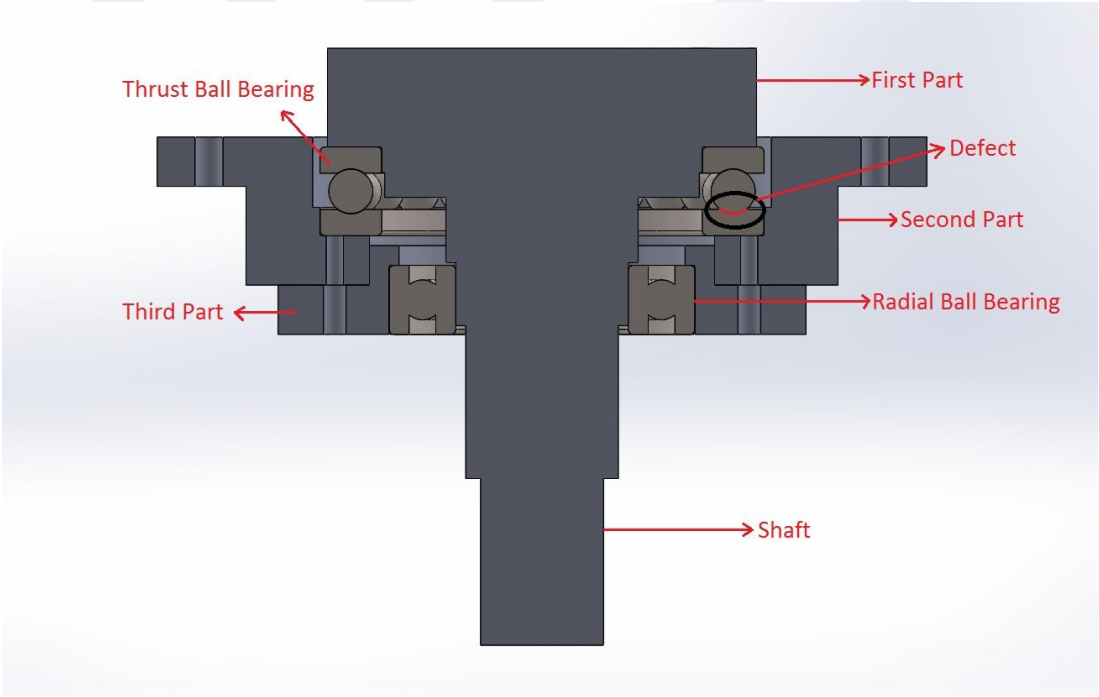

Figure 5.3 Sectional drawing of bearing housing (Personal archive, 2019)

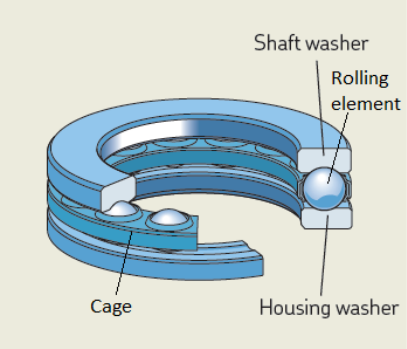

Figure 5.4 Thrust ball bearing components (SKF, 2019)

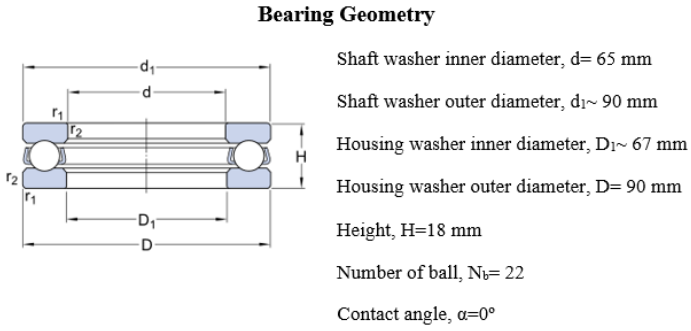

Figure 5.5 Thrust ball bearing geometry - FEB, 51113 (SKF, 2019)

5.2 Instrumentation

The vibration measurements were made by an EMERSON brand CSI2140 model vibration measurement device. The accelerometer type sensor was used. The sensitivity of the sensor is mV/m/s² (±5%). The average number, line number and the point number of the obtained vibration measurements were chosen as 5, 1600, and 4096, respectively.

After measurements uisng the vibration device and the accelerometer, the vibration data were transferred to the computer via the software of the device. Raw vibration data from the computer software were transferred into a text file. The raw vibration data from the text file were converted into various graphics by using some MATLAB programs that were specifically written for this process. In Figure 5.5, the steps of converting raw vibration data from gathering them up to conversion into graphics are shown.

Figure 5.6 Vibration analysis flow chart

5.3 Creation of Defect

Regional faults in the form of a single fault, two faults and four faults are created by using Minimo brand electro erosion machine (Figure 5.6) on the housing washer raceway of the thrust bearing which is used in test setup and three separate damaged bearings were examined. Defects generated on the housing washer ring raceway are shown in Figure 5.7. The amount of defect is about 0.1 mm in depth and 10 mm in length.

Figure 5.7 Minimo brand electro erosion machine

Figure 5.8 Housing washers of thrust bearings that defect generated (Personal archive, 2019)

5.4 Measurement Conditions

The vibration measurements were carried out in two ways – load-1 and load-2 – as mentioned in Section 5.1. The shaft speeds in the measurements are approximately 500, 1000, 1500, 2000, and 2500 RPM, respectively. The aforementioned load and speed parameters were applied for healthy, one defect, two defects and four defects bearings separately and the vibration measurements were observed for all these conditions.

Vibration measurements were taken from axial (P1), horizontal (P2), and vertical (P3) directions onto the shaft axis from points close to thrust bearing on the test rig. Measurement points are shown in Figure 5.8.

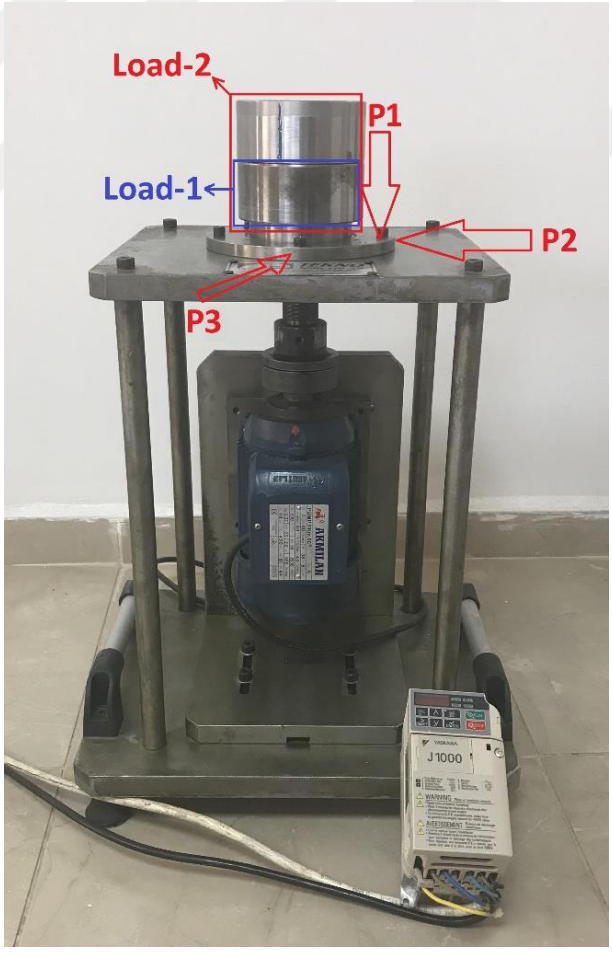

Figure 5.9 Measurement points on the experimental setup (Personal archive, 2019)

CHAPTER SIX
THRUST BEARINGS FAILURE DETECTION WITH VIBRATION ANALYSIS METHODS

6.1 Time Waveform Analysis

The time waveform data consists of vibration amplitudes versus time. It is the raw vibration data and it contains all vibration signals received on the system due to the fact that it does not have any filtering process. There are certain characteristic forms accepted according to the type of damage. However, it can be seen in cases where damage is dominant because there are raw vibration signals. In case of more than one damage, it may be difficult to comment on the waveform characteristic. The time waveform graphs indicate the existance of defect in the bearing but does not give information about the location of the fault (Patidar and Soni, 2013).

6.1.1 Characteristics Time Waveform

In Figures 6.1 and 6.2, experimental waveform samples of healthy and defect bearings are given as reference (Toyota, Niho, Chen and Komura, 2001; Zoladz, Earhart and Fiorucci, 1995). There are differences in the size and shape of the signal between the healthy and defect bearing. It was seen that the waveform of defect bearings has spiky characteristics. When the performed experimental studies were observed and the waveform graphics samples of which were provided in Figure 6.1 and 6.2 are reviewed, it can be concluded that there are characteristic defect waveform graphics for faulty conditions.

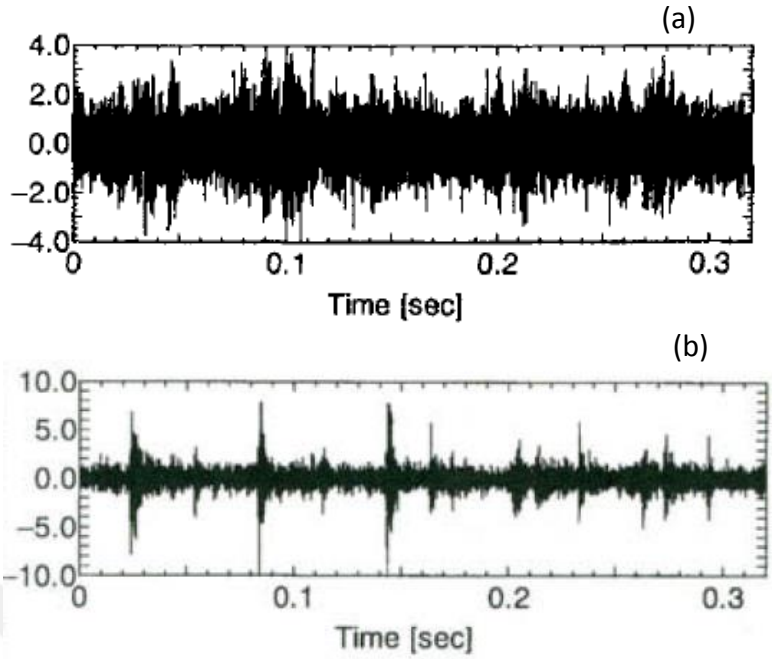

Figure 6.1 Experimental waveform for bearings of different conditions a) healthy bearing b) defect bearing (Toyota, Niho, Chen and Komura, 2001)

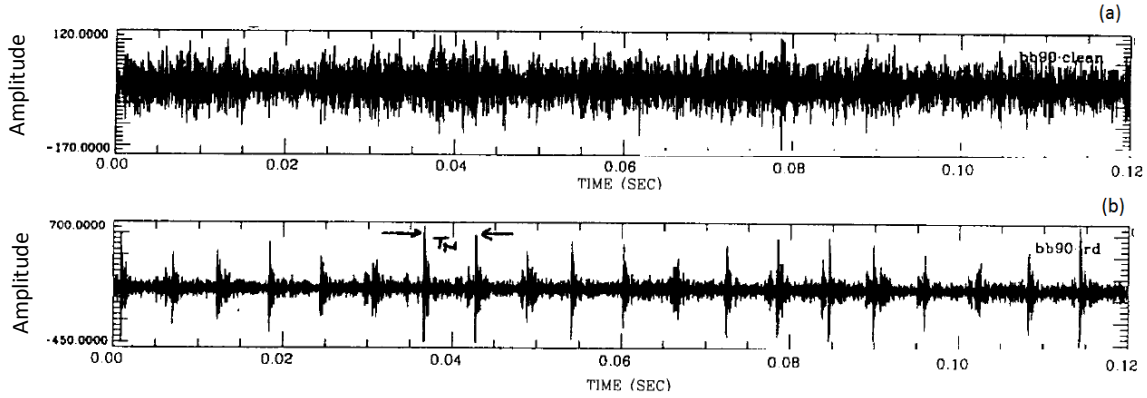

Figure 6.2 Experimental waveform for bearings of different conditions a) healthy bearing b) bearing with inner race defect (Zoladz, Earhart and Fiorucci, 1995)

In Figure 6.3, a waveform graphic showing the unbalance in the system was provided as a reference (Durton, 1999). In the waveform, a sinusoidal pattern that repeats itself in each period can be seen. This condition shows the unbalance in the system.

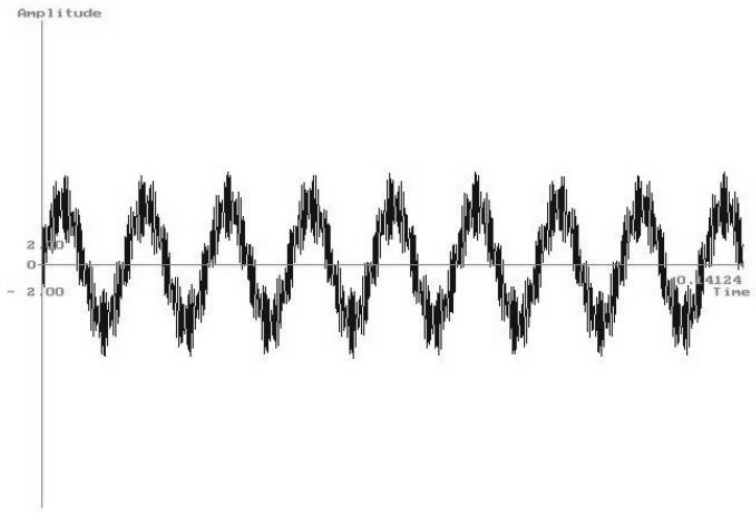

Figure 6.3 Unbalance characteristic waveform for acceleration response (Dunton, 1999)

In Figure 6.4, a waveform graphic showing the misalignment in the system was provided as a reference (Durton, 1999). M and W shapes, which are classic indicators of misalignment, can be seen here. The relative phase angle between 1xRPM and 2xRPM components determines the shape of the waveform graphic. The waveform graphic shown in Figure 6.5 was obtained by rotating the relative phase angle between 1xRPM and 2xRPM 90 degrees.

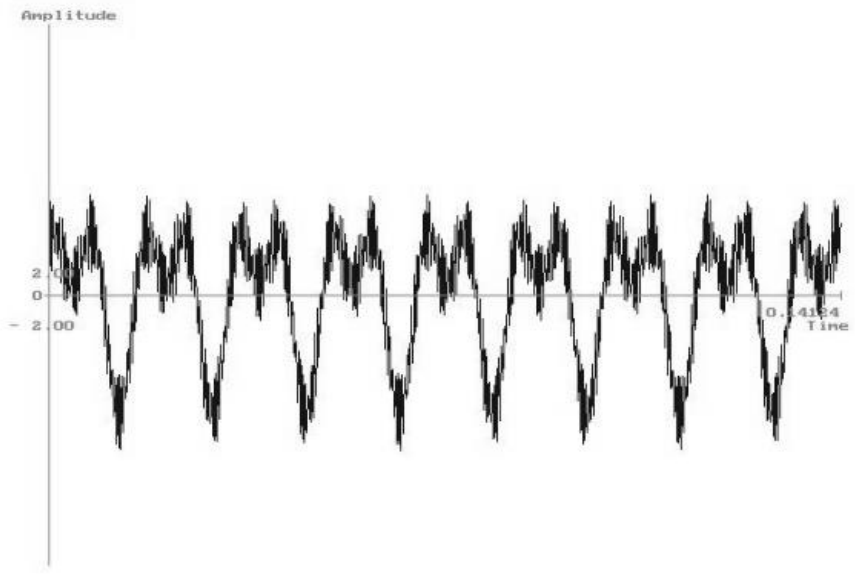

Figure 6.4 Misalignment characteristic waveform (Dunton, 1999)

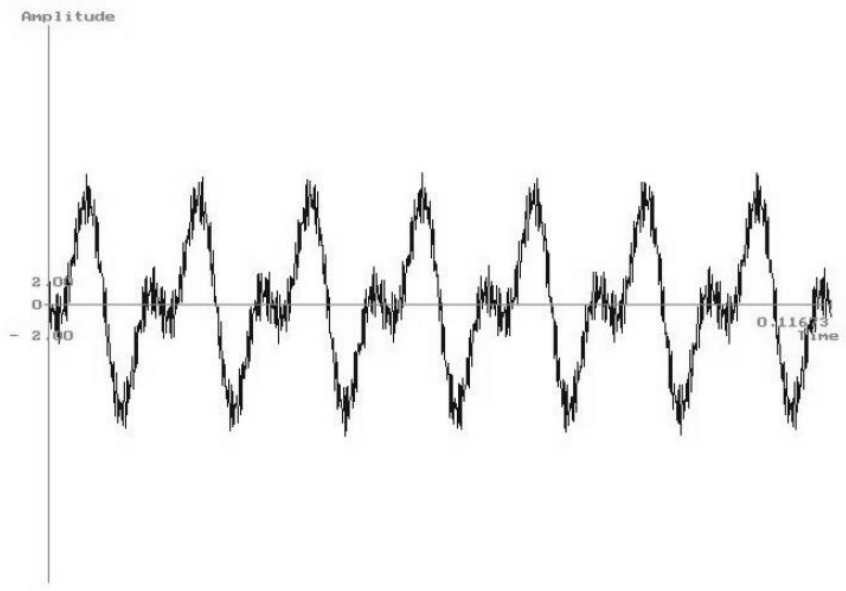

Figure 6.5 Misalignment characteristic waveform phase was changed 90 degrees (Dunton, 1999)

6.1.2 Analysis of Experimental Time Waveform Graphs

In this section, the waveform graphics that were obtained for raw vibration signals were studied for healthy and faulty bearings under two separate loads and between 500-2500 RPM (with 500 RPM increments). The waveform graphics were provided separately for axial (P1), horizontal (P2) and vertical (P3) measurement points.

Time waveforms at P1, P2, and P3 measurement points for 500 RPM under load-1 condition are provided in Figures 6.6, 6.7, and 6.8, respectively. In Figure 6.6, differences are seen between healthy and faulty bearings in terms of the magnitude and the shape of the signal. The fact that the waveforms belonging to two defects and four defects bearings have spiky characteristics shows that they can be used in fault detection of bearings. When Figure 6.7a and 8a is studied, it can be uttered that there is misalignment or imbalance in the system. However, it is seen that misalignment or imbalance are not clear for faulty bearings in 6.7 and 6.8. It can be concluded that the created bearing defect causes this condition.

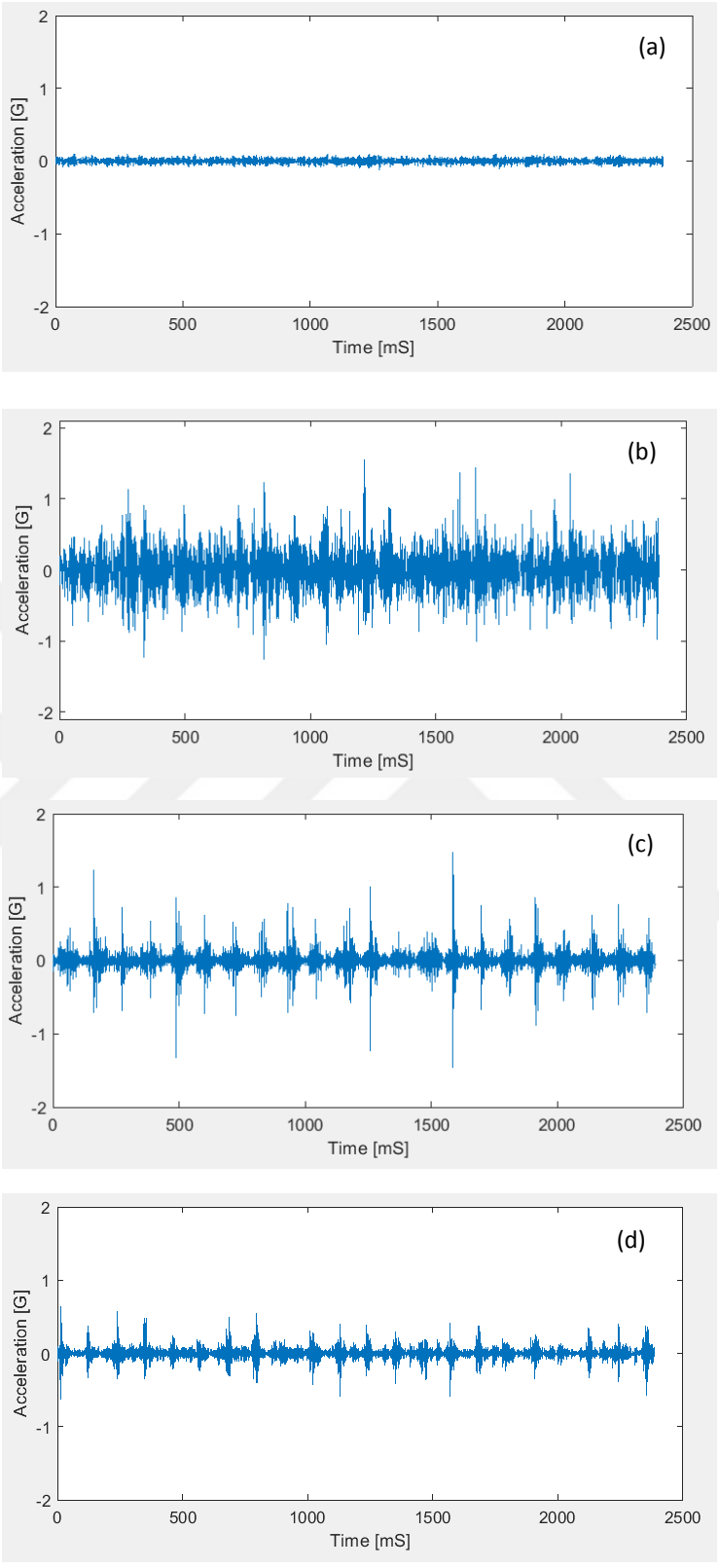

Figure 6.6 Time waveform for load-1 at point P1, 500 RPM a) healthy bearing b) one defect bearing c) two defects bearing d) four defects bearing

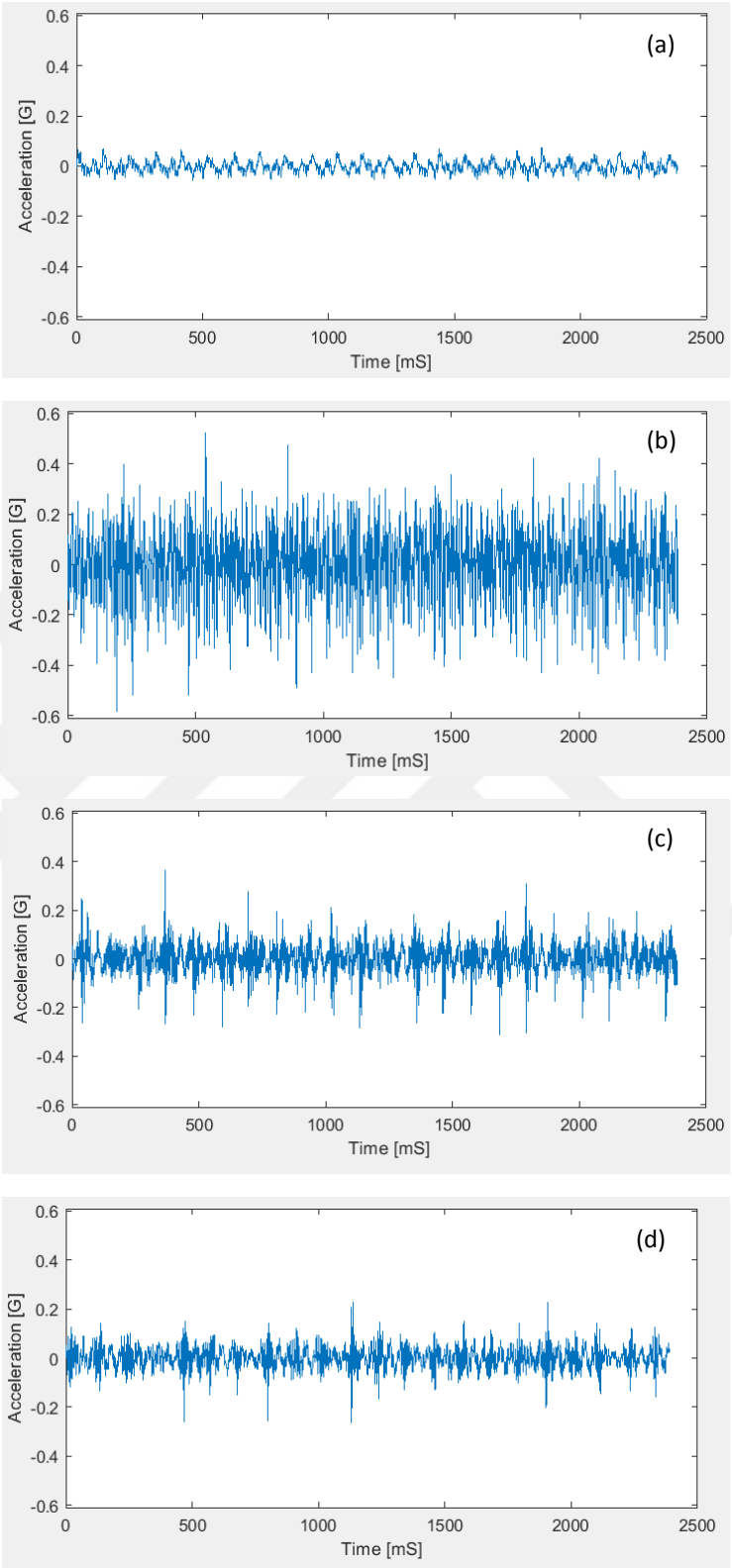

Figure 6.7 Time waveform for load-1 at point P2, 500 RPM a) healthy bearing b) one defect bearing c) two defects bearing d) four defects bearing

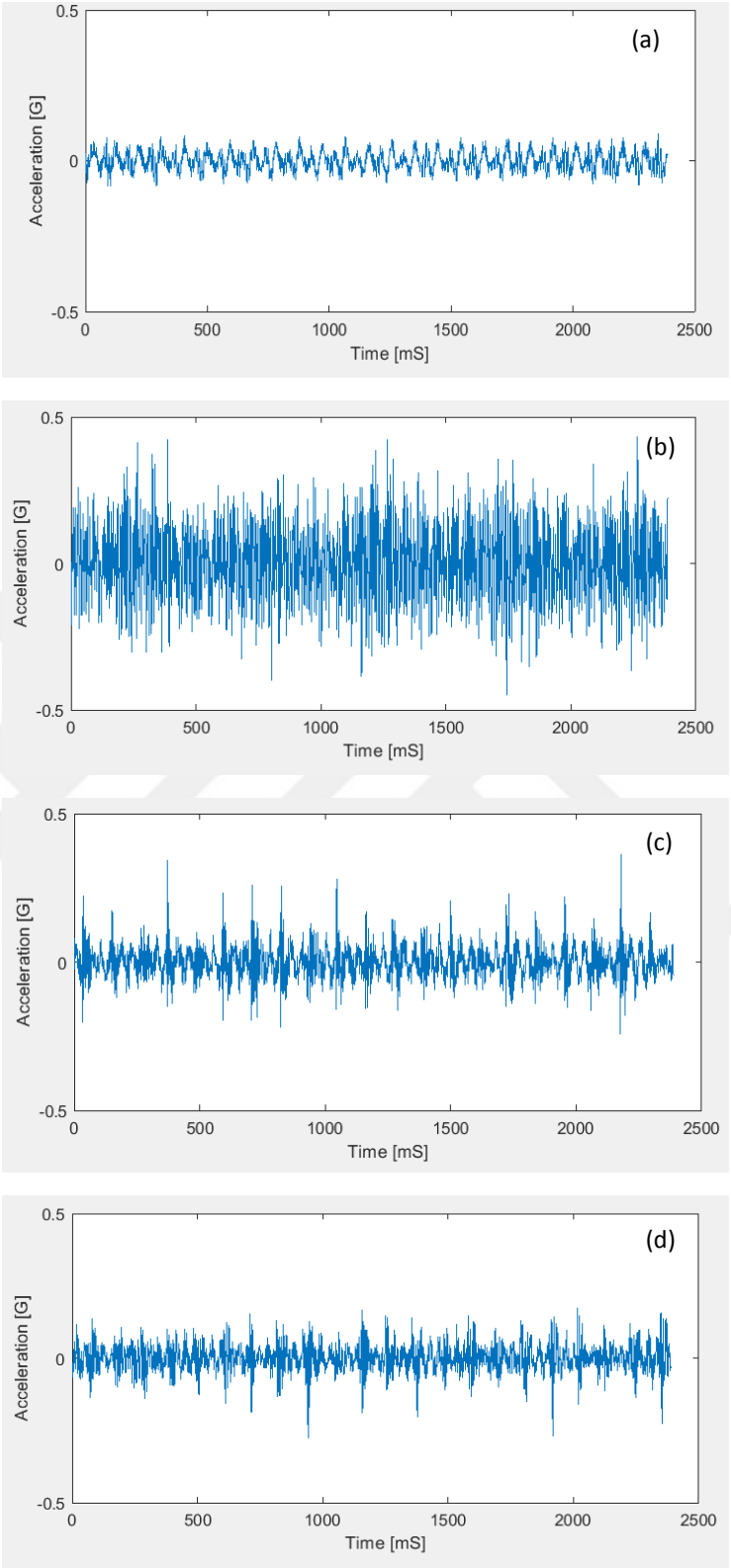

Figure 6.8 Time waveform for load-1 at point P3, 500 RPM a) healthy bearing b) one defect bearing c) two defects bearing d) four defects bearing

Time waveforms at P1, P2, and P3 measurement points for 1000 RPM under load-1 condition are provided in Figures 6.9, 6.10, and 6.11, respectively. The difference between Figure 6.9 and Figure 6.6 is the speed increment. In Figure 6.9, the graphics have a higher amplitude for two and four defects bearings and the graphics have more density. In Figure 6.10 and 6.11, the graphic intense and amplitude for the healthy bearing increase slightly when compared to Figures 6.7 and Figure 6.8. It can be said that the speed increase reveals imbalance and misalignment in the system. Nevertheless, it is not possible to say that there is bearing damage in the system by looking at the faulty graphics in Figure 6.10 and Figure 6.11.

Time waveforms at P1, P2, and P3 measurement points for 1500 RPM under load-1 condition are provided in Figures 6.12, 6.13, and 6.14, respectively. In addition to the speed increment, as expected, the amplitude of the graphic of healthy bearing increased in Figure 6.12 when compared to Figure 6.9. In Figure 6.12, by looking at the graphics of faulty bearings, it can be said that it shows bearing failure. The graphics became a little denser when compared to Figure 6.9. By studying, Figures 6.13 and 6.14, it can be said that there is imbalance in the system. Under condition when there are one and four defects on the bearing (Figures 6.13b and 13d, Figures 6.14b and 14d), it is seen that the imbalance in the system is not clear. It can be concluded that the created bearing defect causes this condition. The graphics of Figures 6.13c and 14c are very intense, therefore an evaluation cannot be done by looking at these graphics.

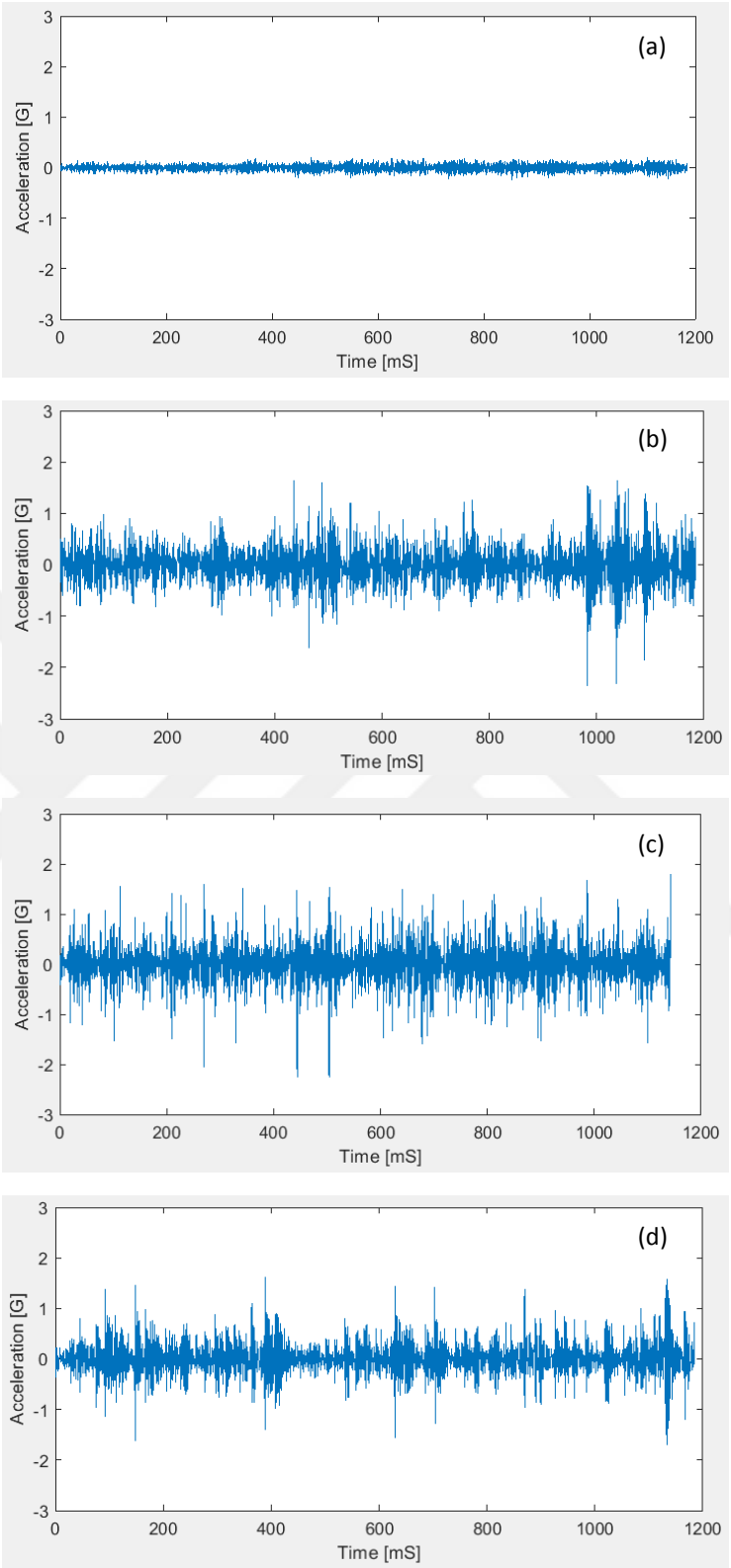

Figure 6.9 Time waveform for load-1 at point P1, 1000 RPM a) healthy bearing b) one defect bearing c) two defects bearing d) four defects bearing

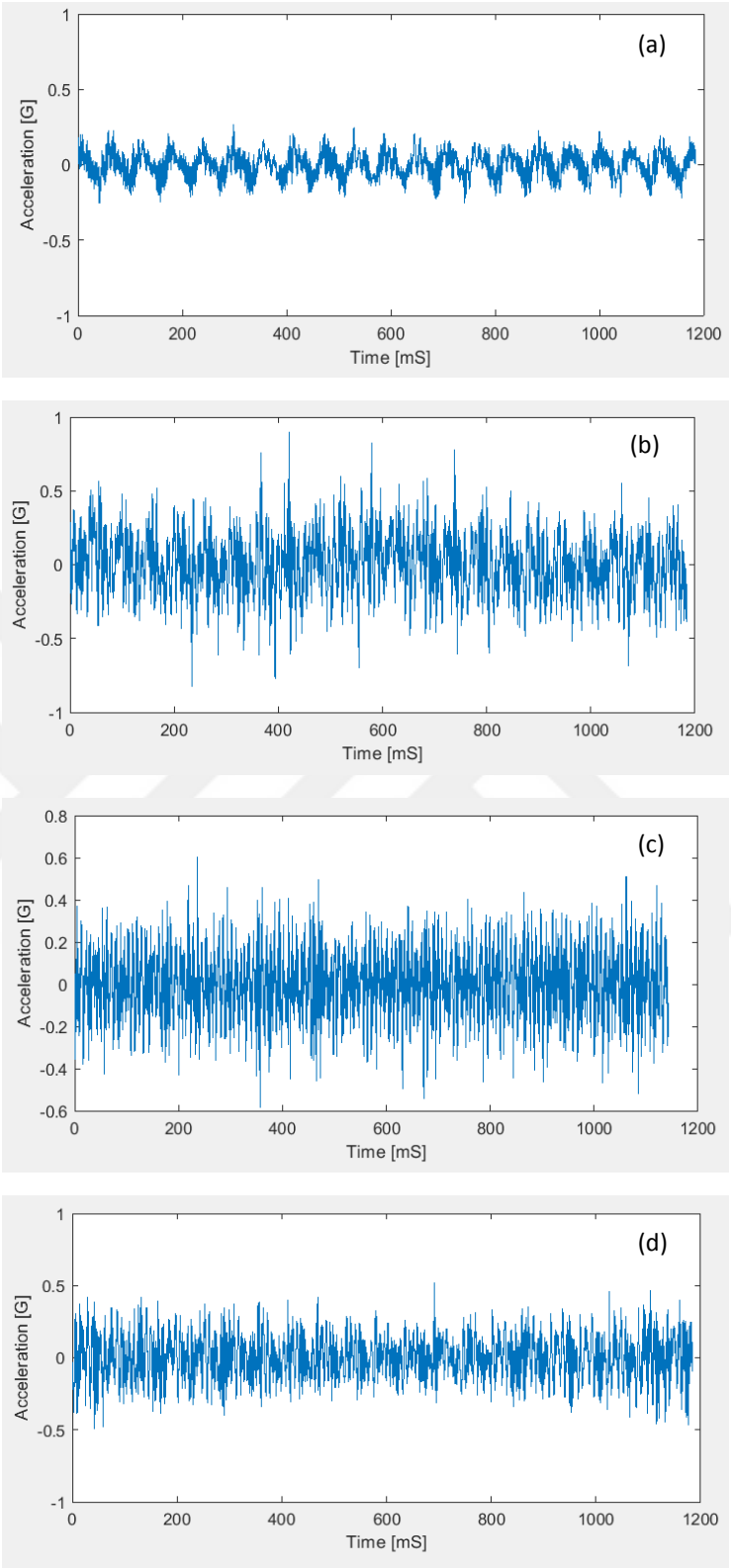

Figure 6.10 Time waveform for load-1 at point P2, 1000 RPM a) healthy bearing b) one defect bearing c) two defects bearing d) four defects bearing

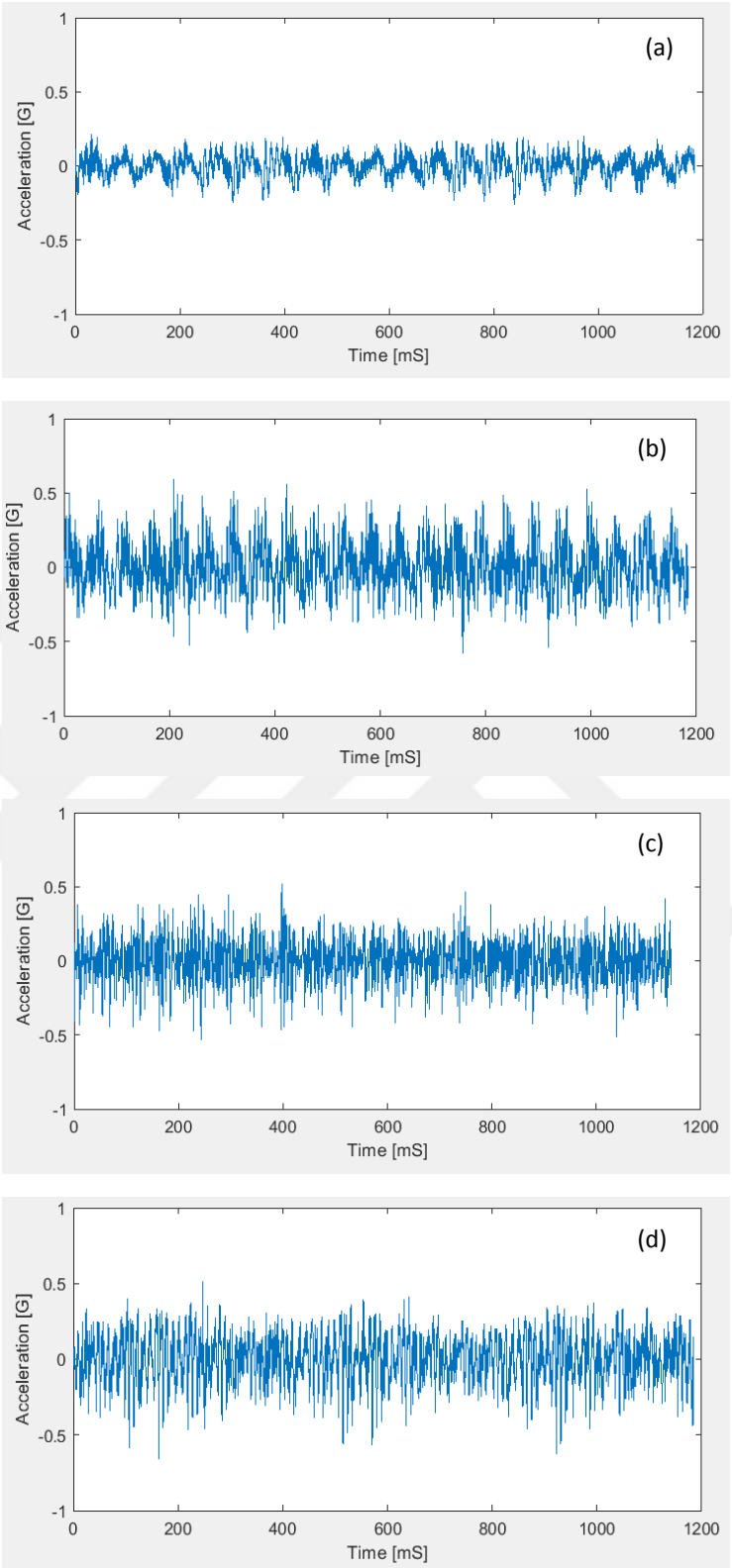

Figure 6.11 Time waveform for load-1 at point P3, 1000 RPM a) healthy bearing b) one defect bearing c) two defects bearing d) four defects bearing

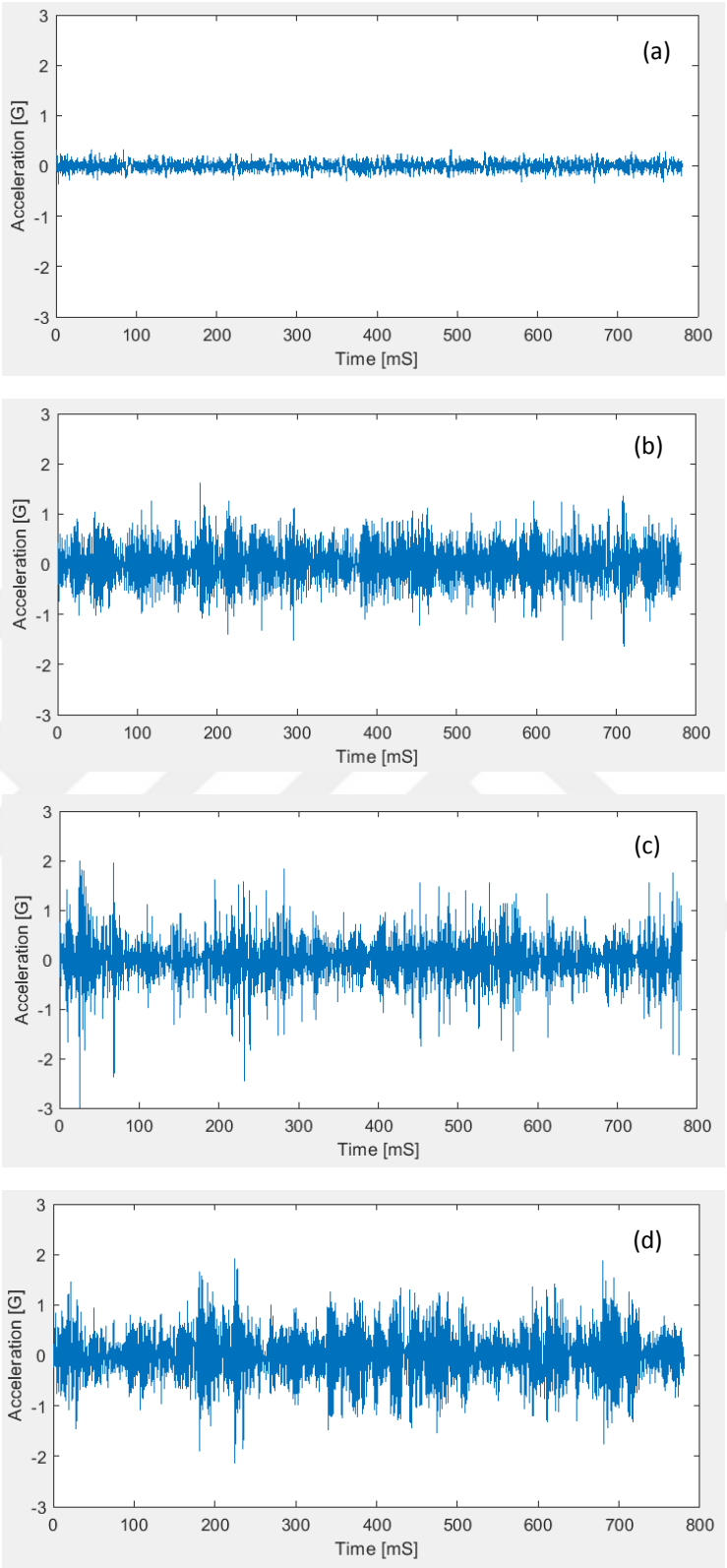

Figure 6.12 Time waveform for load-1 at point P1, 1500 RPM a) healthy bearing b) one defect bearing c) two defects bearing d) four defects bearing

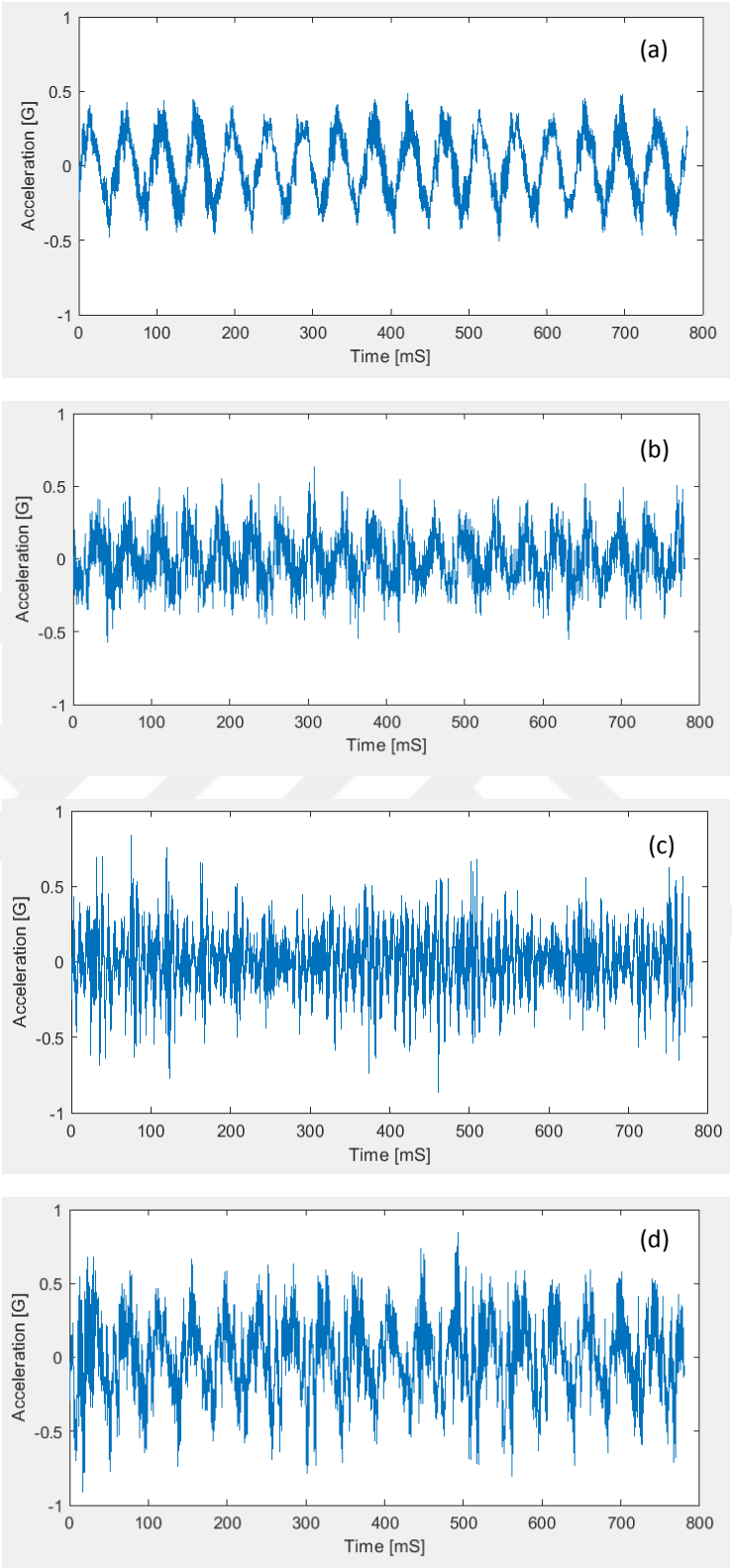

Figure 6.13 Time waveform for load-1 at point P2, 1500 RPM a) healthy bearing b) one defect bearing c) two defects bearing d) four defects bearing

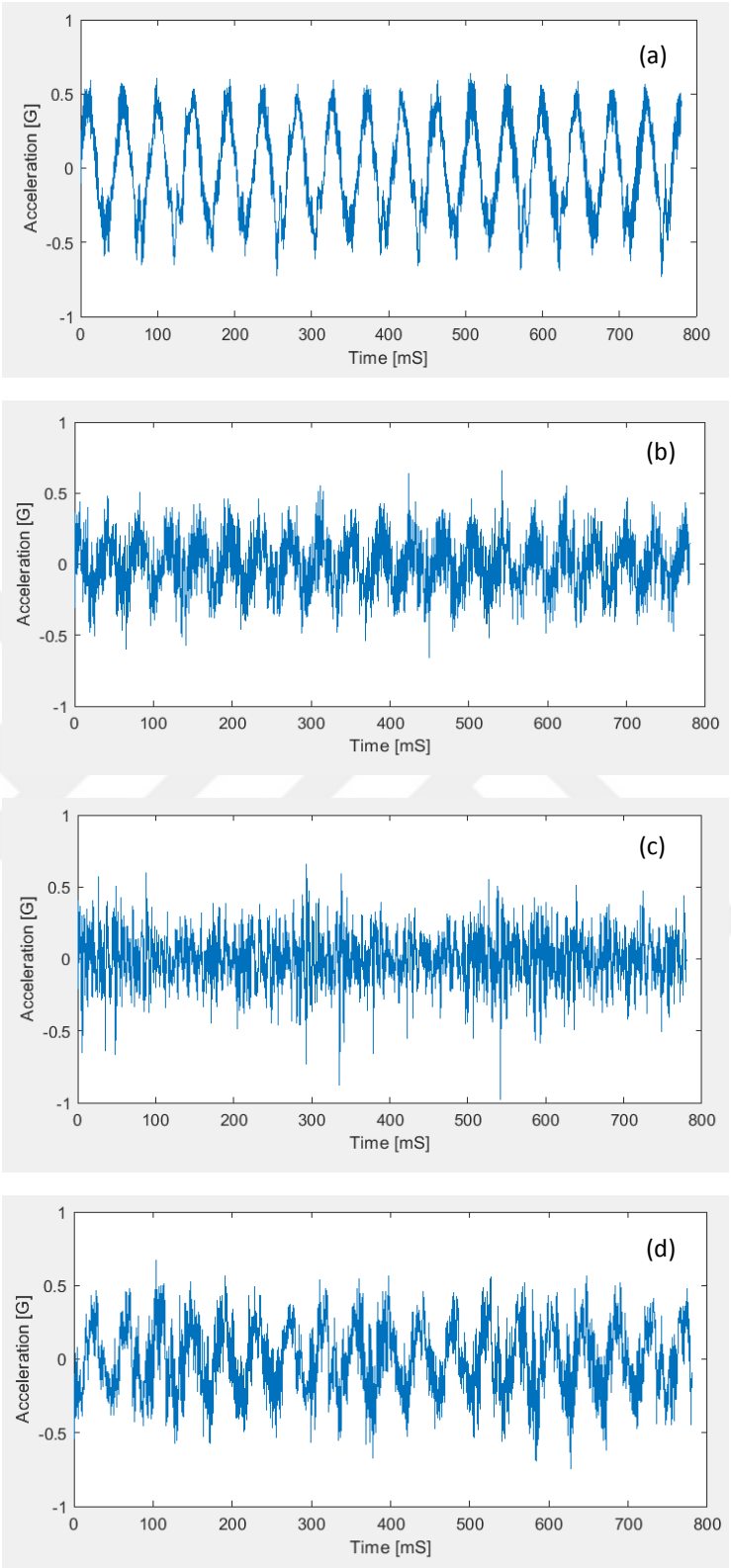

Figure 6.14 Time waveform for load-1 at point P3, 1500 RPM a) healthy bearing b) one defect bearing c) two defects bearing d) four defects bearing

Time waveforms at P1, P2, and P3 measurement points for 1500 RPM under load-2 condition are provided in Figures 6.15, 6.16, and 6.17, respectively. In Figure 6.15, differences are seen between healthy and faulty bearings in terms of the magnitude and the shape of the signal. The fact that the waveforms belonging to faulty bearings have spiky characteristics shows that they can be used in fault detection of bearings. There is an increase in terms of load in Figure 6.15, when compared to Figure 6.12. However, generally speaking, there is not a significant increase in the amplitude. By looking at Figures 6.16a and 6.17a, it can be expressed that there is misalignment and imbalance in the system. In Figures 6.16 and 6.17, misalignment and imbalance condition are seen for damaged bearings in the graphics. Based on the created bearing damage, it can be mentioned that the graphics resulting from the bearing damages have a more intense state than those of the healthy bearings. According to load-1 condition, there was no increase in the amplitude but imbalance and the misalignment in the system can easily be seen.

Time waveforms at P1, P2, and P3 measurement points for 2000 RPM under load-2 condition are provided in Figures 6.18, 6.19, and 6.20, respectively. In Figure 6.18, differences are seen between healthy and faulty bearings in terms of the magnitude and the shape of the signal. Defect detection can be made by studying the waveforms that belong to faulty bearings. The only difference between Figure 6.18 and Figure 6.15 is the shaft speed. It can be said that the amplitude increases as the speed increases. By looking at graphics of Figure 6.19a and 6.20a, it can be expressed that there is misalignment and imbalance in the system. The misalignment and imbalance condition in the system for the faulty bearings in Figure 6.19 and Figure 6.20 can be seen the graphics. As mentioned before, it can be mentioned that the graphics resulting from the bearing damages have a more intense state than the graphics of the healthy bearings. Generally speaking, there is a considerable amount of increase in the amplitude when compared to the measurements at 1500 RPM.

Time waveforms at P1, P2, and P3 measurement points for 2500 RPM under load-2 condition are provided in Figure 6.21, 6.22, and 6.23, respectively. Defect detection can be made by studying specifically Figures 6.21c and 6.21d. It can be suggested that the graphics became more intense thanks to the bearing damages at P2 and P3 measurement points. With the speed increase, the imbalance and misalignment in the system becomes more explicit at the P2 and P3 measurement points. Generally speaking, the assessment for 2000 RPM can also be done for 2500 RPM.

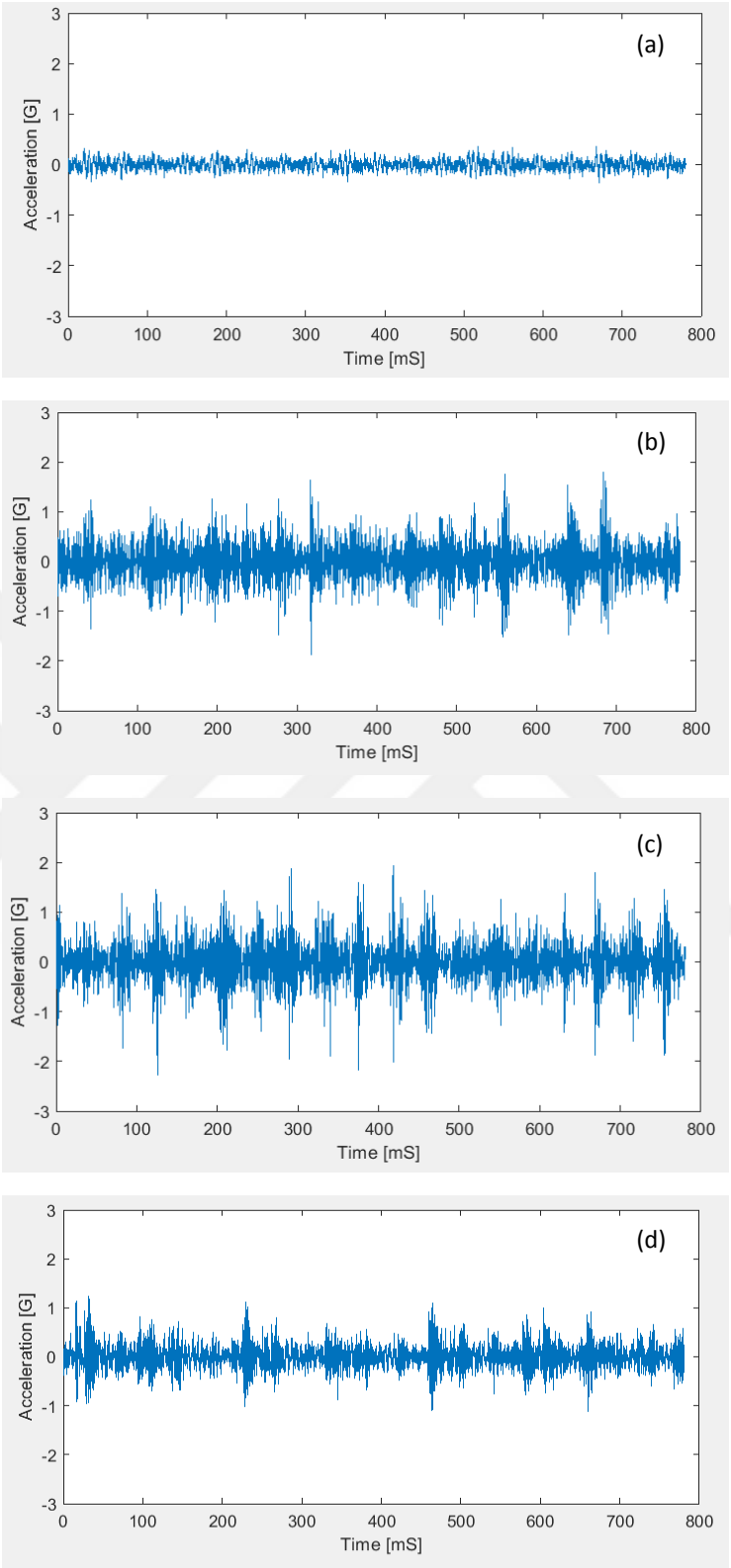

Figure 6.15 Time waveform for load-2 at point P1, 1500 RPM a) healthy bearing b) one defect bearing c) two defects bearing d) four defects bearing

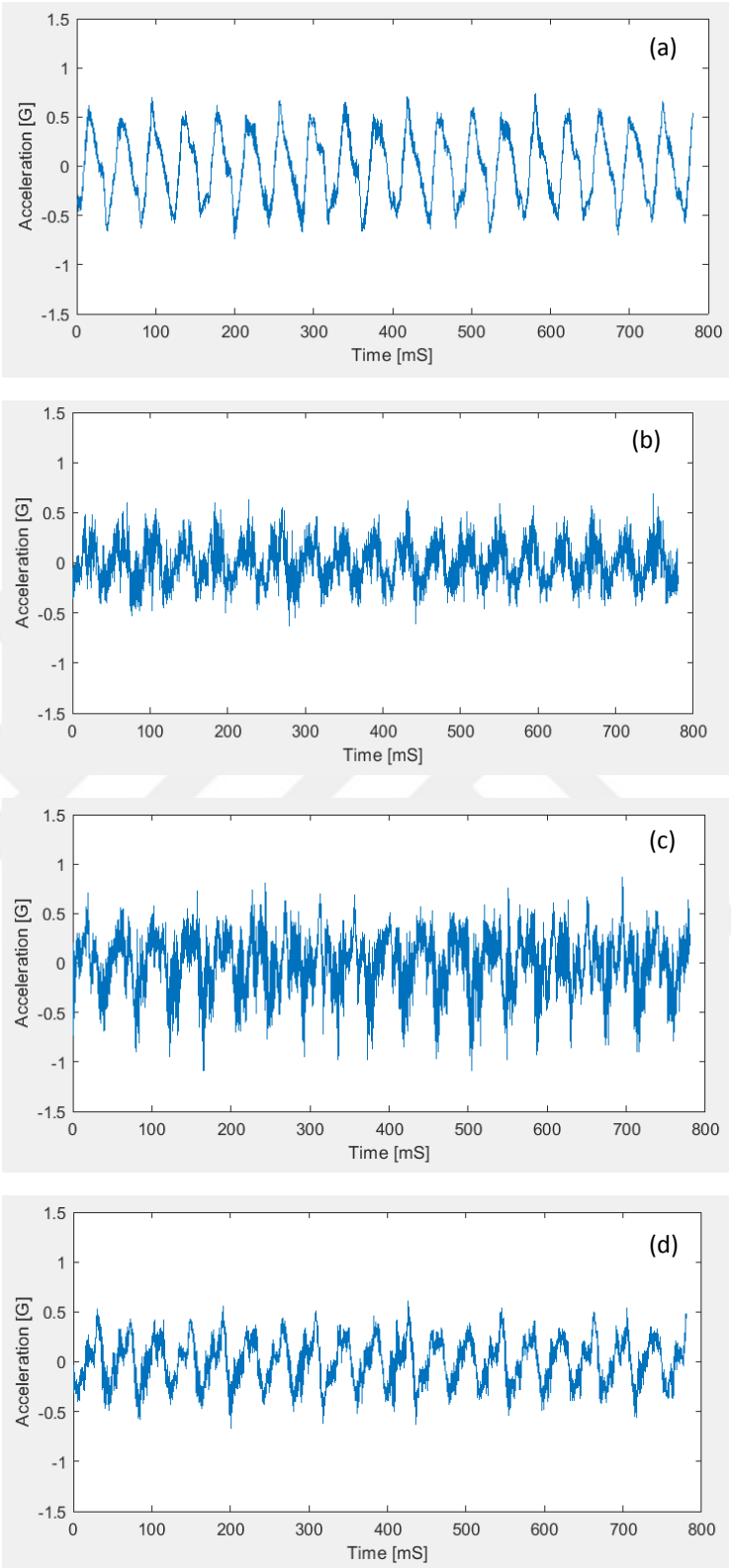

Figure 6.16 Time waveform for load-2 at point P2, 1500 RPM a) healthy bearing b) one defect bearing c) two defects bearing d) four defects bearing

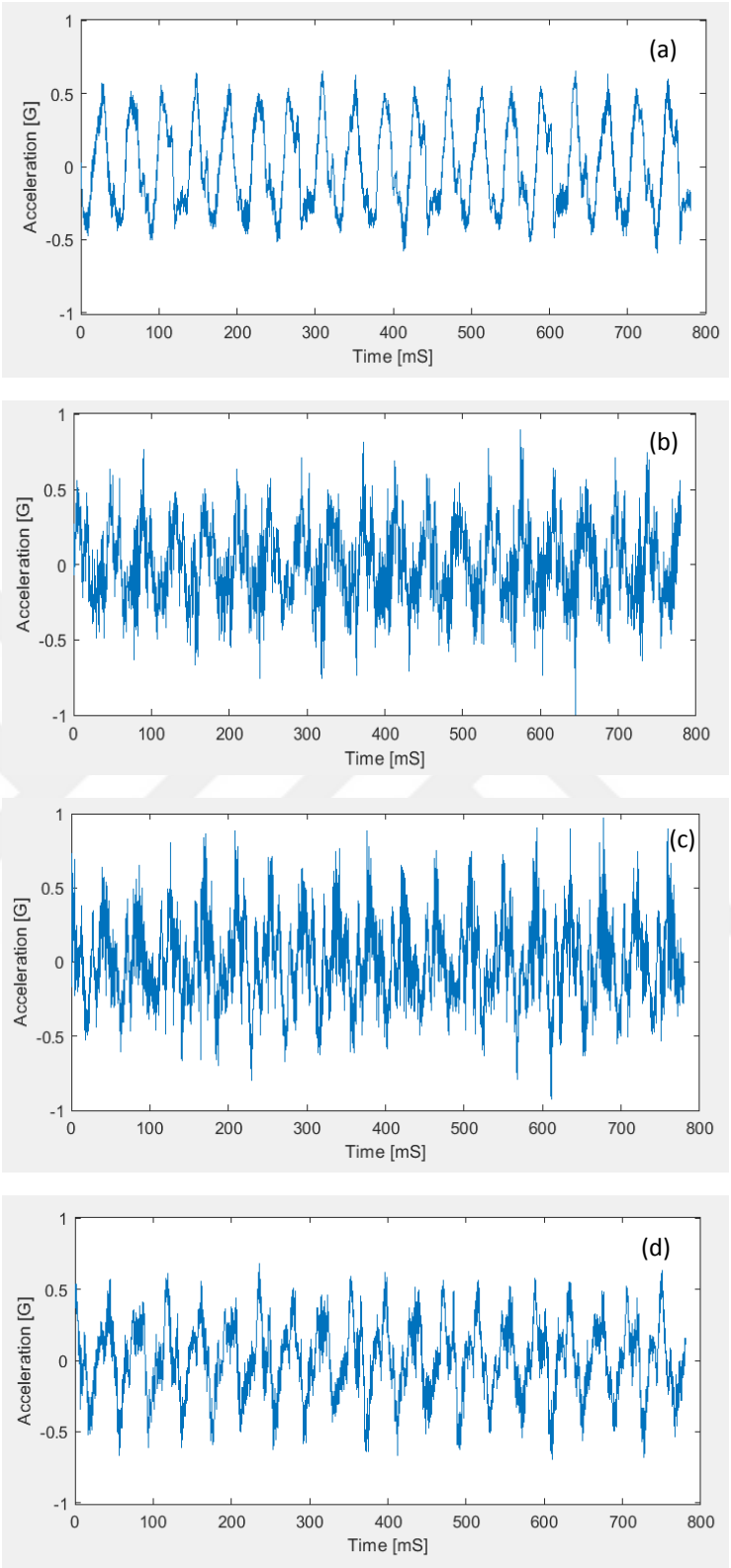

Figure 6.17 Time waveform for load-2 at point P3, 1500 RPM a) healthy bearing b) one defect bearing c) two defects bearing d) four defects bearing

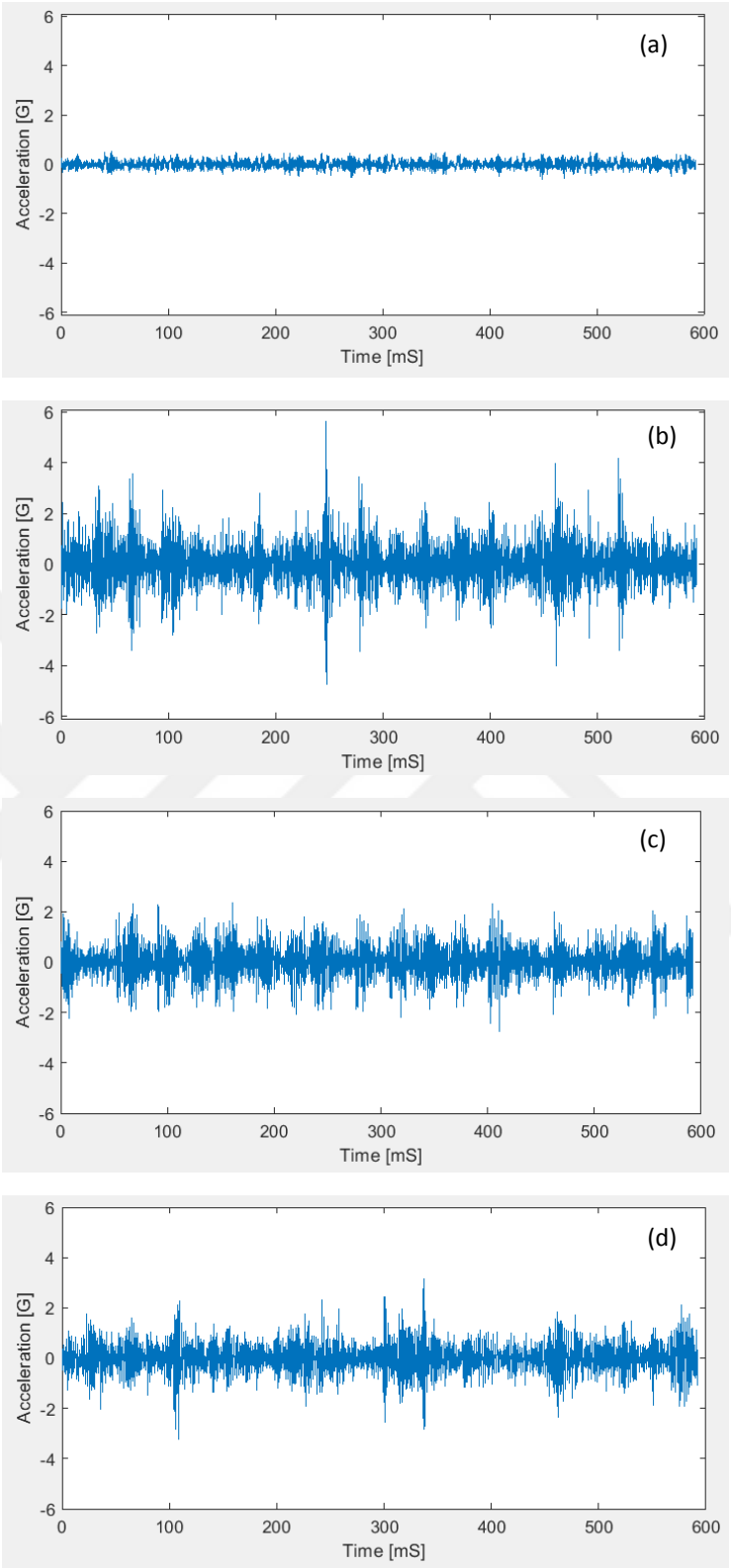

Figure 6.18 Time waveform for load-2 at point P1, 2000 RPM a) healthy bearing b) one defect bearing c) two defects bearing d) four defects bearing

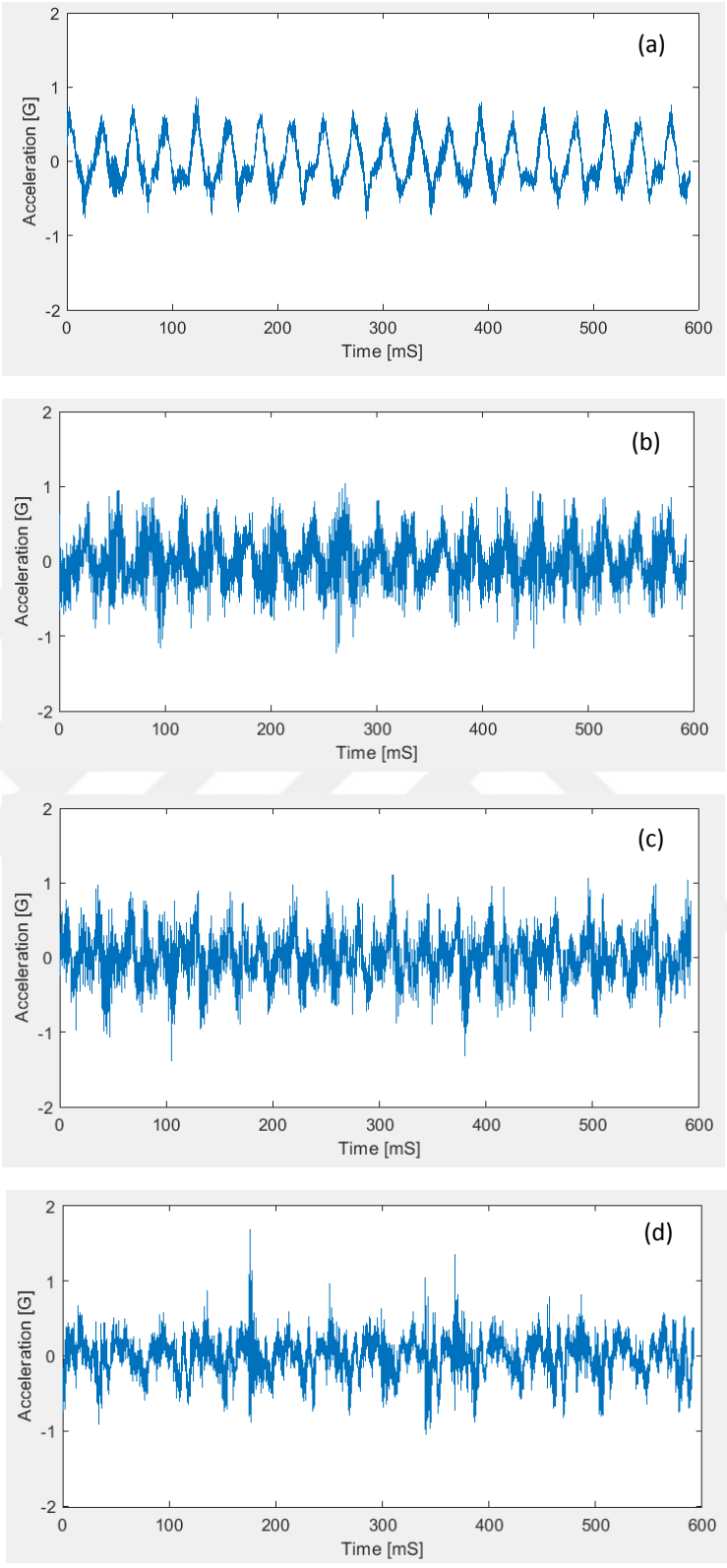

Figure 6.19 Time waveform for load-2 at point P2, 2000 RPM a) healthy bearing b) one defect bearing c) two defects bearing d) four defects bearing

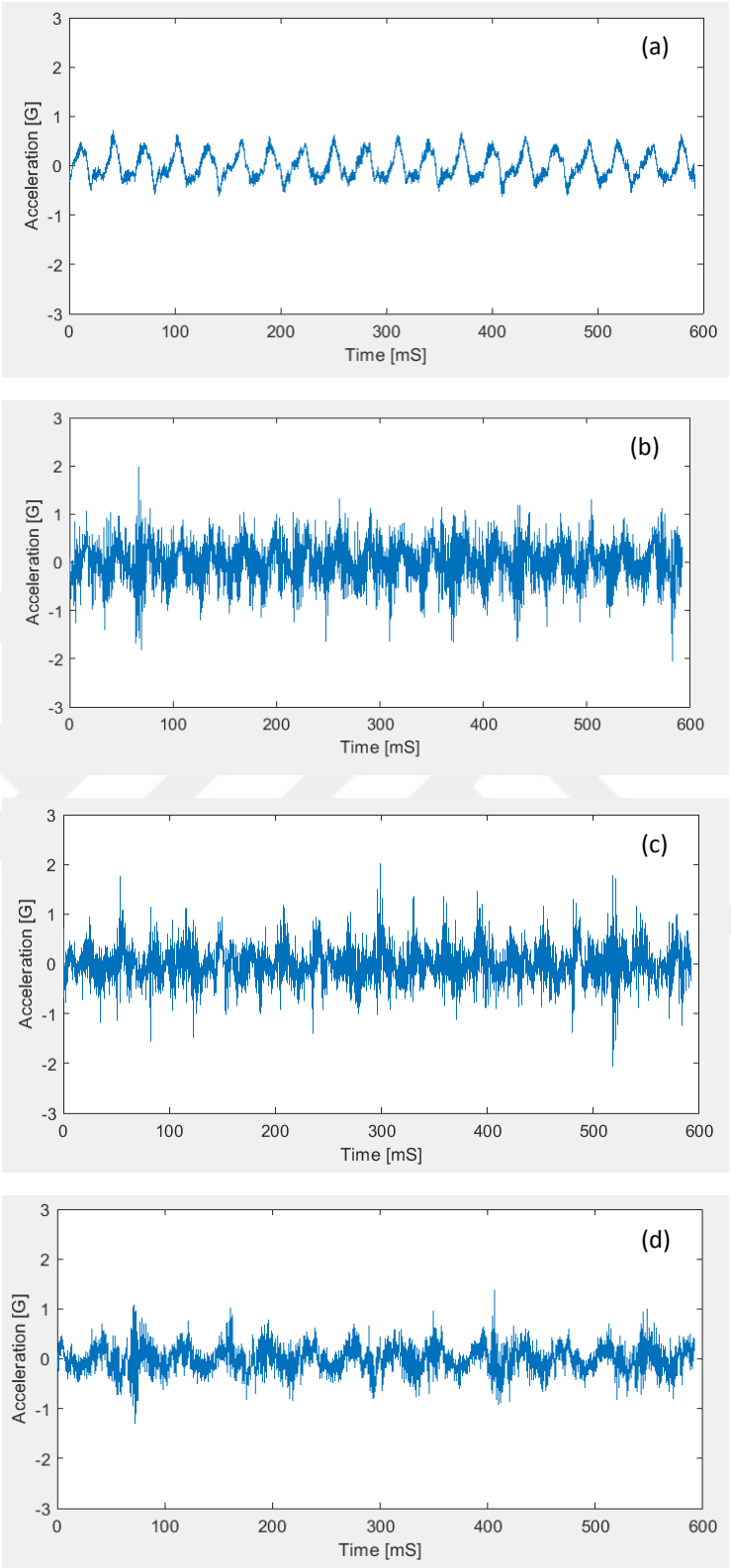

Figure 6.20 Time waveform for load-2 at point P3, 2000 RPM a) healthy bearing b) one defect bearing c) two defects bearing d) four defects bearing

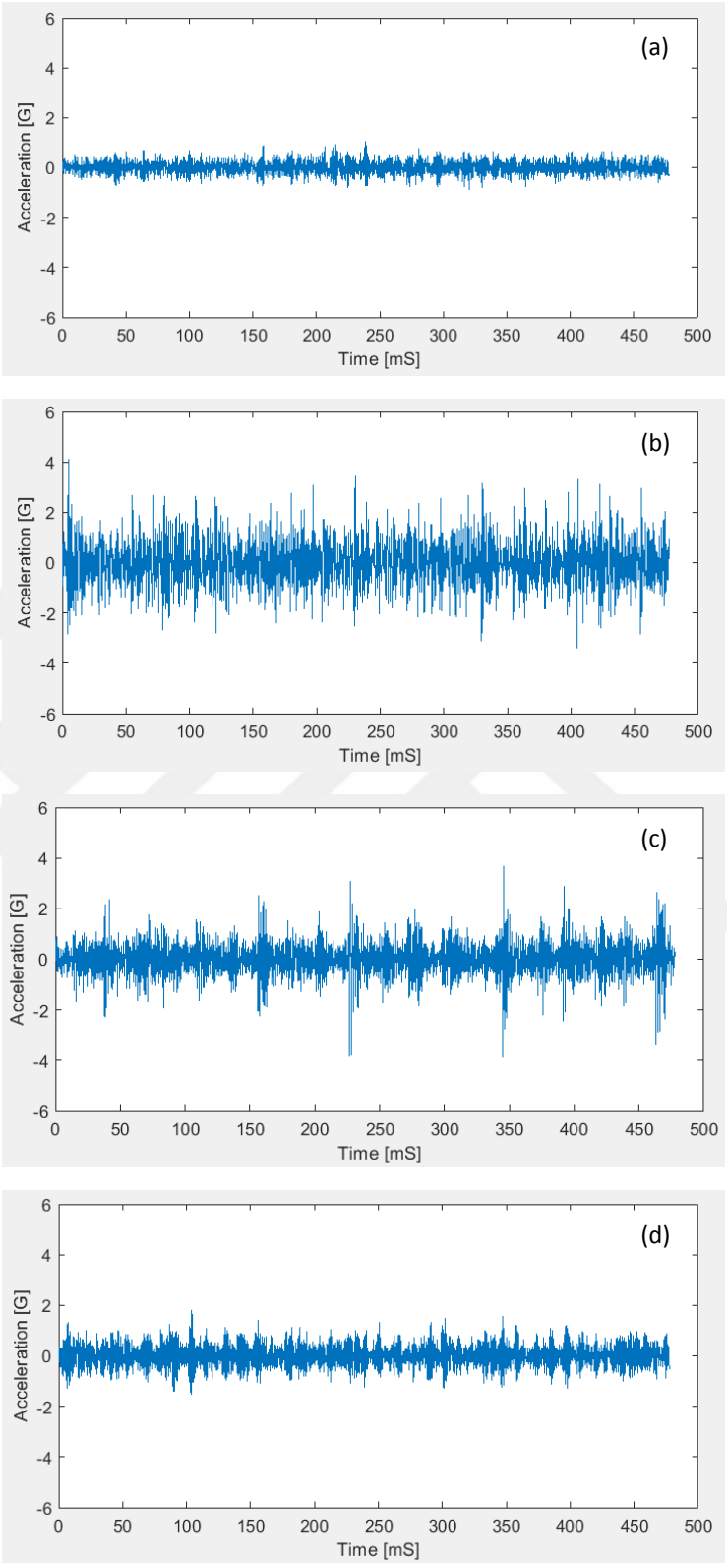

Figure 6.21 Time waveform for load-2 at point P1, 2500 RPM a) healthy bearing b) one defect bearing c) two defects bearing d) four defects bearing

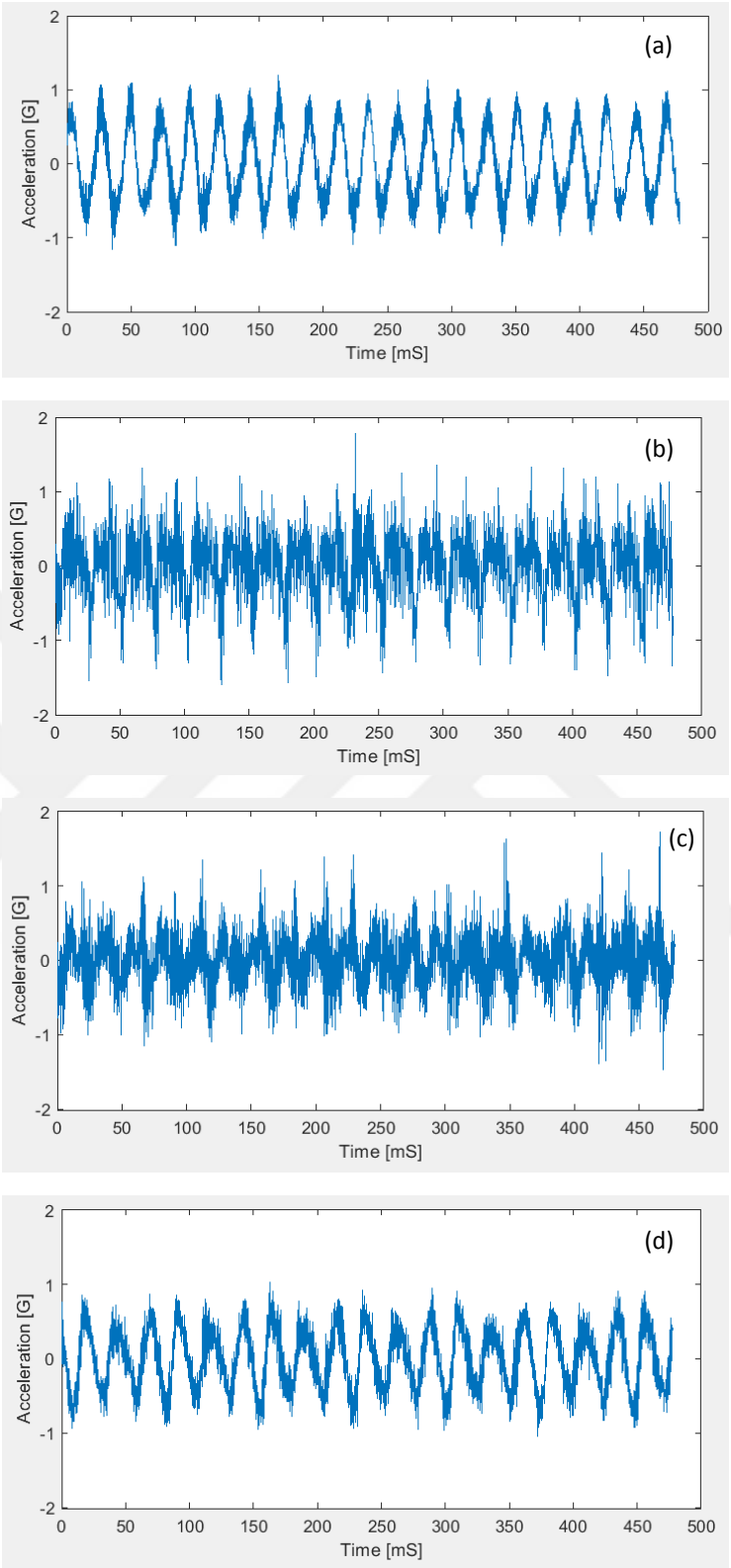

Figure 6.22 Time waveform for load-2 at point P2, 2500 RPM a) healthy bearing b) one defect bearing c) two defects bearing d) four defects bearing

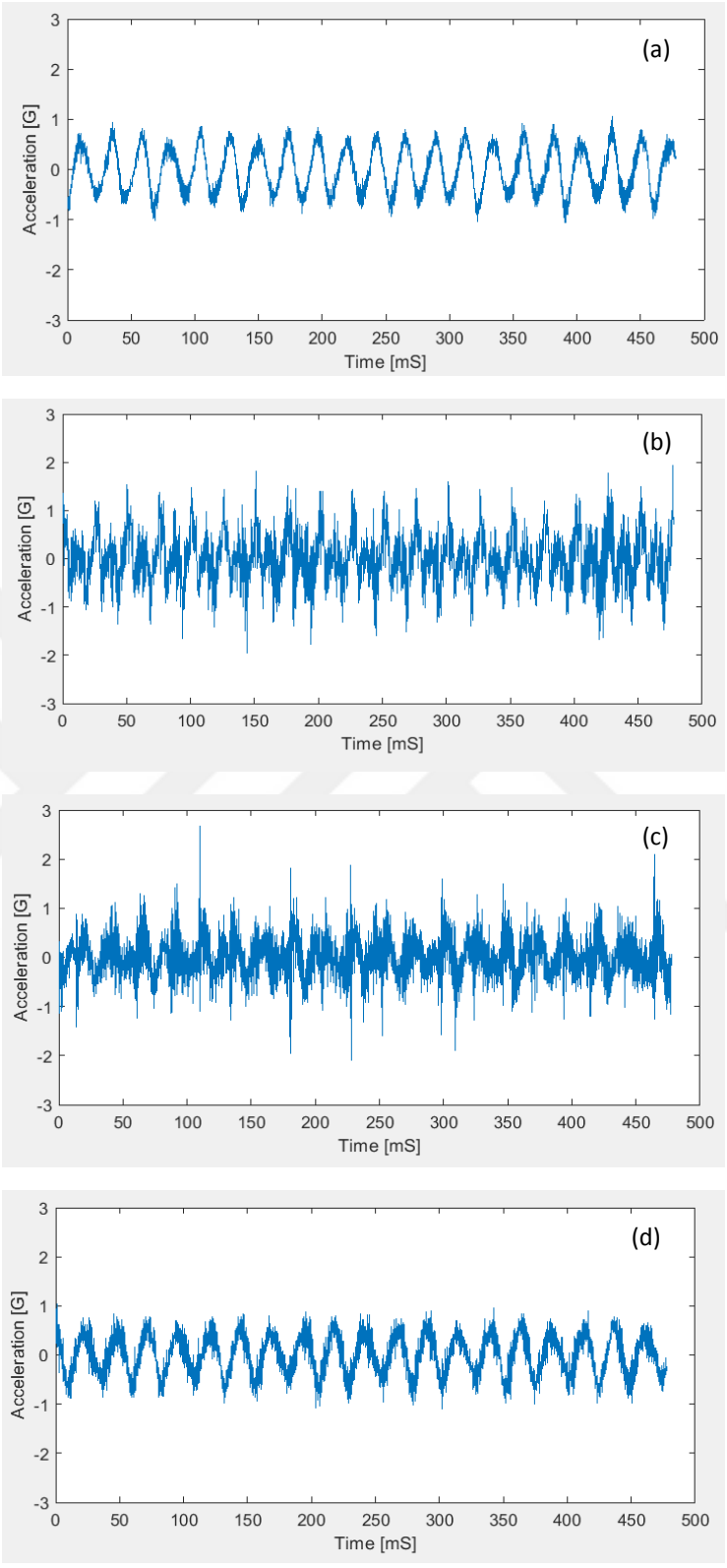

Figure 6.23 Time waveform for load-2 at point P3, 2500 RPM a) healthy bearing b) one defect bearing c) two defects bearing d) four defects bearing

6.2 Comparison of Raw Statistical Indicators

In this section, from the thrust bearing; defect analysis was performed for raw and filtered signals by utilizing peak to peak, RMS, crest factor and kurtosis, which were calculated for the vibration data obtained in healthy, single fault, two-faults and four-faults cases. The vibration data can be adjusted to the shaft axis for two separate load conditions between 500 and 2500 RPM; taken from axial (P1), horizontal (P2) and vertical (P3) points.

6.2.1 For Axial Measurement Point (P1)

In the case of load-1, the statistical parameters calculated from the vibration data taken from point P1 are shown in Figure 6.24 Peak to peak and RMS values are effective parameters for fault detection for all shaft speeds. However, generally, it can not be said that both parameters show an increase in value due to the increase in defect. The Crest factor value can be used to determine the defect regardless from the number of defect. It can be said that it easily shows defect at low RPM, especially at 500 RPM. But, at higher speeds, it can not be as successful as at low speeds. Kurtosis value is a suitable parameter that can be used for fault detection between 500 and 1000 RPM. However, as seen in the case of a single fault at 1500, 2000 and 2500 RPM, four-faults cases at 2500 RPM, it can not be used in error detection at high revolutions.

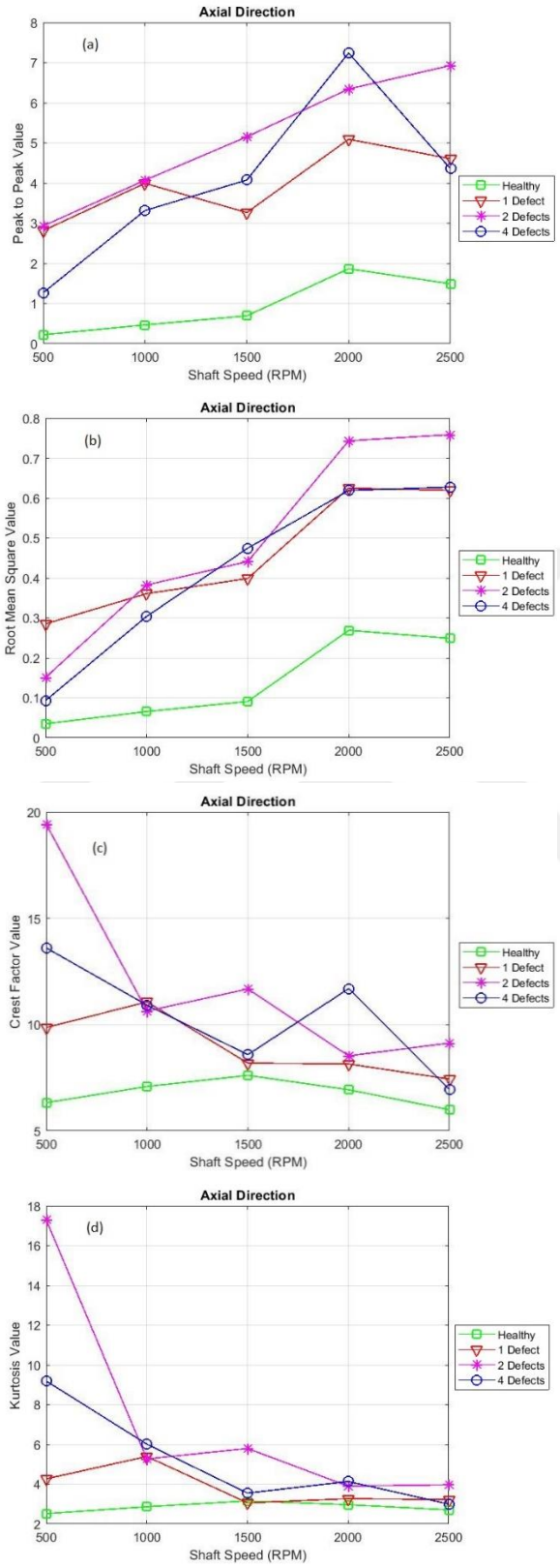

Figure 6.24 Statistical parameters for load-1 a) peak to peak b) RMS c) crest factor d) kurtosis

In the load-2 condition, the statistical parameters which are calculated from the vibration data taken from the structure in axial direction are shown in Figure 6.25. Peak to peak and RMS values as shown in Figure 6.25a and 6.25b are effective parameters in fault detection for all defect conditions and shaft speeds. However, due to the increase in the number of load, increase of values can not be mentioned. Crest and Kurtosis values can be used as fault indication at low speeds of 500 and 1000 RPM as in the case of load-1. Especially, crest and kurtosis values of single fault and four-faults bearings at 2500 RPM gave results close to healthy status conditions. Considering the results of Kurtosis and crest values in 1500, 2000 and 2500 RPM that belongs to defect conditions, it is seen that it does not give a clear result as 1000 and 1500 RPM values in general. It can be said that the load-2 situation gives similar results with the load-1 situation.

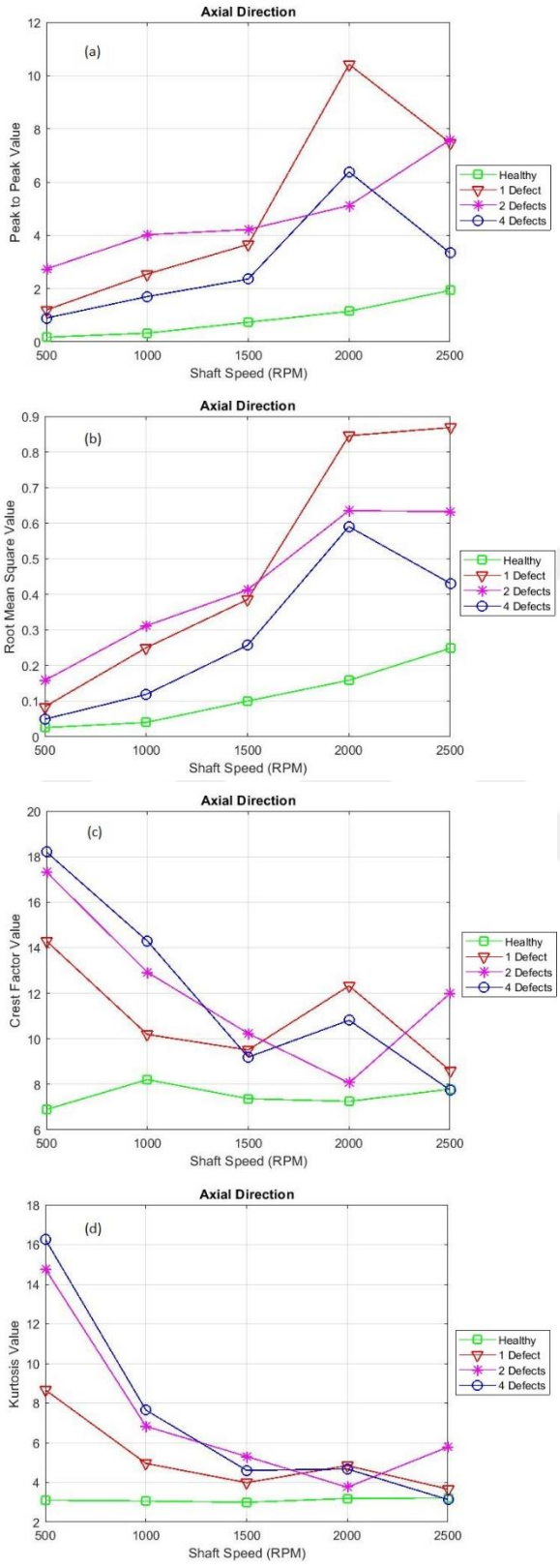

Figure 6.25 Statistical parameters for load-2 a) peak to peak b) RMS c) crest factor d) kurtosis

6.2.2 For Horizontal Measurement Point (P2)

In the condition of the load-1, the statistical parameters which are calculated from the vibration data taken from the structure at point P2 are shown in Figure 6.26. The peak to peak values of the defect bearings are higher than the values of the healthy bearing. However, it is not as high as the ratio between the peak to peak values of healthy and defect situations in axial measurements. It is observed that RMS does not give good results for defect detection. It can be seen that the crest factor value can be used for detection of defect situations at all revolutions. Crest factor and kurtosis values give very good results for single and four-faults bearings, especially at 500 RPM. However, in the measurements taken in the axial direction at the 500 RPM, the value of kurtosis for two-fault bearing is 17.31 while for same bearing at here is 5.88.

In the condition of the load-2, the statistical parameters which are calculated from the vibration data taken from the structure at point P2 are shown in Figure 6.27. In a general sense, the peak to peak value returned high in defect conditions. Nonetheless, it is seen that one and four defects bearing at 1500 RPM and four defects bearing at 2500 RPM returned higher values. In general terms, it is not appropriate for defect detection. A similar condition is valid for RMS value at 1000, 2000, and 2500 RPM. In fact, the RMS value of the healthy bearing at 2500 RPM returned a higher RMS value than that of the defect bearing. Crest factor and kurtosis values yield similar results at load-1 condition. Notwithstanding, when it is foreseen that values go up depending on the increase in the load amount, generally speaking it cannot be suggested that there is a significant increase in the values. Under load-2 condition, while the kurtosis value is 14.77 at the axial measurement point for four defects bearing at 500 RPM, the value at the horizontal measurement point is 4.01.

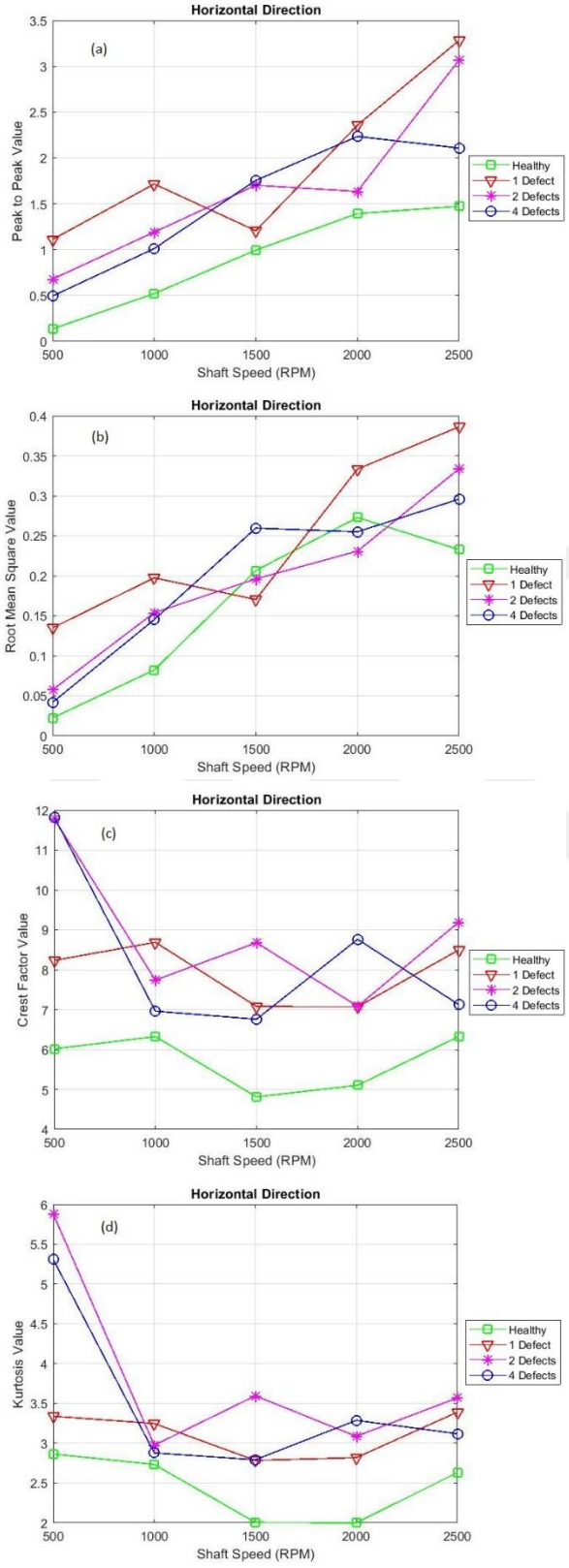

Figure 6.26 Statistical parameters for load-1 a) peak to peak b) RMS c) crest factor d) kurtosis

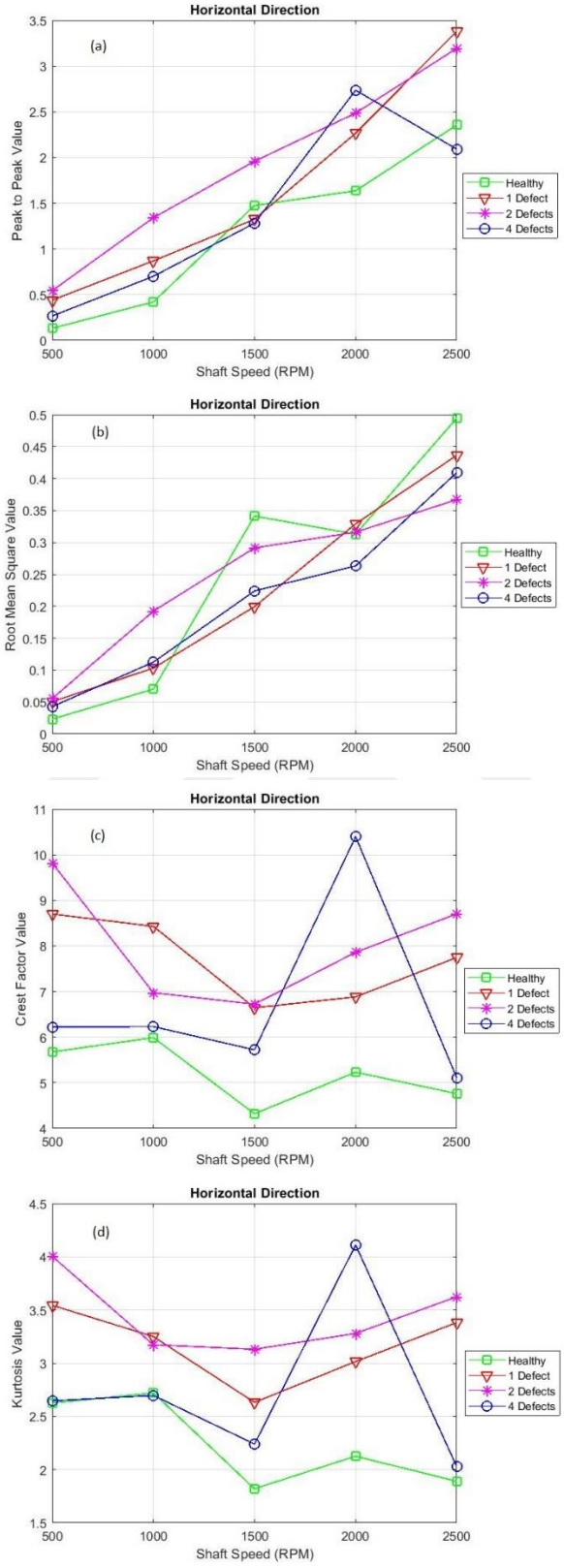

Figure 6.27 Statistical parameters for load-2 a) peak to peak b) RMS c) crest factor d) kurtosis

6.2.3 For Vertical Measurement Point (P3)

In the condition of the load-1, the statistical parameters which are calculated from the vibration data taken from the structure at point P3 are shown in Figure 6.28. The peak to peak value is almost identical for healthy and defect bearings at 1500 RPM. For other rotational speeds, although the values of the defect bearings are higher, the defect rate is lower than the axial measurements as in the horizontal measurements. RMS value is not seen as a suitable parameter for defect detection as in horizontal measurements. Crest factor value can be used for defect detection. Kurtosis values are seen similar to kurtosis values in horizontal measurement results. In addition, at 2000 RPM, it can be said that the kurtosis value of two faults is relatively high.

In the condition of the load-2, the statistical parameters which are calculated from the vibration data taken from the structure at point P3 are shown in Figure 6.29. Generally speaking, peak to peak value is higher for defects bearings. However, it cannot be suggested that this shows the existence of a defect in general. The RMS values – just as in the load-1 condition – do not seem to be an appropriate parameter for defect detection. The crest factor and kurtosis values of the defects bearings at all revolutions except for the 1000 RPM result higher values than healthy bearings. Usually, crest factor and kurtosis return higher values under faulty conditions. Nevertheless, as in the horizontal measurements, while it was foreseen that values can go up depending on the load amount increase, it cannot be suggested that there is a significant increase in these values in a general sense.

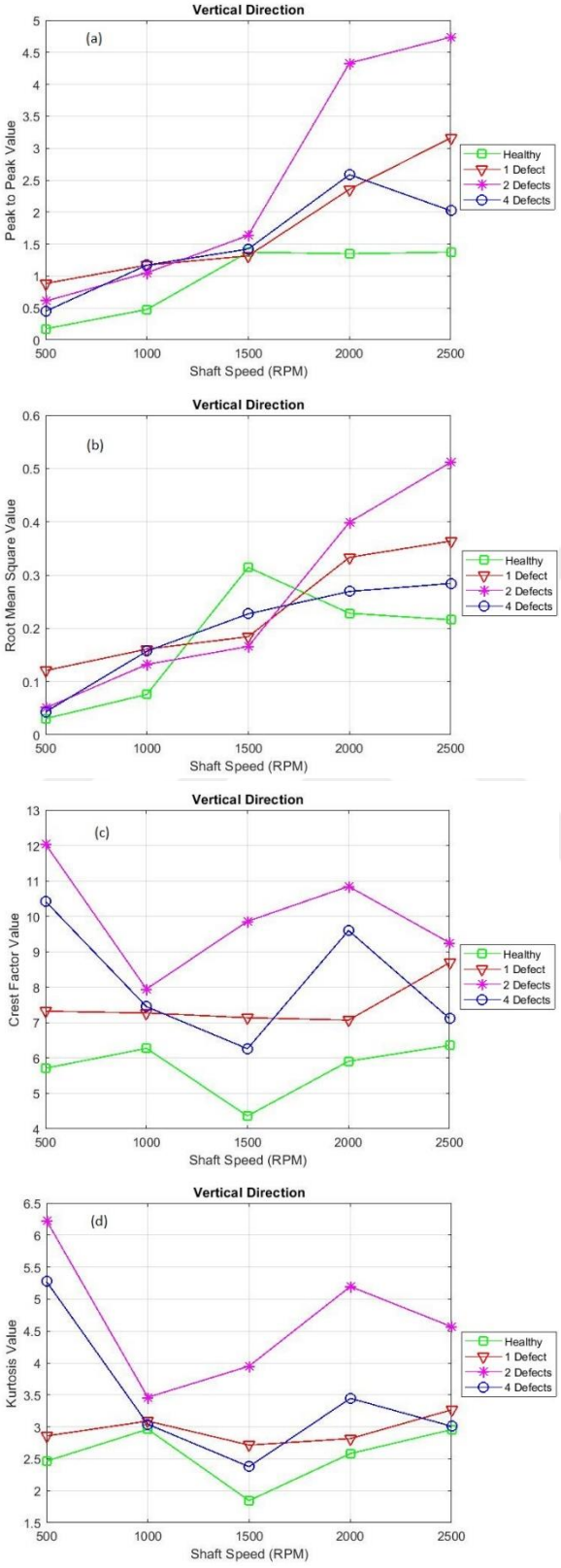

Figure 6.28 Statistical parameters for load-1 a) peak to peak b) RMS c) crest factor d) kurtosis

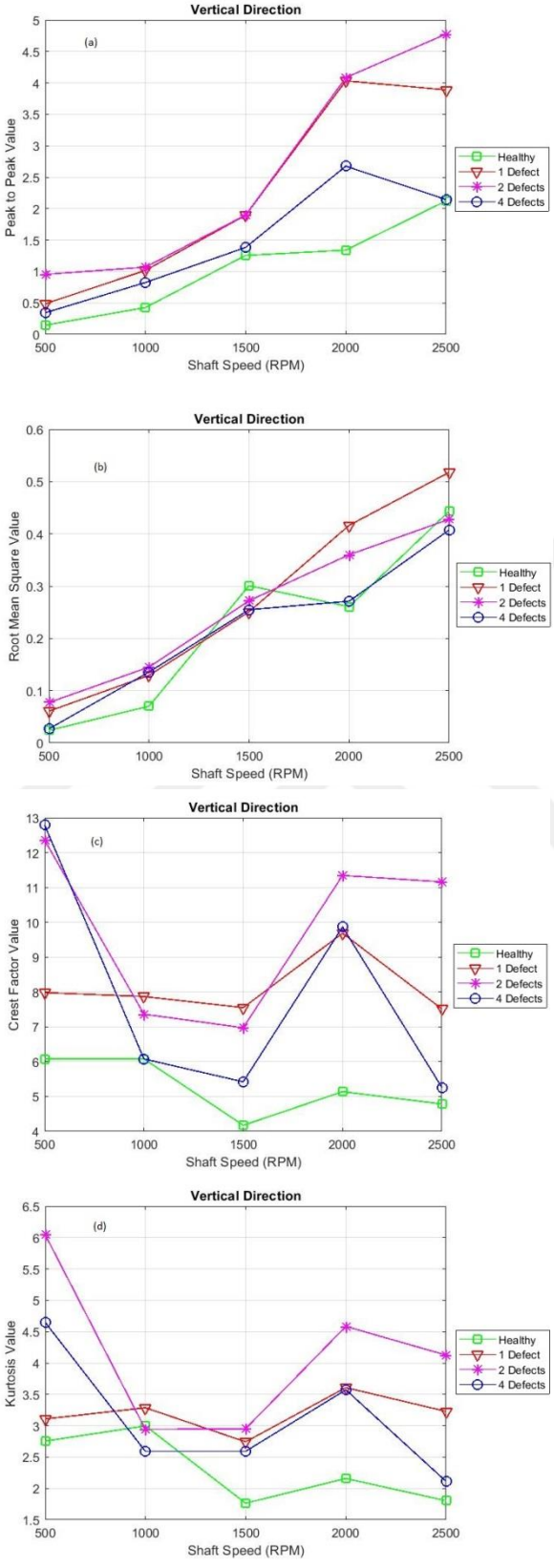

Figure 6.29 Statistical parameters for load-2 a) peak to peak b) RMS c) crest factor d) kurtosis

6.3 Filtering of Vibration Signals

As mentioned in the Section 6.1, defect detection can be performed by using time-domain statistical parameters. However, there may be improprieties such as unbalance, misalignment and looseness in addition to bearing damage in the system. The values which are obtained through the method used do not show the source of the damage while showing the damaged condition in the system.

Vibration signals lose their spiky properties due to reduced impact time at high speeds and therefore override time domain parameters. The difficulty of detecting the fault at high speeds can be overcome by filtering the vibration signal in some frequency bands (Kıral & Karagülle, 2003). In Table 6.1, the load-1 and in Table 6.2, the load-2, 2500 RPM, filtered vibration signals for the points of P1, P2 and P3, their raw states and change percentages are given. Vibration signals were filtered using Butterworth filter from the fourth order in the MATLAB program and increasing by 250 Hz in the range 0-2000 Hz.

It is seen that filtering the peak to peak and RMS values at axial measurement points yields good results for defect detection. Still, the same cannot be suggested for crest factor and kurtosis. It is seen that the filtering that is carried out following the load amount increase for one defect and two defects bearings returns better results. It is observed that filtering under load-1 condition at horizontal measurement point returns negative results. Under load-2 condition, it seen that filtering with peak to peak and RMS values return positive results. Except for some exceptions, filtering in both load conditions at vertical measurement point did not yield positive results.

Table 6.1 Raw and filtered statistical parameters for load-1 at the speed 2500 RPM a) P1 b) P2 c) P3

(a)				
Statistical Parameter	**Ratio**	**Raw**	**Filtered (Mean)**	**Change (%)**
Peak to Peak Value	1 defected/healthy	3.09	3.67	18.94
	2 defected/healthy	4.64	5.51	18.55
	4 defected/healthy	2.92	3.58	22.59
Root Mean Square Value (RMS)	1 defected/healthy	2.49	3.59	44.11
	2 defected/healthy	3.05	4.32	41.89
	4 defected/healthy	2.52	3.30	30.86
Crest Factor Value	1 defected/healthy	1.24	0.97	-21.98
	2 defected/healthy	1.52	1.18	-22.35
	4 defected/healthy	1.16	1.13	-2.19
Kurtosis Value	1 defected/healthy	1.19	0.99	-17.04
	2 defected/healthy	1.47	1.30	-11.07
	4 defected/healthy	1.11	1.26	13.37

(b)				
Statistical Parameter	**Ratio**	**Raw**	**Filtered (Mean)**	**Change (%)**
Peak to Peak Value	1 defected/healthy	2.23	1.52	-31.58
	2 defected/healthy	2.08	1.91	-8.52
	4 defected/healthy	1.43	1.44	0.39
Root Mean Square Value (RMS)	1 defected/healthy	1.66	1.09	-34.19
	2 defected/healthy	1.43	1.56	9.14
	4 defected/healthy	1.27	1.20	-5.47
Crest Factor Value	1 defected/healthy	1.34	1.11	-17.54
	2 defected/healthy	1.45	1.06	-27.21
	4 defected/healthy	1.14	1.12	0.75
Kurtosis Value	1 defected/healthy	1.29	1.20	-6.59
	2 defected/healthy	1.36	1.14	-16.34
	4 defected/healthy	1.19	1.24	4.36

(c)				
Statistical Parameter	**Ratio**	**Raw**	**Filtered (Mean)**	**Change (%)**
Peak to Peak Value	1 defected/healthy	2.3	1.79	-22.34
	2 defected/healthy	3.45	1.88	-45.57
	4 defected/healthy	1.47	1.42	-3.65
Root Mean Square Value (RMS)	1 defected/healthy	1.68	1.44	-14.50
	2 defected/healthy	2.37	1.36	-42.76
	4 defected/healthy	1.32	1.11	-15.39
Crest Factor Value	1 defected/healthy	1.37	1.11	-18.66
	2 defected/healthy	1.46	1.22	-16.18
	4 defected/healthy	1.12	1.23	9.96
Kurtosis Value	1 defected/healthy	1.10	1.13	2.69
	2 defected/healthy	1.54	1.27	-18.07
	4 defected/healthy	1.02	1.26	23.86

Table 6.2 Raw and filtered statistical parameters for load-2 at the speed 2500 RPM a) P1 b) P2 c) P3

(a)				
Statistical Parameter	**Ratio**	**Raw**	**Filtered (Mean)**	**Change (%)**
Peak to Peak Value	1 defected/healthy	3.87	7.71	99.56
	2 defected/healthy	3.92	6.58	67.86
	4 defected/healthy	1.73	1.36	-21.06
Root Mean Square Value (RMS)	1 defected/healthy	3.50	6.57	88.02
	2 defected/healthy	2.55	3.78	48.41
	4 defected/healthy	1.73	1.28	-26.27
Crest Factor Value	1 defected/healthy	1.11	1.14	2.93
	2 defected/healthy	1.54	1.52	-1.00
	4 defected/healthy	1.00	1.08	8.35
Kurtosis Value	1 defected/healthy	1.14	1.17	2.90
	2 defected/healthy	1.80	1.93	6.96
	4 defected/healthy	0.97	1.12	14.57

(b)				
Statistical Parameter	**Ratio**	**Raw**	**Filtered (Mean)**	**Change (%)**
Peak to Peak Value	1 defected/healthy	1.44	1.67	16.52
	2 defected/healthy	1.36	1.57	15.64
	4 defected/healthy	0.89	0.93	4.31
Root Mean Square Value (RMS)	1 defected/healthy	0.88	1.21	37.06
	2 defected/healthy	0.74	0.91	22.80
	4 defected/healthy	0.83	0.84	1.23
Crest Factor Value	1 defected/healthy	1.63	0.91	-44.33
	2 defected/healthy	1.83	1.13	-38.20
	4 defected/healthy	1.07	0.97	-9.91
Kurtosis Value	1 defected/healthy	1.79	0.97	-45.71
	2 defected/healthy	1.92	1.48	-22.80
	4 defected/healthy	1.07	0.90	-16.33

(b)				
Statistical Parameter	**Ratio**	**Raw**	**Filtered (Mean)**	**Change (%)**
Peak to Peak Value	1 defected/healthy	1.44	1.67	16.52
	2 defected/healthy	1.36	1.57	15.64
	4 defected/healthy	0.89	0.93	4.31
Root Mean Square Value (RMS)	1 defected/healthy	0.88	1.21	37.06
	2 defected/healthy	0.74	0.91	22.80
	4 defected/healthy	0.83	0.84	1.23
Crest Factor Value	1 defected/healthy	1.63	0.91	-44.33
	2 defected/healthy	1.83	1.13	-38.20
	4 defected/healthy	1.07	0.97	-9.91
Kurtosis Value	1 defected/healthy	1.79	0.97	-45.71
	2 defected/healthy	1.92	1.48	-22.80
	4 defected/healthy	1.07	0.90	-16.33

6.4 Frequency Spectrum Analysis

Another vibration analysis method is frequency spectrum analysis. The main indication for bearing defects is bearing characteristic frequencies. The presence of one of the defect frequencies in the direct or processed frequency spectrum is the strong sign of damage (Kıral and Karagülle, 2003).

6.4.1 Bearing Characteristic Frequencies

Bearings, rings and rolling elements have surface roughness even in very small amounts. For this reason, healthy bearings also produce defect frequencies. The equations of bearing characteristic frequencies are shown below.

$$\text{Fundamental Train (case) Frequency} = \text{FTF} = \frac{S}{2} \times \left(1 - \frac{Bd}{Pd} \times \cos\phi\right) \tag{6.1}$$

$$\text{Ball Pass Frequency of the Inner Race} = \text{BPFI} = \frac{Nb}{2} \times Sx \left(1 + \frac{Bd}{Pd} \times \cos\phi\right) \tag{6.2}$$

$$\text{Ball Pass Frequency of the Outer Race} = \text{BPFO} = \frac{Nb}{2} \times Sx \left(1 - \frac{Bd}{Pd} \times \cos\phi\right) \tag{6.3}$$

$$\text{Ball Spin Frequency} = \text{BSF} = \frac{Pd}{2Bd} \times Sx\left[\left(1 - \left(\frac{Bd}{Pd}\right)^2 \times (\cos\phi)^2\right]\right. \tag{6.4}$$

The sembols used in above equations are

S: Shaft speed
B_d: Ball or roller diameter
P_d: Pitch diameter
N_b: Number of balls or rollers
θ: Contact angle

The geometry of the thrust ball bearing type 51113 used in the test rig is given in Section 5.1. Ball pass frequency of the outer race (housing washer) of 51113 for different shaft speeds are given Table 6.3.

Table 6.3 Characteristic defect frequencies and harmonics of 51113 thrust ball bearing

Shaft speed (Hz)	1xBPFO (Hz)	2xBPFO (Hz)	3xBPFO (Hz)	4xBPFO (Hz)	5xBPFO (Hz)
7.747	85.22	170.44	255.66	340.88	426.1
24.93	274.23	548.46	822.69	1096.92	1371.15
16.90	185.90	371.80	557.70	743.60	929.50
17.06	187.66	375.32	562.98	750.64	938.30
16.05	176.55	353.10	529.65	706.20	882.75
32.83	361.13	722.26	1083.39	1444.52	
42.78	470.58	941.16	1411.74		

6.4.2 The Fast Fourier Transform

The frequency spectrums are obtained using Fast Fourier Transform (FFT). In this study, the frequency spectrums were obtained using the MATLAB program. Fourier transformation is calculated for a discrete time signal with the equation below.

$$x(k) = \sum_{n=0}^{N-1} x(n) e^{-jn\omega_k} \quad (k = 0,1, \dots, N-1) \tag{6.5}$$

6.4.3 Analysis of Experimental Frequency Spectrum Graphs

In this section, bearing defect frequencies for healthy and faulty bearings were compared by providing frequency spectrums. Samples were presented so that the effects of load and speed variables in the system can be seen. The spectrum graphics were provided separately for axial (P1), horizontal (P2), and vertical (P3) measurement points. The experimental characteristic fault frequencies and harmonics that were obtained for the housing washer yielded similar results with the theoretical calculations. The rotational speeds, the ball pass frequency of the outer race (BPFO), and the harmonics were marked in the graphics.

Under load-2 condition, the frequency spectrum graphics of healthy and one defect bearings at P1, P2, and P3 measurement points for 7.75 Hz are given in Figure 6.30, Figure 6.31, and Figure 6.32, respectively. In Figure 6.30, the amplitude of BPFO and its harmonics for a one defect bearing seems to be more than that of the healthy bearing. It can be used for bearing defect detection. In Figures 6.31 and 6.32, the amplitude of BPFO and its harmonics for a one defect bearing seems to be more than that of the healthy bearing. It is seen that the amplitudes of BPFO and its harmonics at P1 measurement point are higher than those of P2 and P3 measure points.

Under load-2 condition, the frequency spectrum graphics of healthy and one defect bearings at P1, P2, and P3 measurement points for 24.93 Hz are given in Figure 6.33, Figure 6.34, and Figure 6.35, respectively. In all graphics, the amplitudes of BPFO and its harmonics for a one defect bearing returned higher than those of healthy bearings. The bearing failure shows it itself in all graphics. However, the amplitude value obtained at P1 point is more than others. The revolution frequencies (1XRPM) at the P2 and P3 (Figures 6.34a and 6.35a) measuring points for healthy bearings shows the imbalance in the system. These frequencies are also available (Figures 6.34b and 6.35b) in the graphics for one defect bearings. Still, revolution frequencies (1XRPM) are lower than those for healthy bearings. It can be concluded that the created bearing failure caused this condition.

If Figure 6.30 and Figure 6.33 need to be compared, the only variable in the system is speed. It can be uttered that amplitudes of BPFO and its harmonics increase thanks to the effect of the speed. Again, thanks to the effect of the speed, it can be said that the imbalance in the system at P2 and P3 points becomes more visible.

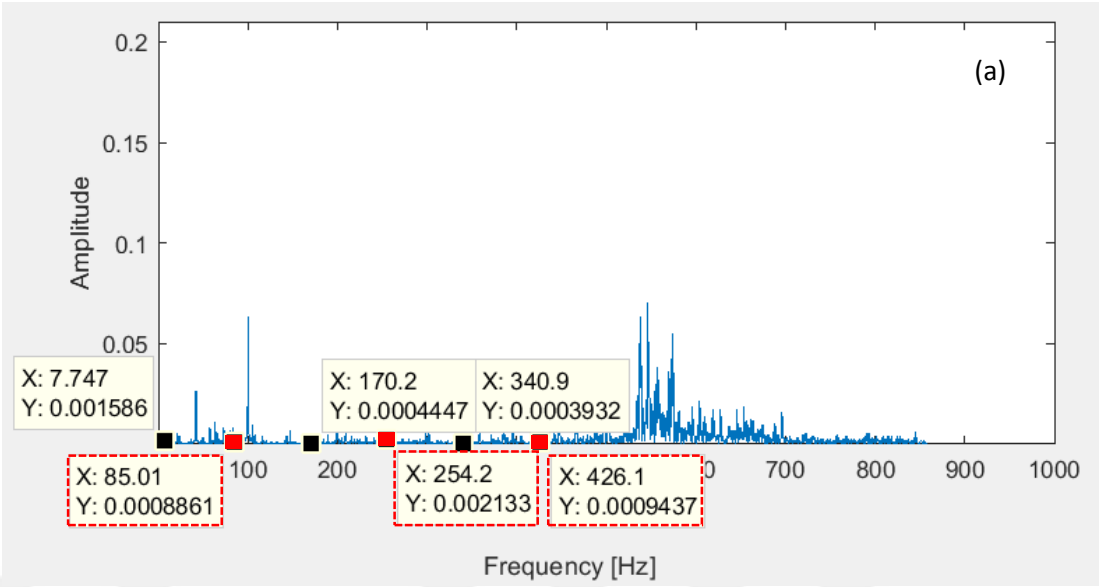

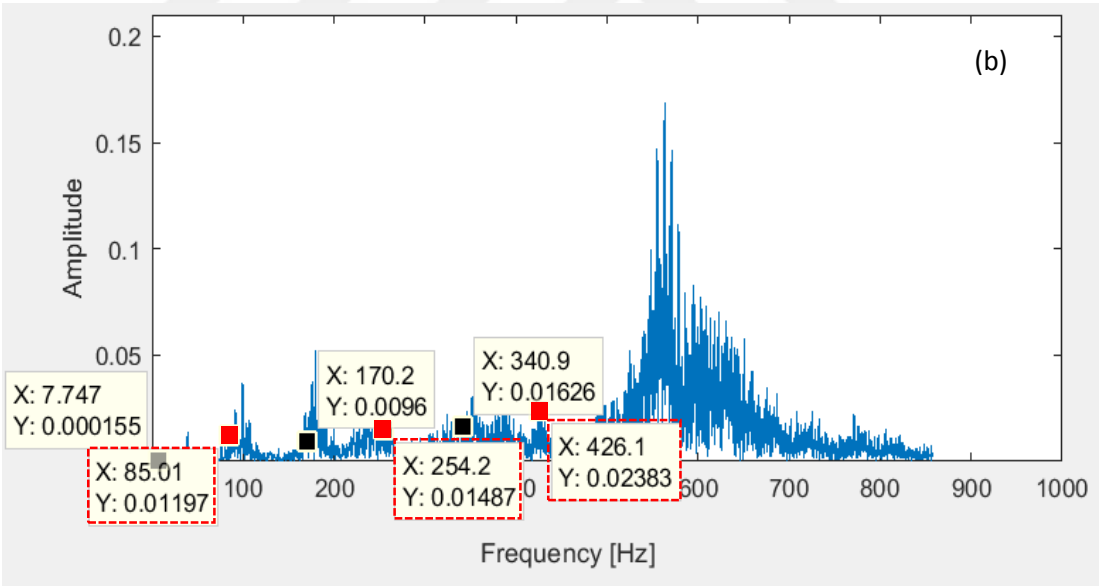

Figure 6.30 Load-2 case, at P1 point, 7.75 Hz a) healthy bearing b) one defect bearing

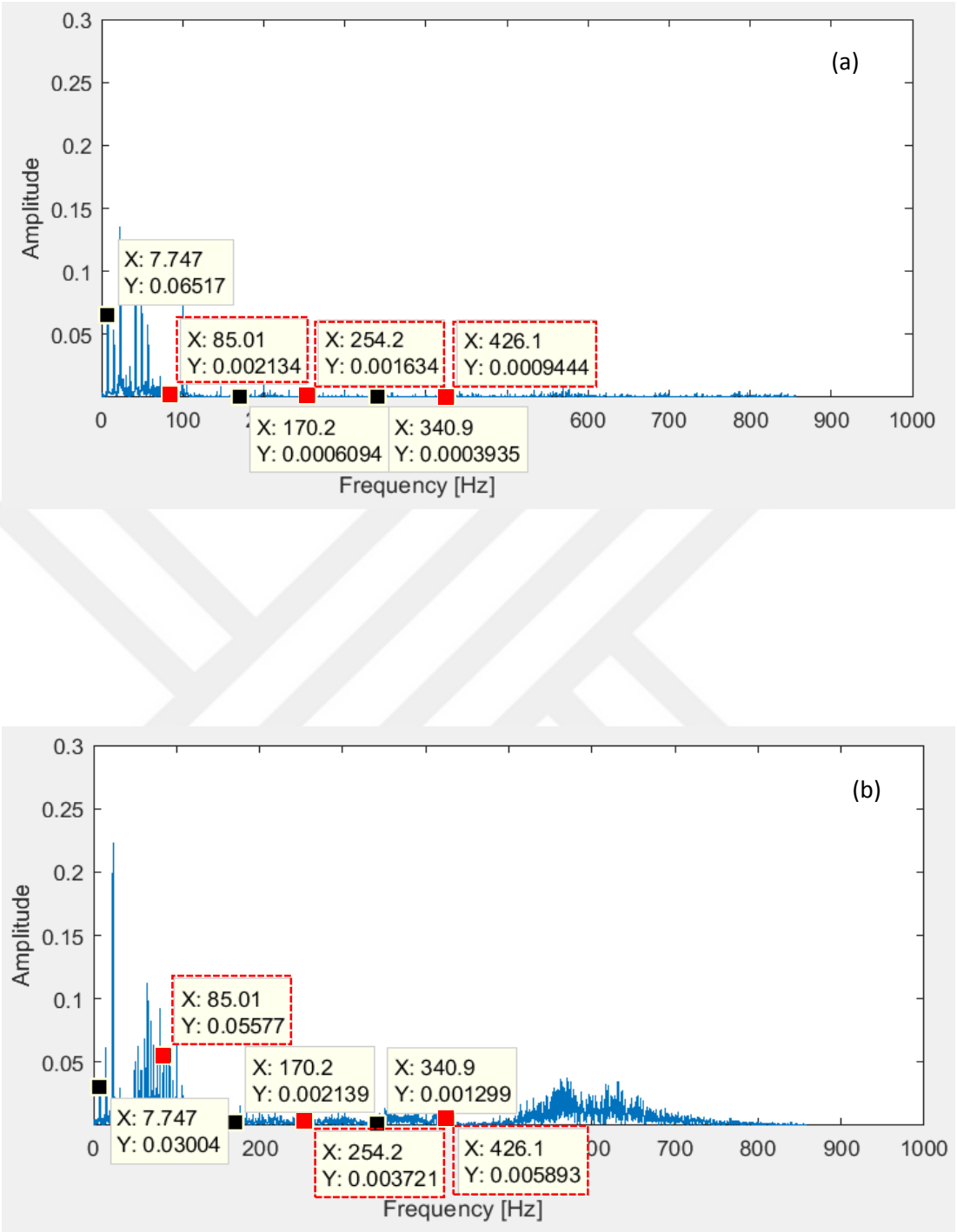

Figure 6.31 Load-2 case, at P2 point, 7.75 Hz a) healthy bearing b) one defect bearing

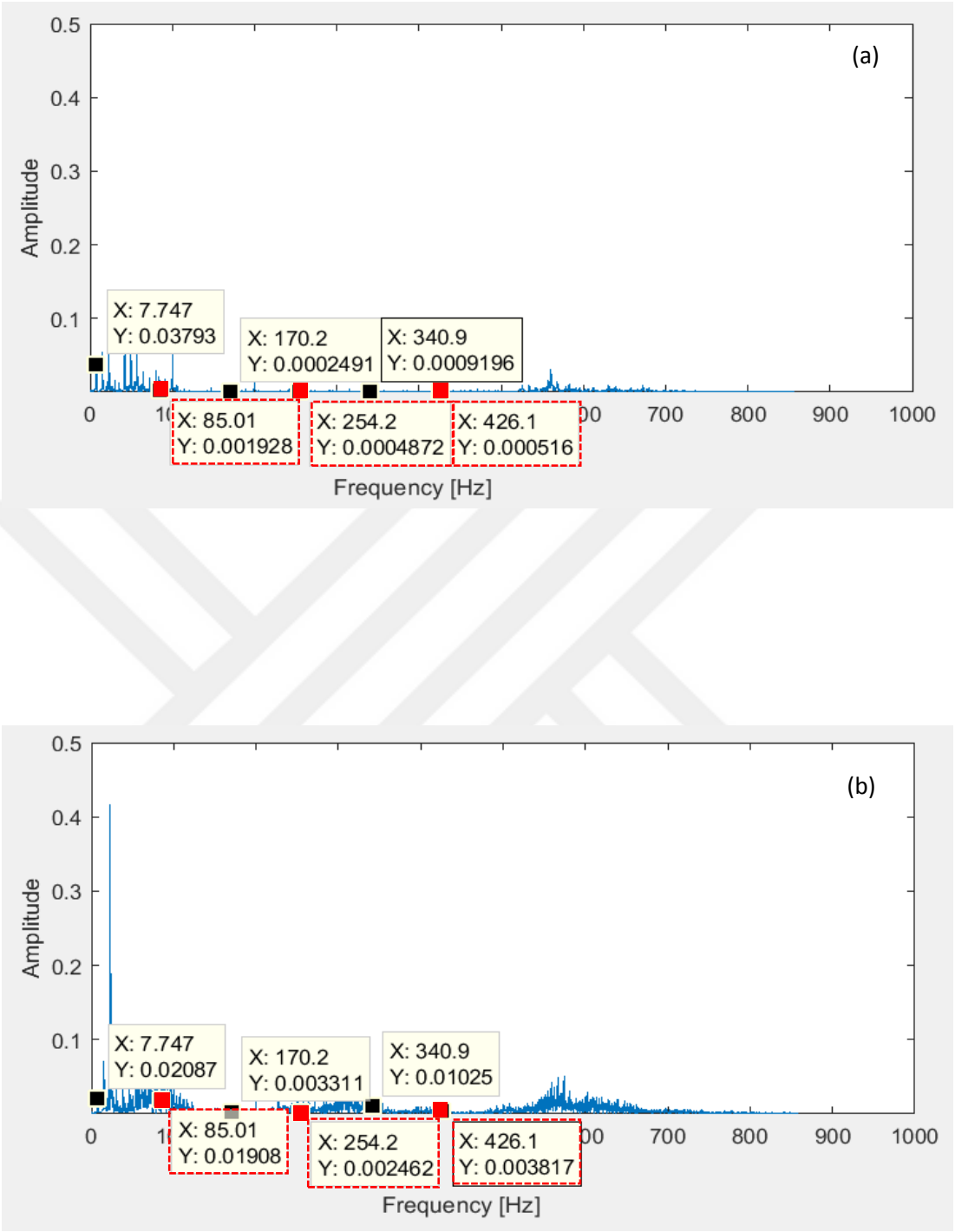

Figure 6.32 Load-2 case, at P3 point, 7.75 Hz a) healthy bearing b) one defect bearing

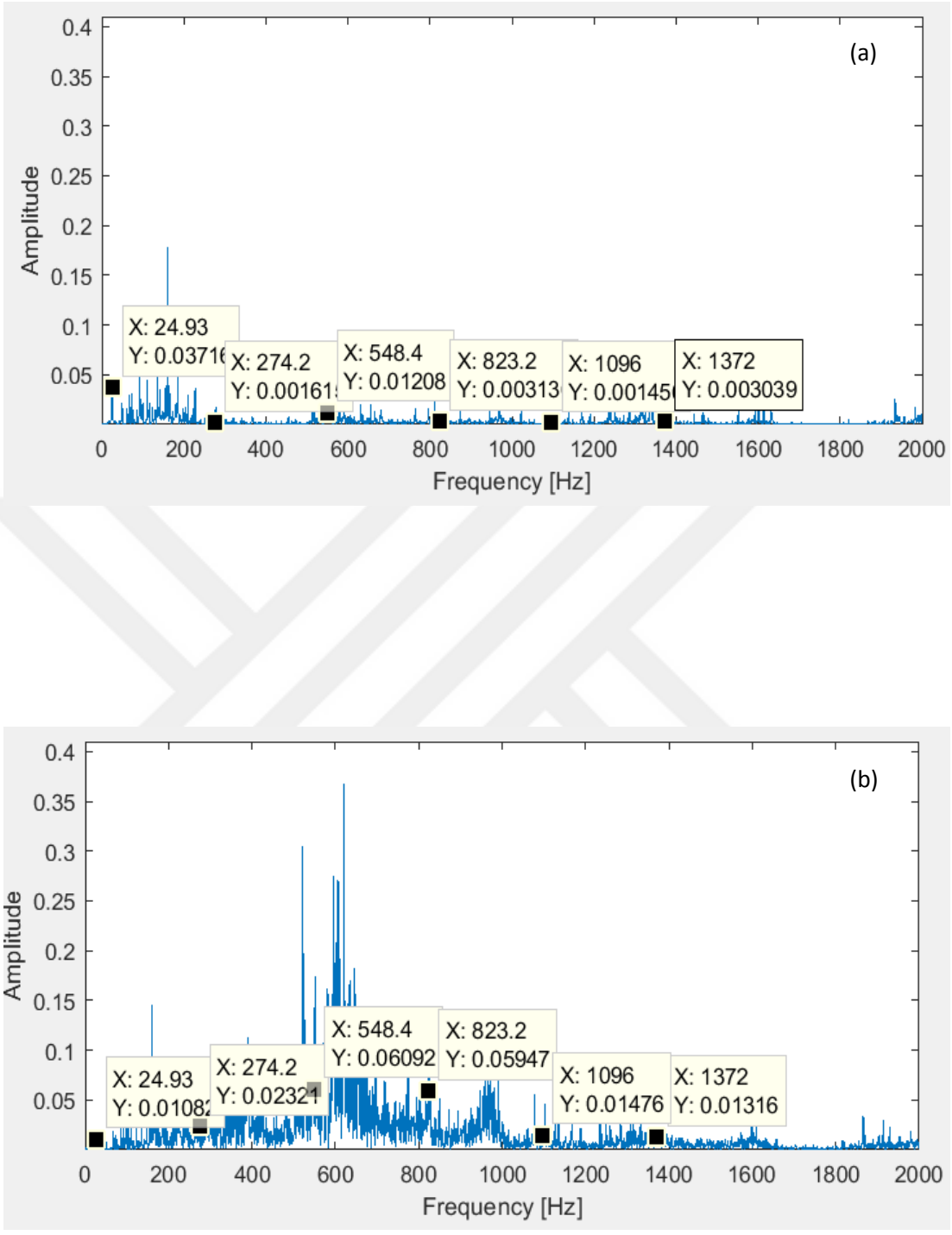

Figure 6.33 Load-2 case, at P1 point, 24.93 Hz a) healthy bearing b) one defect bearing

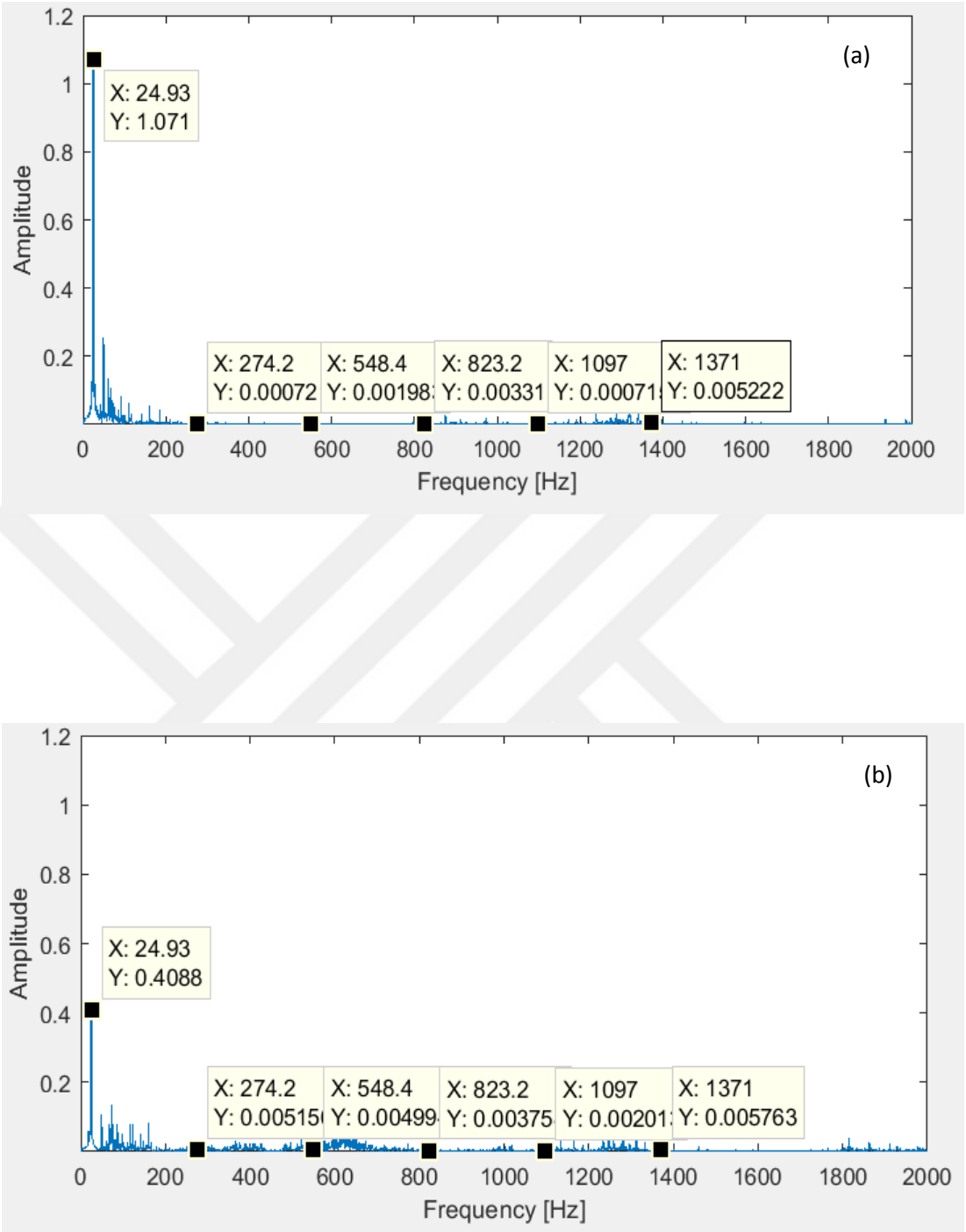

Figure 6.34 Load-2 case, at P2 point, 24.93 Hz a) healthy bearing b) one defect bearing

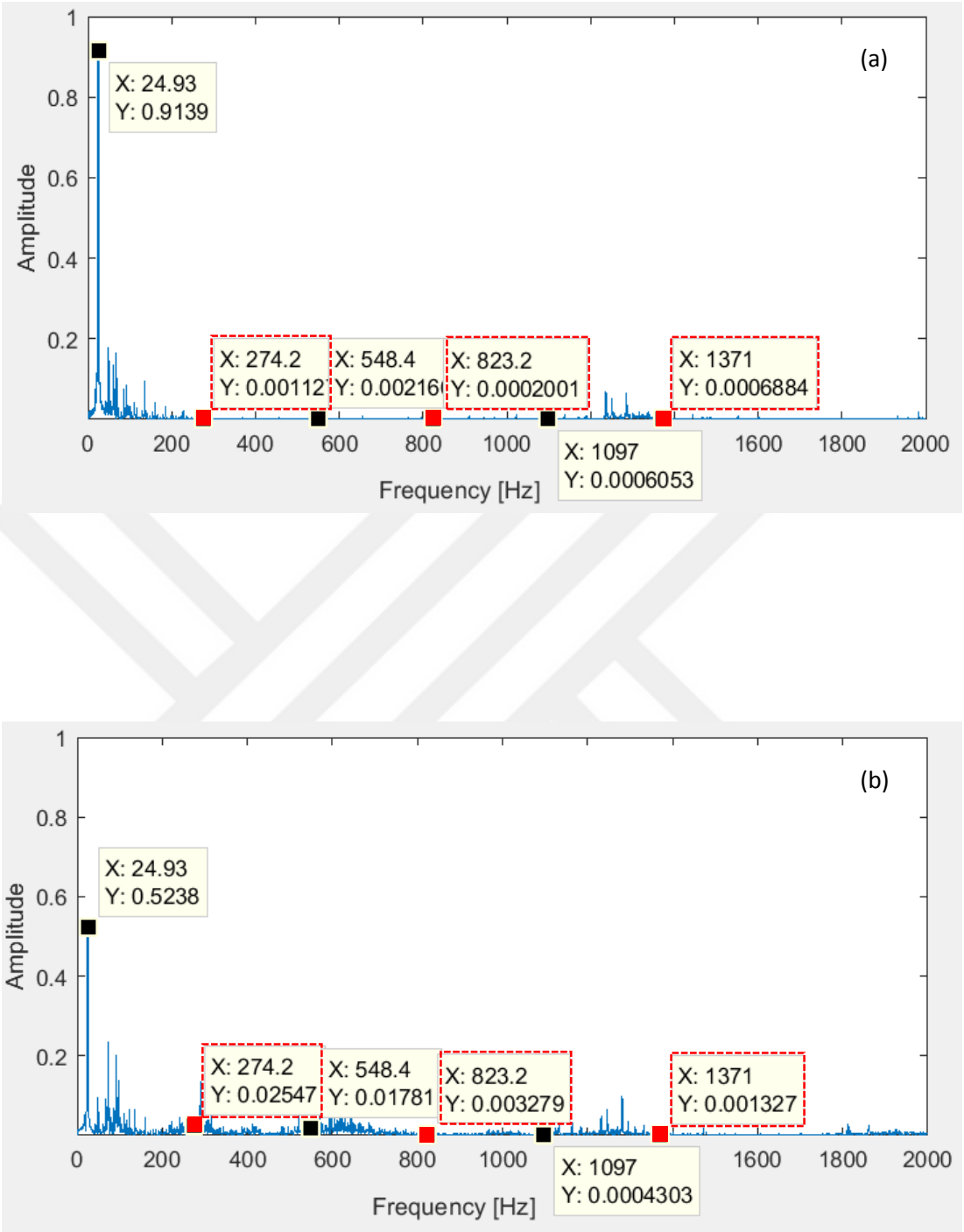

Figure 6.35 Load-2 case, at P3 point, 24.93 Hz a) healthy bearing b) one defect bearing

Under load-1 condition, the frequency spectrum graphics of healthy (16,9 Hz) and two defects (17,06 Hz) bearings at P1, P2, and P3 measurement points are given in Figure 6.36, Figure 6.37, and Figure 6.38, respectively. The vibration data were obtained at shaft speeds of 1014 RPM (16,09 Hz) for healthy bearings and of 1024 RPM (17,06 Hz) for two defects bearings. Due to the fact that these are very approximate revolution speeds, comparisons were made by ignoring small changes in the shaft speed. For healthy and two defects bearings, BPFO and its harmonics were obtained according to their speeds. In all measurement points, it is seen that the amplitudes of BPFO and its harmonics for two defects bearing is more than those of the healthy bearing. The point where two defects bearing has the highest values of BPFO and its harmonics is the P1 measurement point. It is seen that the amplitude of revolutions that show the imbalance in the system at P2 and P3 measurement points for healthy bearing is higher than that of faulty bearing. It can be concluded that the created bearing failure led to this.

Under load-2 condition, the frequency spectrum graphics of healthy and two defects bearings at P1, P2, and P3 measurement points for 16.05 Hz are given in Figure 6.39, Figure 6.40, and Figure 6.41, respectively. It provided similar results with Load-1 condition, as aforementioned. It cannot be said that increase in load amount leads to increase in amplitude of BPFO and its harmonics.

Under load-1 condition, the frequency spectrum graphics of healthy and four defects bearings at P1, P2, and P3 measurement points for 32.83 Hz are given in Figure 6.42, Figure 6.43, and Figure 6.44, respectively. In all graphics, the amplitudes of BPFO and its harmonics for a four defects bearing returned much higher than those of healthy bearings. The amplitude values especially obtained from the P1 point are more than others. The amplitude of the imbalance in the system can be seen in Figures 6.43a and 6.44a. The imbalance in the system can be seen in parallel to the bearing failure in the graphics of Figures 6.43b and 6.44b. Yet, it can be suggested that the amplitude of imbalance decreases because of bearing failure.

Under load-2 condition, the frequency spectrum graphics of healthy and two defects bearings at P1, P2, and P3 measurement points for 42.78 Hz are given in Figure 6.45, Figure 6.46, and Figure 6.47, respectively. Similar results to other graphics showed up. The bearing failure can clearly be seen especially at P1 point. Due to high speed and load-2 condition, the imbalance value in the system has higher amplitudes at P2 and P3 measurement points.

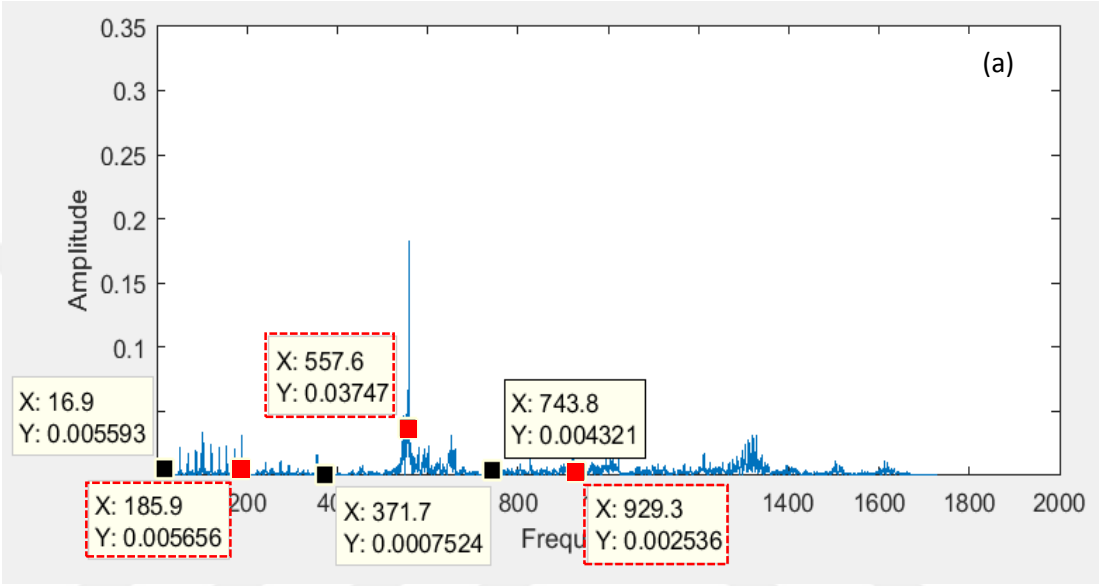

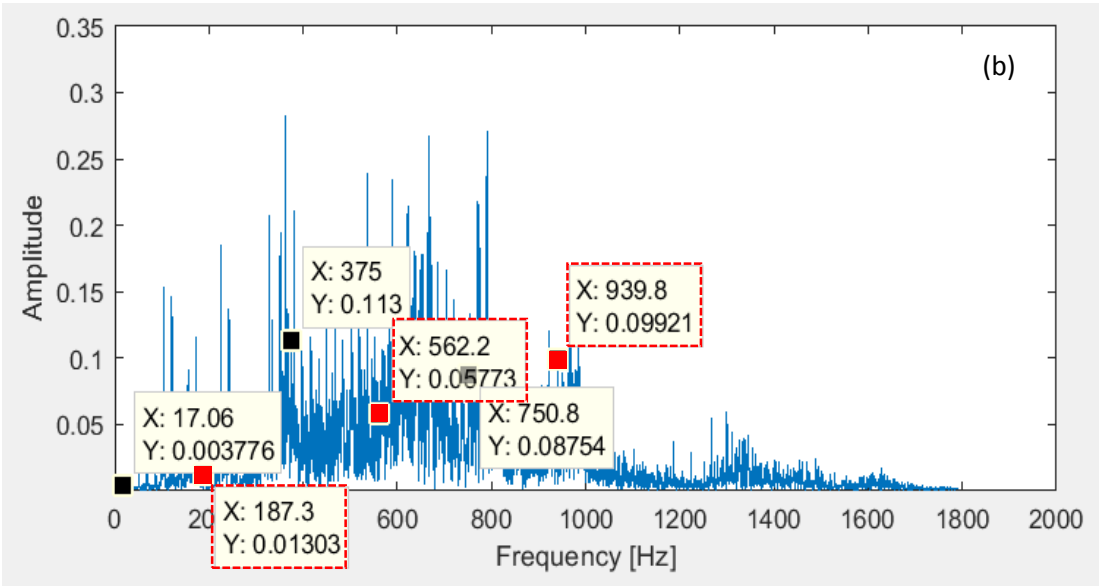

Figure 6.36 Load-1 case, at P1 point a) 16.9 Hz, healthy bearing b) 17.06 Hz, two defects bearing

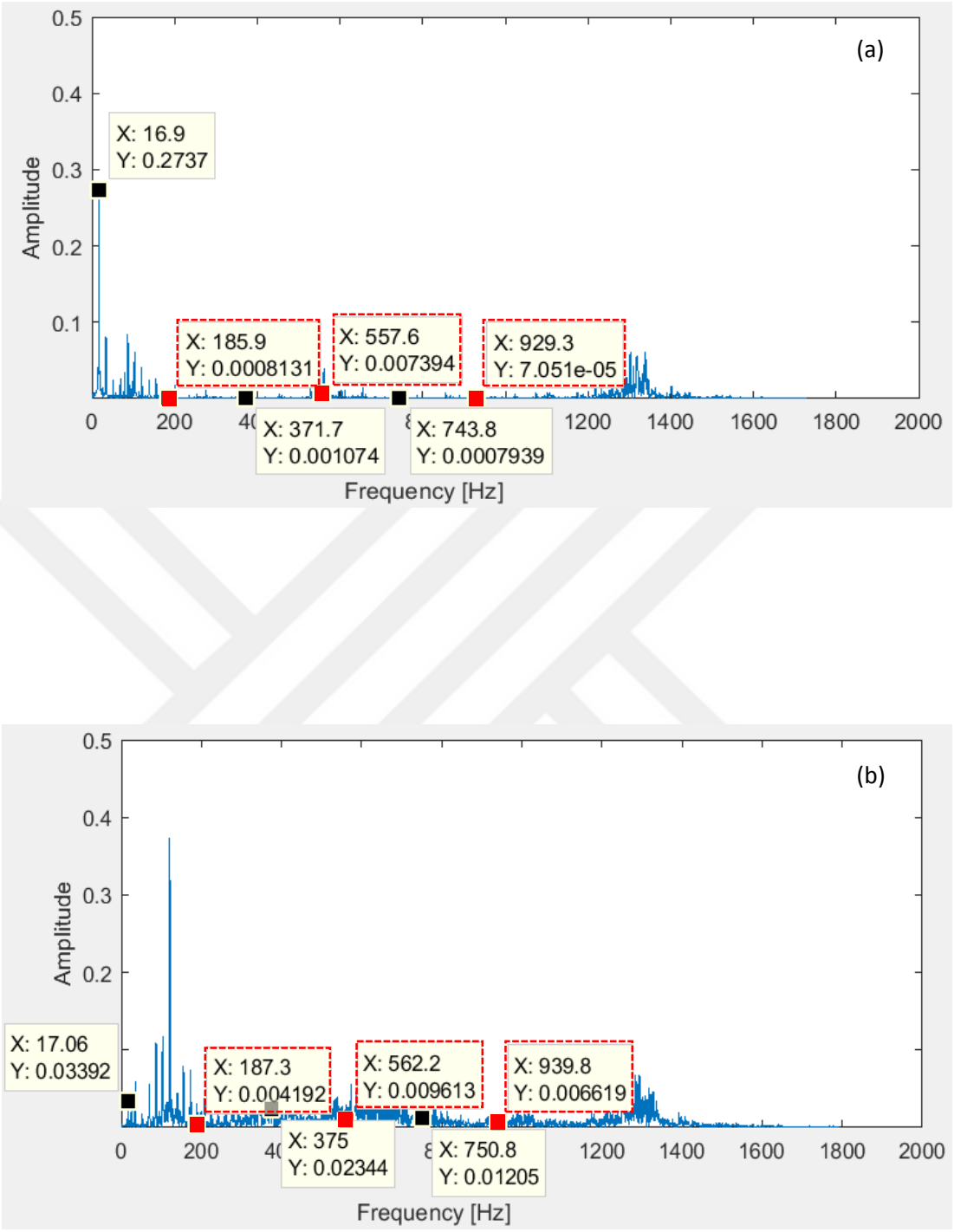

Figure 6.37 Load-1 case, at P2 point a) 16.9 Hz, healthy bearing b) 17.06 Hz, two defects bearing

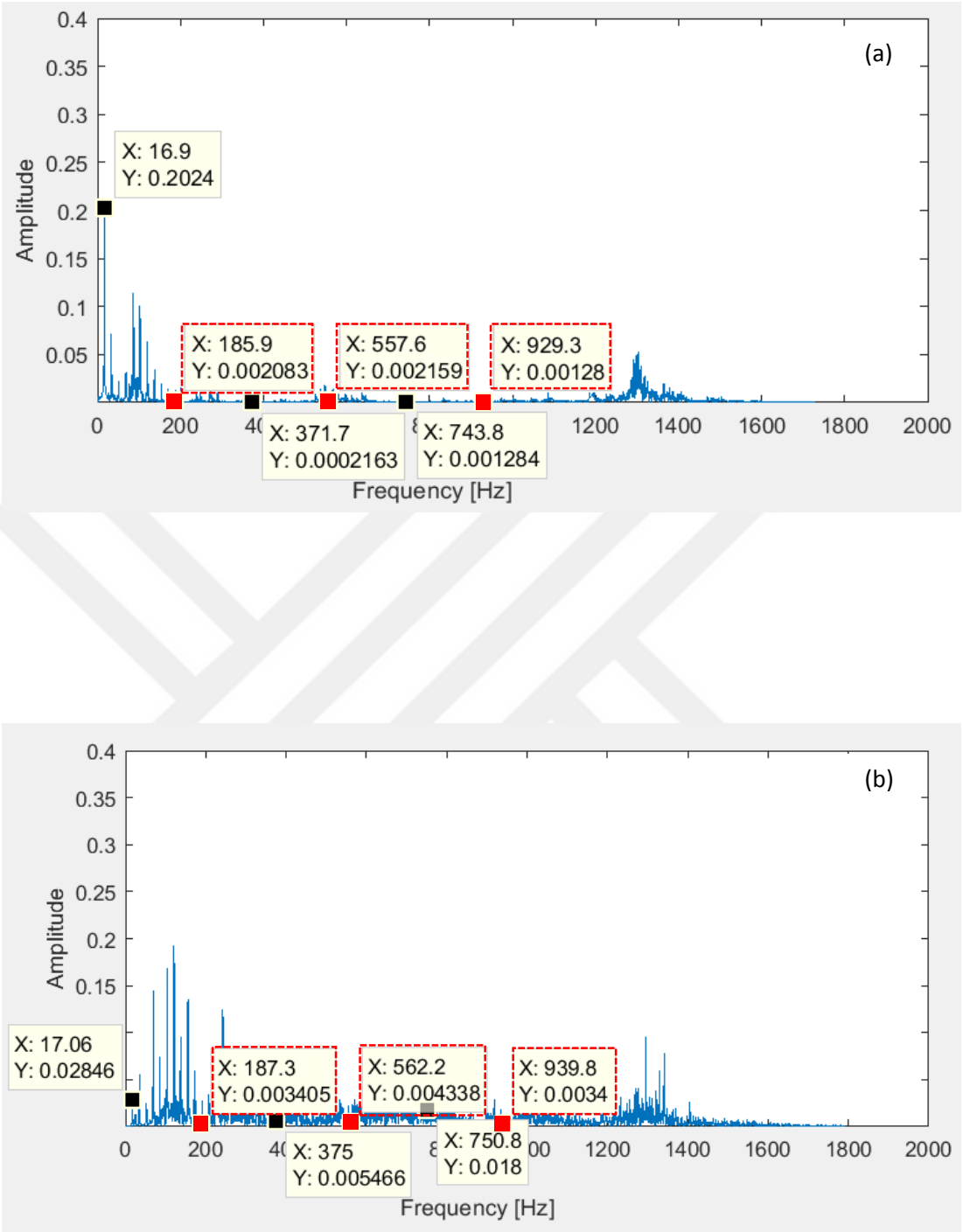

Figure 6.38 Load-1 case, at P3 point a) 16.9 Hz, healthy bearing b) 17.06 Hz, two defects bearing

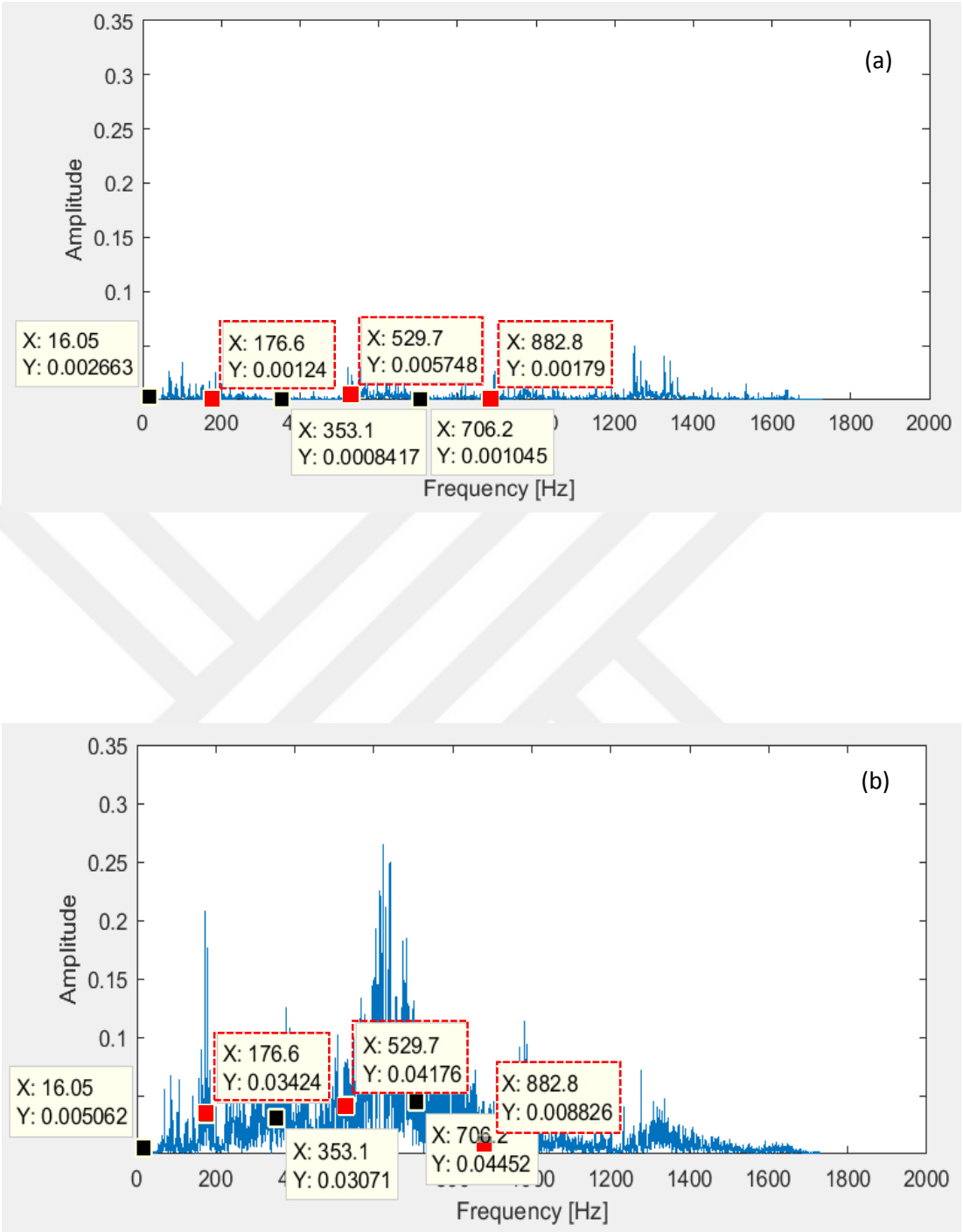

Figure 6.39 Load-2 case, at P1 point a) 16.05 Hz, healthy bearing b) 16.05 Hz, two defects bearing

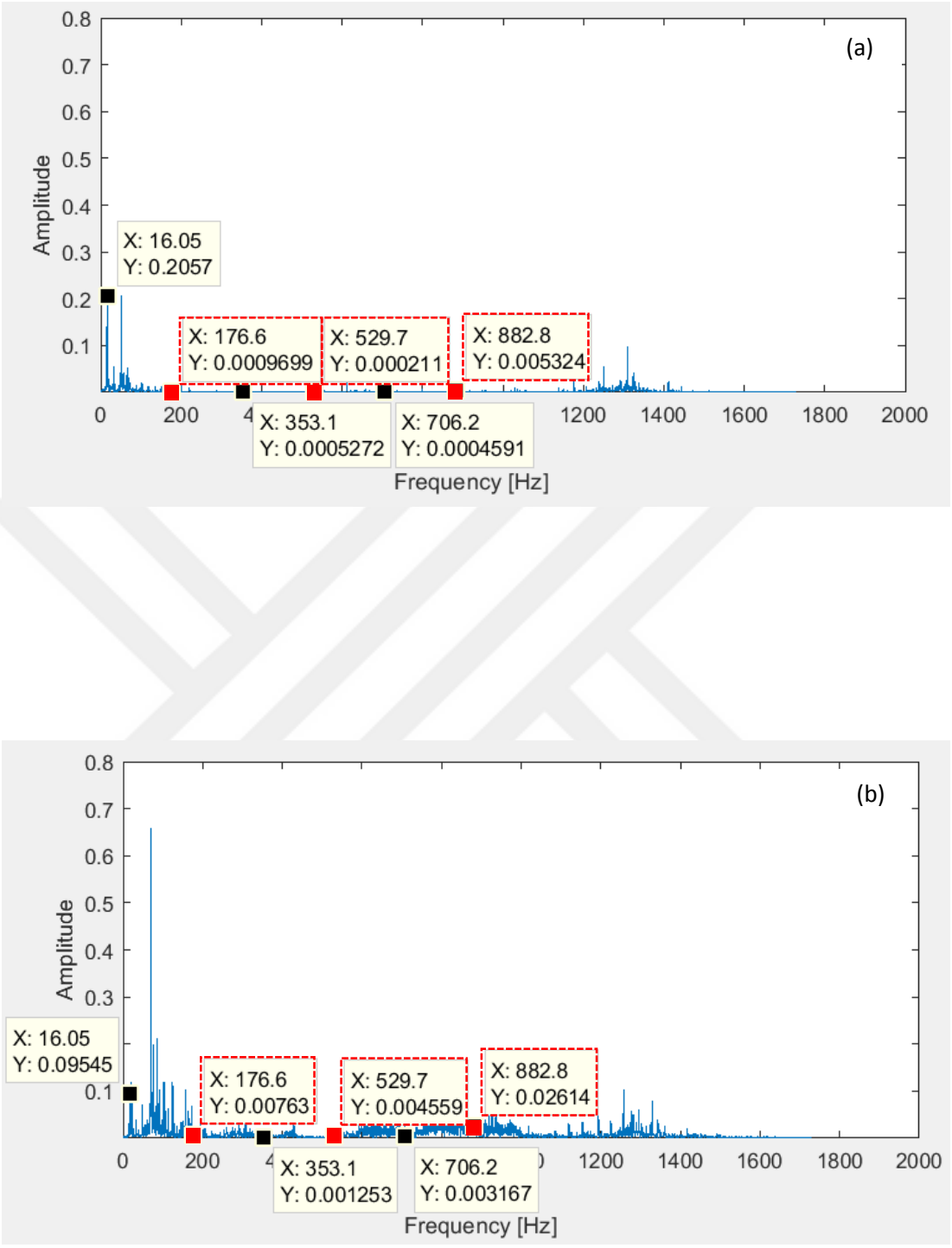

Figure 6.40 Load-2 case, at P2 point a) 16.05 Hz, healthy bearing b) 16.05 Hz, two defects bearing

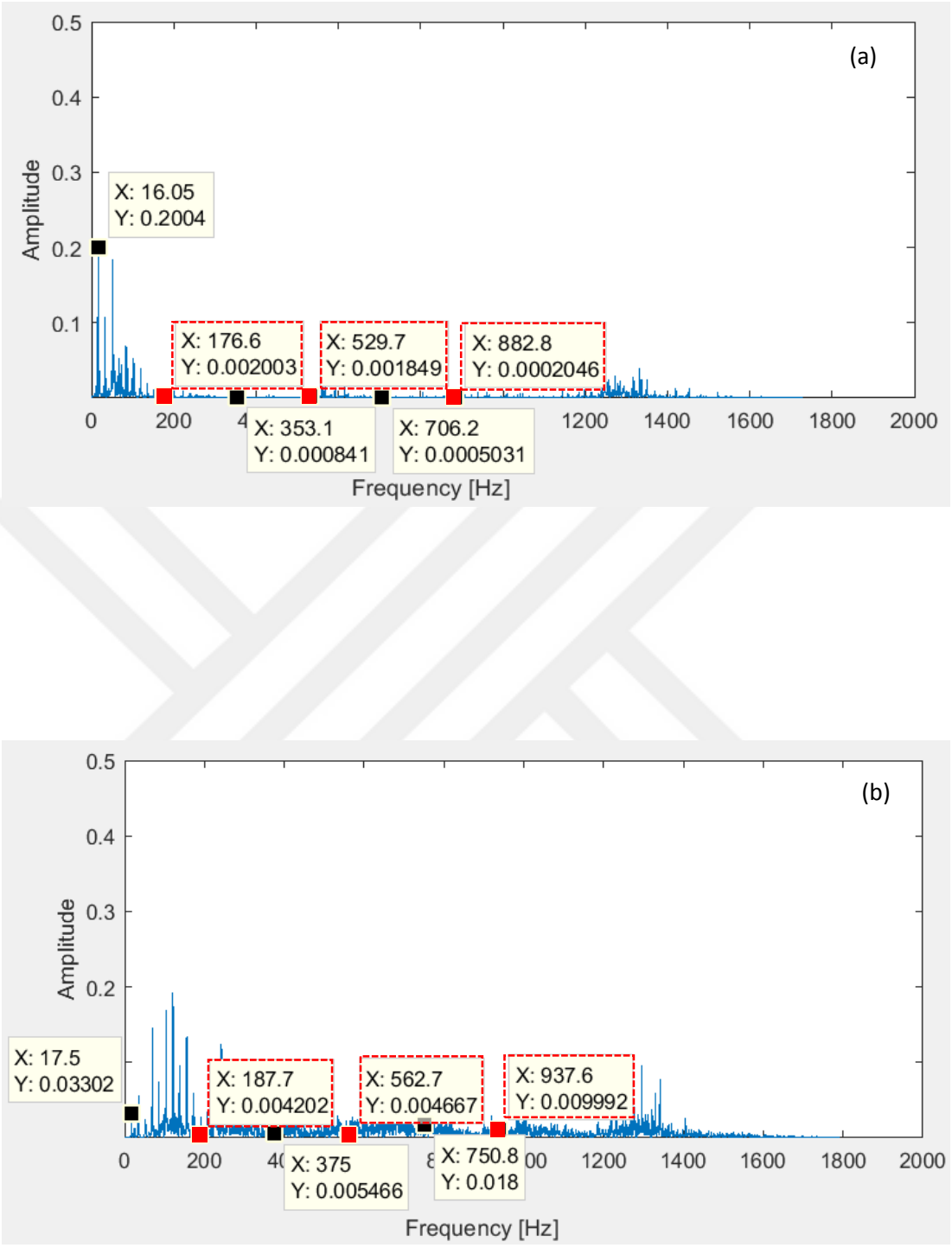

Figure 6.41 Load-2 case, at P3 point a) 16.05 Hz, healthy bearing b) 17.5 Hz, two defects bearing

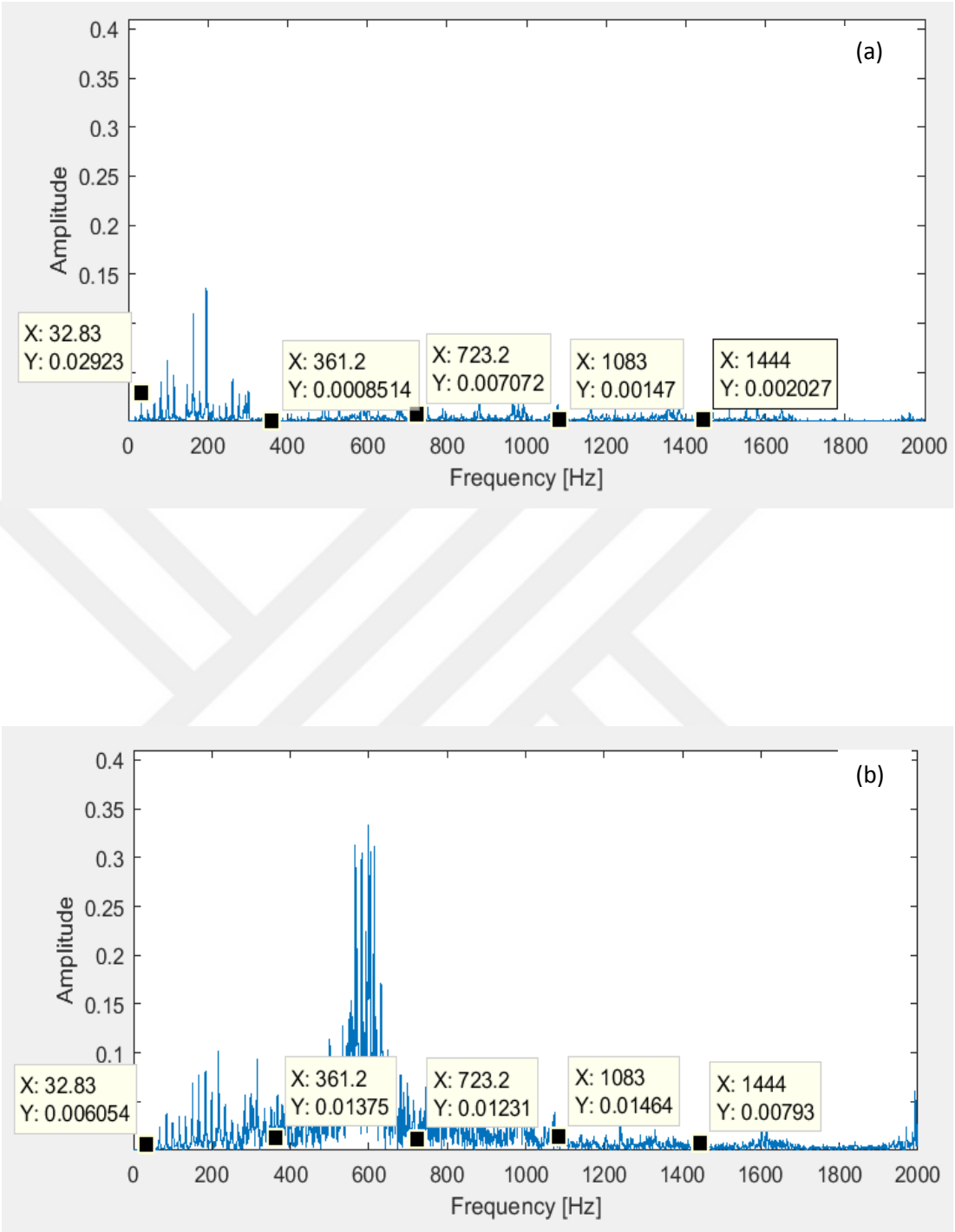

Figure 6.42 Load-1 case, at P1 point, 32.83 Hz a) healthy bearing b) four defects bearing

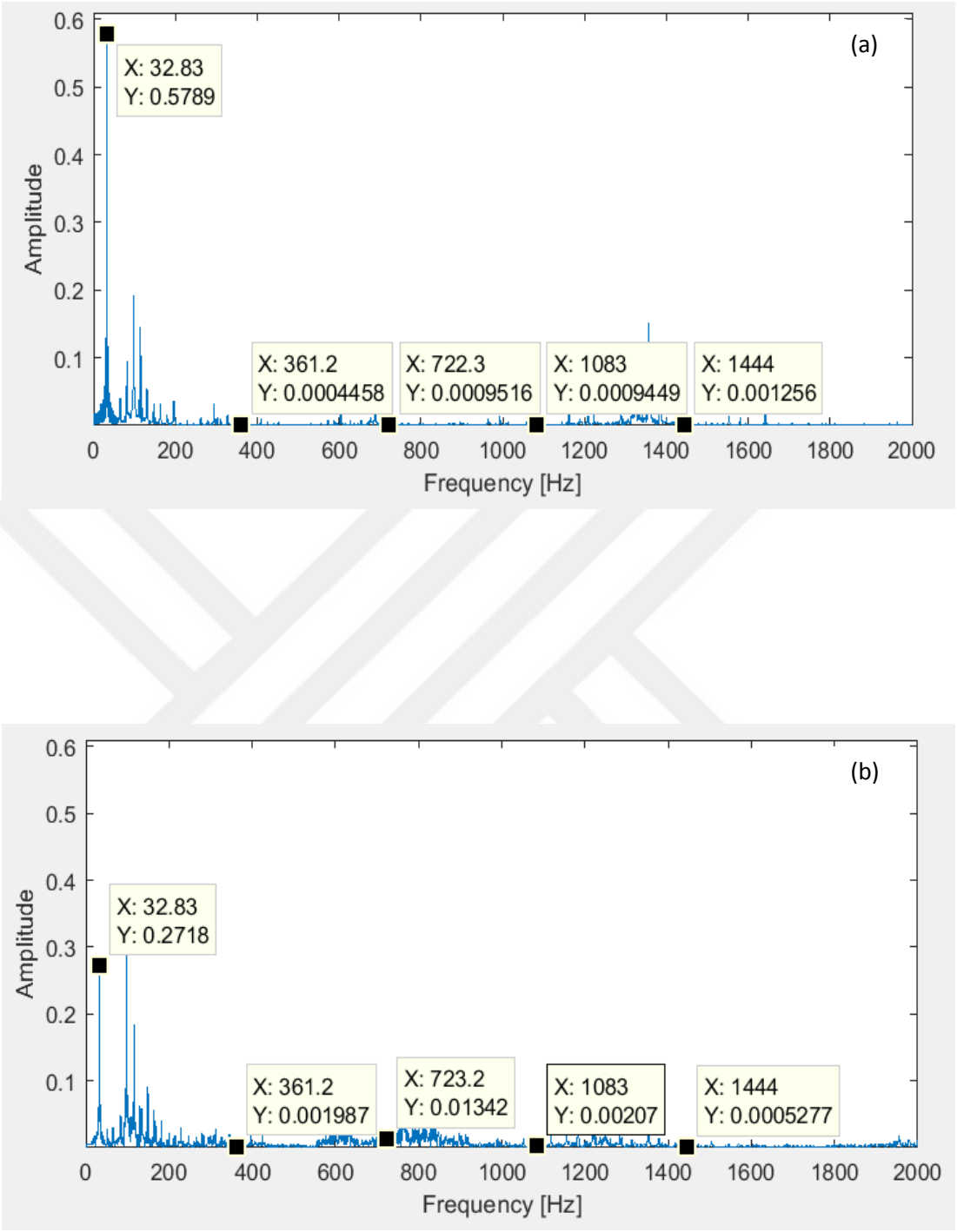

Figure 6.43 Load-1 case, at P2 point, 32.83 Hz a) healthy bearing b) four defects bearing

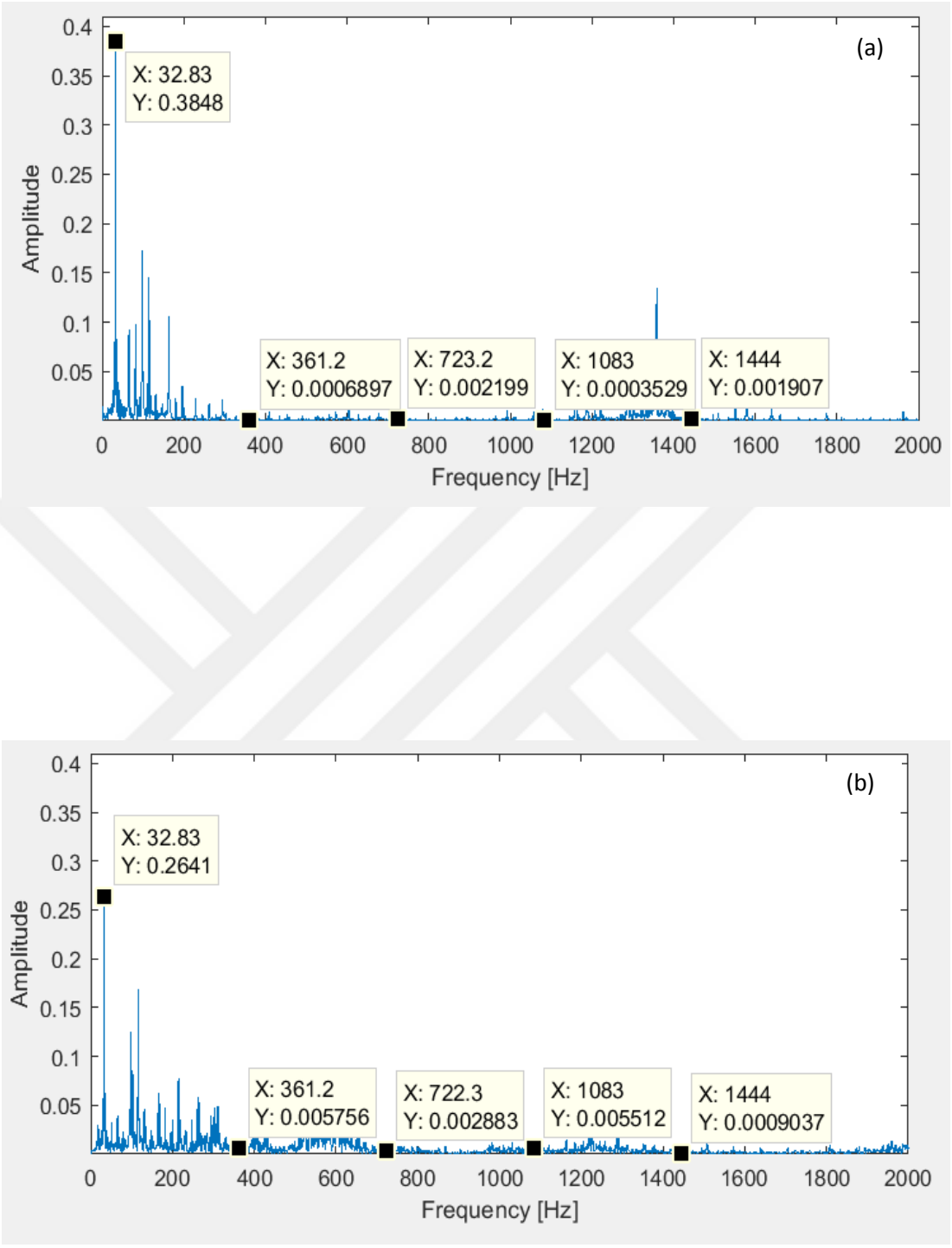

Figure 6.44 Load-1 case, at P3 point, 32.83 Hz a) healthy bearing b) four defects bearing

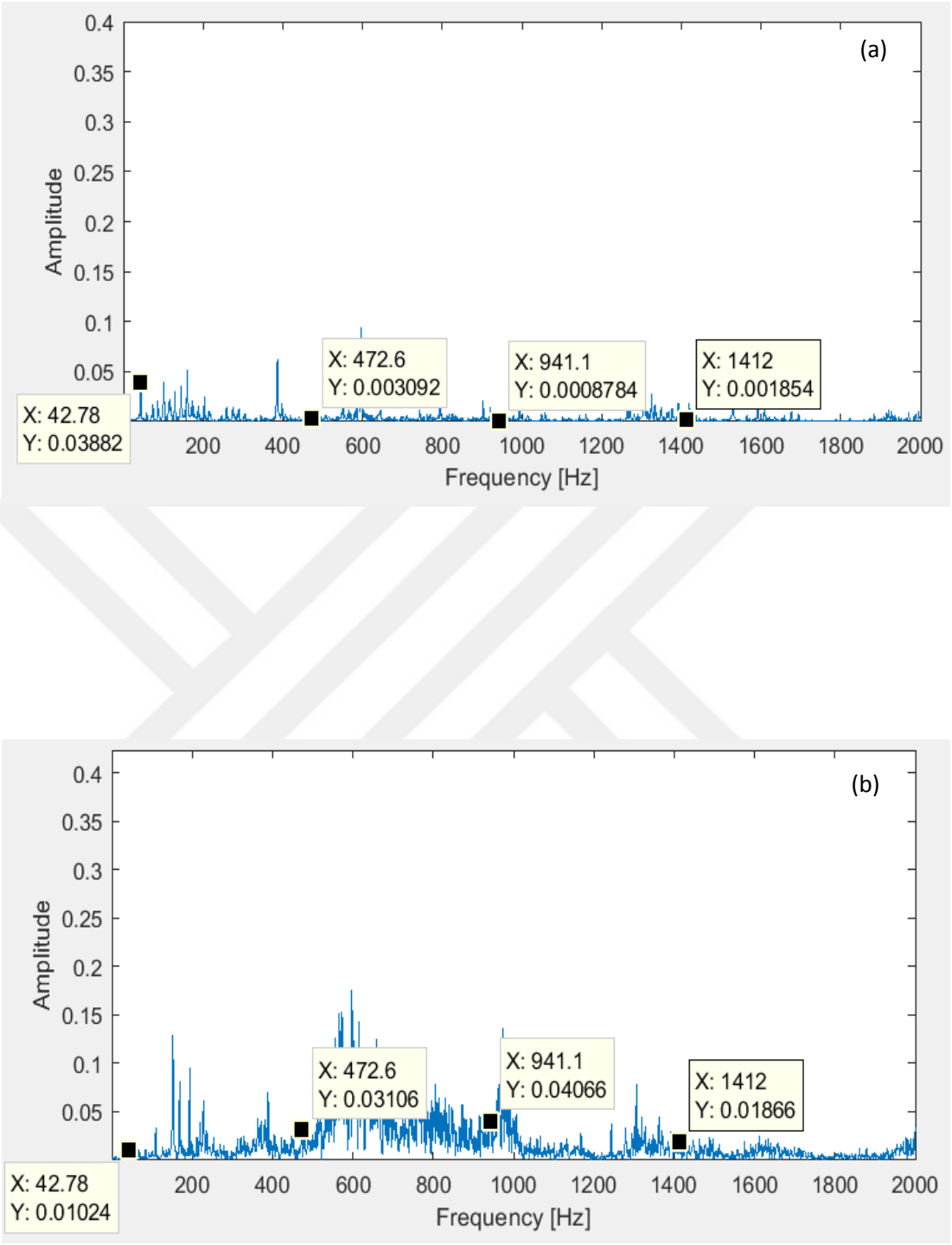

Figure 6.45 Load-2 case, at P1 point, 42.78 Hz a) healthy bearing b) two defects bearing

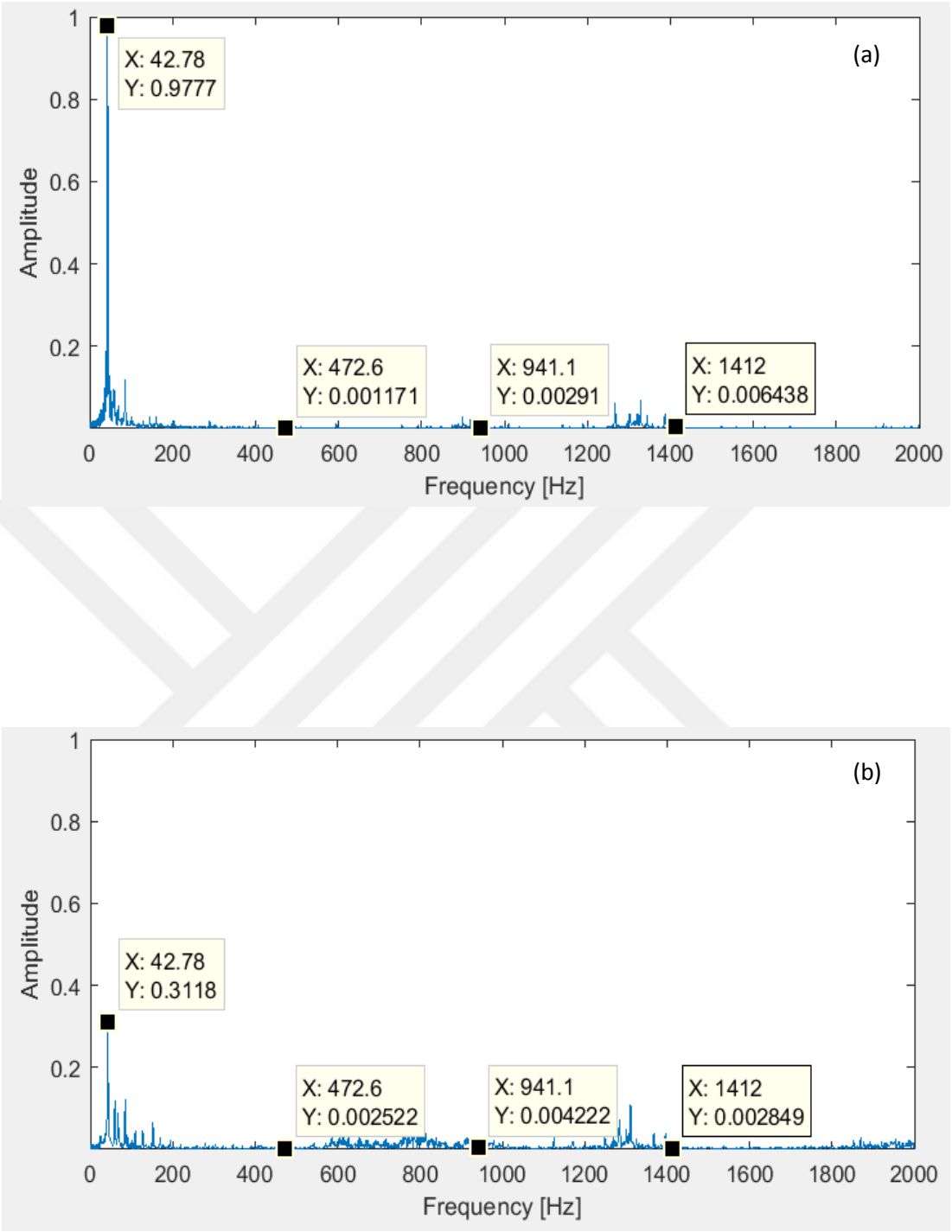

Figure 6.46 Load-2 case, at P2 point, 42.78 Hz a) healthy bearing b) two defects bearing

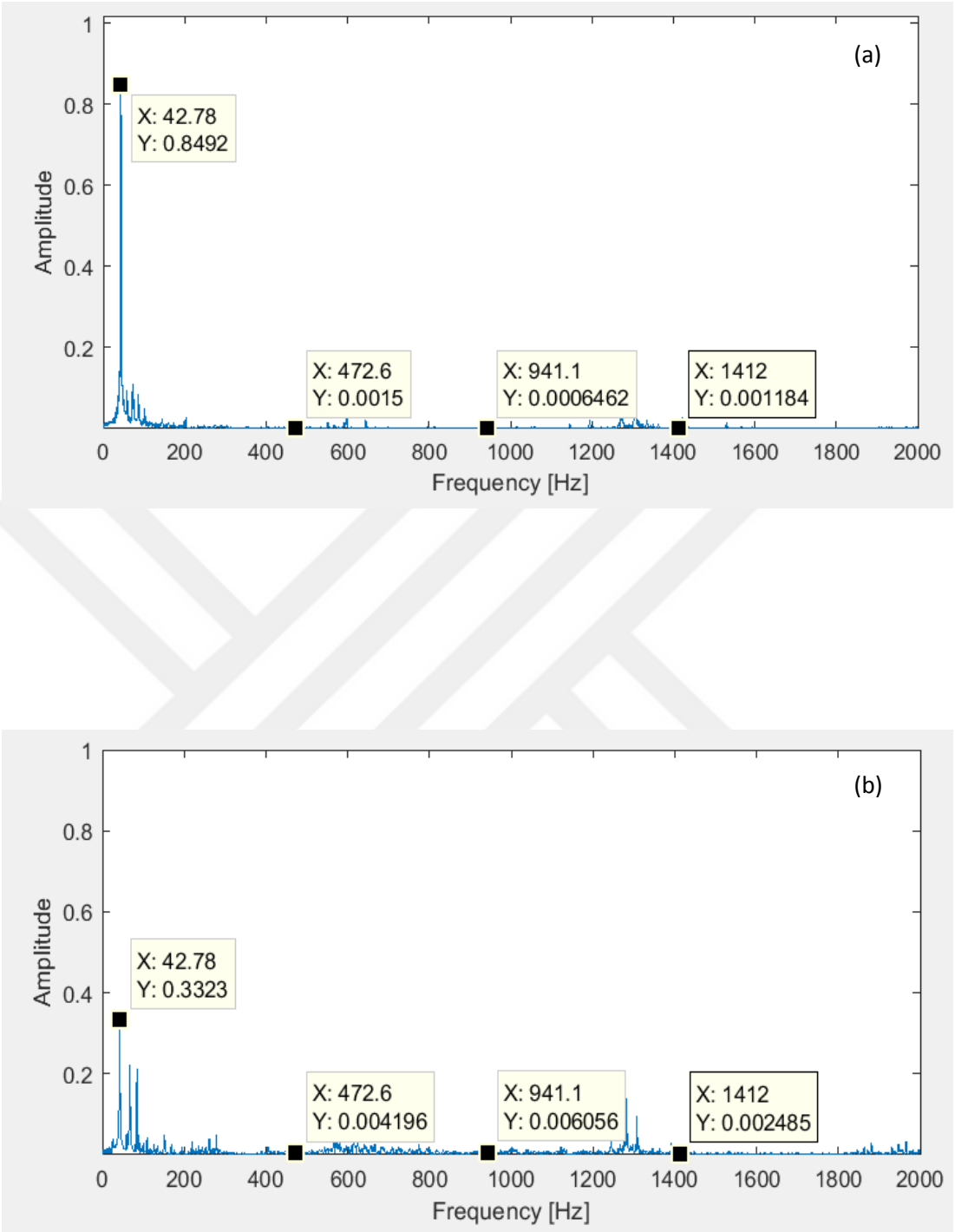

Figure 6.47 Load-2 case, at P3 point, 42.78 Hz a) healthy bearing b) two defects bearing

CHAPTER SEVEN
CONCLUSIONS

In this study, the condition of thrust bearing was monitored through vibration signals by creating one, two, and four defect points on the housing washer raceway. The vibration measurements were carried out at different rotational speeds and under two different load conditions. The vibration measurements were taken from axial, horizontal, and vertical measure points on a location closer to the thrust bearing. Statistical parameters were compared for healthy and faulty conditions. It was shown that good results can be provided by filtering the vibration signals. Time waveform samples of healthy and faulty bearings at different revolution speeds were presented. The effect of faulty bearings on time waveforms was evaluated. Samples of different revolution speeds from frequency spectrums for healthy and faulty bearings were presented. The shaft rotation speed and housing washer bearing defect frequency and its harmonics were provided in graphics. Results were evaluated for three different measurement points.

From the results presented in this study, the following points of discussion are summarized:

- Statistical indicators such as peak to peak, root mean square, crest factor, and kurtosis can be used in the defect detection of bearings. However, due to the fact that these parameters do not show the source of the failure, measurement point is crucial.

- In thrust bearings, for axial measurement points, peak to peak, root mean square, crest factor and kurtosis yield good results in fault detection. While peak to peak and RMS values return good results at all speeds, crest factor and kurtosis values return good results only at lower speeds.

- Depending on the amount of the failure, the increase of statistical indicators values is out of the question.

- Depending on the increase in load and speed, it cannot be said that there is a clear increase in the values of statistical indicators.

- The results obtained from vertical and horizontal measurement points yield similar results for statistical indicators.

- Values of statistical indicators obtained for faulty bearings at vertical and horizontal measurement points are higher than the values obtained for the healthy bearing. Although, there are exceptions and generally the values are lower than axial measurement point.

- Better results can be obtained by filtering statistical indicators at definite frequency intervals.

- Due to the fact that statistical indicators do not show the origin of the damage, they cannot be used standalone for defect detection. If the evaluation should be done over the statistical indicators only, then the vibration measurements should be taken in the axial direction.

- Time waveform graphics for axial measurement points have high vibration values and bearing characteristic damage graphics under faulty conditions.

- In the waveform graphics obtained from vertical and horizontal measurement points for healthy bearing, damages such as imbalance and misalignment can clearly be seen. However, it gets difficult to make any comments on imbalance or misalignment by looking at the graphics obtained from the faulty bearing. At vertical and horizontal measurement points, it will not be correct to make an assessment on the damage by studying only the waveform graphics if there are more than one fault in the system.

- It cannot be suggested that there is a net increase in the structure of waveform graphics depending on the increase in the amount of the damage.

- For time waveforms, the results obtained from vertical and horizontal measurement points generally returned similar outcomes.

- Depending on the increase in the shaft speed, it can be said that there is an increase in the vibration amplitude of waveform graphics in general.

- The imbalance in the system became clearer on the frequency spectrum when the shaft speed of the healthy bearing increased. In the frequency spectrums of the damaged bearings, the imbalance amplitude slightly decreased under same conditions. The reason of this is the bearing failure.

- At the axial, vertical, and horizontal measurement points on frequency spectrums, BPFO and harmonics have a higher amplitude value in the damaged bearings than healthy bearings. Theoretical and experimental results coincide with each other.

- While frequency spectrums are used in fault detection clearly, axial measurement point especially for thrust bearings yields the best results for defect detection.

- When a general assessment is made, the most appropriate sensor position for vibration analysis on thrust bearings is the axial direction.

- By only using only time domain parameters on thrust bearings, defect detection cannot be done. The frequency domain should be focused since it shows the source of the failure.

REFERENCES

Alfredson, R. J., Aust, M. I. E. & Mathew J. (1985). Frequency domain methods for monitoring the condition of rolling element bearings. *Mechanical Engineering Transactions in Australia, 10*(2), 108-112.

Alfredson, R. J., Aust, M. I. E., & Mathew J. (1985). Time domain methods for monitoring the condition of rolling element bearings. *Mechnical Engineering Transaction in Australi*a, *10*(2), 102-107.

Barden bearing failure: causes and cures. (n.d.), 9-13. Retrieved January 20, 2019, from https://www.schaeffler.com/remotemedien/media/_shared_media/08_media_library/01_publications/barden/brochure_2/downloads_24/barden_bearing_failures_us_en.pdf.

Bearing timeline, (n.d.). Retrieved February 4, 2019, from https://www.americanbearings.org/page/bearing_timeline.

Choudhury, A., & Tandon, N. (2006). Vibration response of rolling element bearings in a rotor bearing system to a local defect under radial load. *Journal of Tribology, 128*, 252-261.

Damped free vibration, (2007). Retrieved April 15, 2019, from http://www.wikizero.biz/index.php?q=aHR0cHM6Ly91cGxvYWQud2lraW1lZGlhLm9yZy93aWtpcGVkaWEvY29tbW9ucy84Lzg3L0RhbXBlZF9GcmVlX1ZpYnJhdGlvbi5wbmc.

Dunton, T. A. (1999). *Technologies inc: an introduction to time waveform analysis. universal.* Retrieved April 22, 2019, from http://www.unitechinc.com/pdf/IntroductiontoTimeWaveformAnalysis.pdf.

Dyer, D., & Stewart, R. M. (1978). Detection of rolling element bearing damage by statistical vibration analysis. *Journal of Mechanical Design*, *100*(2), 229–235.

FAG rolling bearing damage, (2001), 38. Retrieved February 4, 2019, from http://www.endas.com/images/Appic/PDF/FileUploadPDFTRinsert00456000.pdf.

Geometrical parameters of engine bearings, (2019). Retrieved April 7, 2019, from http://www.substech.com/dokuwiki/doku.php?id=geometrical_parameters_of_engine_bearings.

Jayaswal, P., Wadhwani, A. K., & Mulchandani, K. B. (2008). Machine fault signature analysis. *International Journal of Rotating Machinery*, 1-10.

Jensen, T., & Brown, D. N. (n.d.). *Brüel & Kjaer: machine-condition monitoring using vibration analysis.* Retrieved January 20, 2019, from https://www.bksv.com/media/doc/bo0253.pdf.

Kelm, R., & Pavelek, D. (2018). *Vibration institute: orbit analysis, 4.* Retrieved April 8, 2019, from http://www.vibration.org/Presentation/May%202018/Rays%20Stuff/Orbit%20Analysis%200518-1.pdf.

Kim, Y. H., Tan, A. C. C., Mathew, J., & Yang, B. S. (2006). Condition monitoring of low speed bearings: a comparative study of the ultrasound technique versus vibration measurements. *World Congress on Engineering Asset Management*, *29*, 1-10.

Kiral Z., & Karagülle, H. (2006). Vibration analysis of rolling element bearings with various defects under the action of an unbalanced force. *Mechanical Systems and Signal Processing*, *20*, 1967-1991.

Kiral, Z. (2002). *Simulation and analysis of vibration signals generated by rolling element bearings with defects*. Phd Thesis, Dokuz Eylül University, İzmir.

Kiral, Z., & Karagülle, H. (2003). Simulation and analysis of vibration signals generated by rolling element bearings with defects. *Tribology International, 36*, 667-678.

Koyo ball & roller bearings: failure, causes and countermeasures, (2015), 6-13. Retrieved March 20, 2019, from http://donoupoglou.gr/wp/wp-content/uploads/2015/03/catb3001e.pdf.

Kurtosis, (2009). Retrieved February 5, 2019, from http://azimadli.com/vibman/kurtosis.htm.

Leonardo and the strife-ridden renaissance, (n.d.). Retrieved February 8, 2019, from https://en.unesco.org/courier/octubre-1974/leonardo-and-strife-ridden-renaissance.

Liu, H., Wang, J., & Lu, C. (2013). Rolling bearing fault detection based on the teager energy operator and elman neural network. *Mathematical Problems in Engineering, 2013*(1), 1-10.

Mathew, J., & Alfredson, R. J. (1984). The condition monitoring of rolling element bearings using vibration analysis. *Journal of Vibration, Acoustics, Stress, and Reliability in Design, 106*(3), 447-453.

McFadden, P. D., & Smith, J. D. (1984). Model for the vibration produced by a single point defect in a rolling element bearing. *Journal of Sound and Vibration, 96*(1), 69-82.

Metravib technologies, (n.d.). Retrieved February 5, 2019, from http://www.plant-maintenance.com/articles/bearing_vibration_monitoring.pdf.

Nabhan, A., Nouby, M., Sami, A. M., & Mousa, M. O. (2016). Vibration analysis of deep groove ball bearing with outer race defect using ABAQUS. *Journal of Low Frequency Noise Vibration and Active Control*, *35*(4), 312-325.

NTN bearing care and maintenance of bearings, (2017), 10. Retrieved January 20, 2019, from https://www.ntn-snr.com/sites/default/files/2017-03/care_and_maintenance_of_bearings_en.pdf.

Orhan, S., Aktürk, N., & Çelik, V. (2006). Vibration monitoring for defect diagnosis of rolling element bearings as a predictive maintenance tool: Comprehensive case studies. *NDT & E International*, *39*(4), 293-298.

Patel, R. K., Agrawal, S., & Joshi, N. C. (2012). Induction motor bearing fault identification using vibration measurement. *Conference: Engineering and Systems (SCES)*, 1-5.

Patidar, S., & Soni, P. K. (2013). An overview on vibration analysis techniques for the diagnosis of rolling element bearing faults. *International Journal of Engineering Trends and Technology (IJETT)*, *4*(5), 1804-1809.

Rao, S. S. (2004). *Mechanical vibrations*. (5th ed.). Pearson Education, 17-922.

Roller type rolling guides, (n.d.). Retrieved April 7, 2019, from https://www.ikont.com/L2oU/7eMf-ZHvfu.html.

Scheffer, C. (Ed.). (2004). *Practical machinery vibration analysis and predictive maintenance*. Oxford: Elsevier, 17.

Segla, M., Wang, F., & Wang, S. (2012). Bearing fault diagnosis with an improved high frequency resonance technique. *IEEE 10th International Conference on Industrial Informatics*, 580-585.

Simple harmonic motion, (n.d). Retrieved April 8, 2019, from https://www.augusta.k12.va.us/cms/lib01/VA01000173/Centricity/Domain/396/Simple_Harmonic_Motion_(SHM).pdfc.

SKF gauging machine health with "overall" vibration, (n.d.). Retrieved April 15, 2019, from https://www.skf.com/group/services/services-and-solutions/introduction-to-condition-monitoring/gauging-machine-health.html.

SKF rulman bakım ve yağlama ürünleri, (2008), Turkey, İstanbul.

SKF rulmanların tanımı, (2013), Turkey, İstanbul.

SKF super-precision double direction angular contact thrust ball bearings, (2012). Retrieved April 8, 2019, from https://www.skf.com/binary/21-279300/Super-precision-double-direction-angular-contact-thrust-ball-bearings-BTW-series_10097_3_EN.pdf.

SKF thrust ball bearings, (2014). Retrieved February 8, 2019, from http://sopetra.com.br/view/catalogo/rolamentos-axiais-de-esferas-catalogo.pdf.

Sundyne pumps training-vibrations, (2018), France, Djon.

Tandon, N., & Choudhury, A. (1999). A review of vibration and acoustics measurement methods for the detection of defects in rolling element bearings. *Tribology International*, *32*, 469-480.

Toyota, T., Niho, T., Chen, P., & Komura, H. (2001). Condition monitoring and diagnosis of rotating machinery by orthogonal expansion of vibration signal. A.G. Starr, & R. B. K. N. Rao, (Ed), *Condition Monitoring and Diagnostic Engineering Management* (730-731). Manchester, UK: Elsevier.

Types of ball bearings, (2012). Retrieved April 8, 2019, from https://nptel.ac.in/courses/116102012/bearings/types%20of%20ball%20bearings.html.

Williams, T., Ribadeneira, X., Billington, S., & Kurfess, T. (2001). Rolling element bearing diagnostics in run-to-failure lifetime testing. *Mechanical System and Signal Processing*, *15*(5), 979-993.

Yiğit, A. (2008). *Detection of rolling element bearing faults via vibration analysis*. Msc Thesis, Dokuz Eylül University, İzmir.

Ziebell, A., Schöppl, O., Haubner, R., & Konegger, T. (2015). Identification of bearing defects in hybrid thrust ball bearings by vibration analysis. *Materials Science Forum*, 825-826, 844-851.

Zoladz, T., Earhart, E., & Fiorucci, T. (1995). Bearing defect signature analysis using advanced nonlinear signal analysis in a controlled enviroment. *NASA Technical Memorandum*, *93*(10), 16.

APPENDICES

For vibration data; creating of waveform and spectrum graphs and obtaining statistical indicators.

```
clc;clear
dat=load('F:\DATA\E_N2_2500.txt');
tm=dat(:,1);
acc=dat(:,2);
 d=acc;
byt=length(d);
 dt=(tm(2)-tm(1))/1000;
fs=1/dt;
subplot(2,2,1),plot(tm,d)
xlabel('Time [mS]'),ylabel('Acceleration [G]')
sigmin=min(d);
sigmax=max(d);
 %*************************************************************************
display ('=======================================')
p2p=sigmax-sigmin                % peak to peak
rms=sqrt(sum(d.^2)/length(d))       % rms
cf=p2p/rms                       % crest factor
kurtosis=sum((d-mean(d)).^4)/(length(d).*(std(d)^4)) % kurtosis
%*************************************************************************
display
('=========================================================')
nfft=256*32;
f_fft=abs(fft(d,nfft))*dt*2*pi;
wf=(0:(nfft/2-1))/(nfft/2)*(fs/2);
f_fft=f_fft(1:length(f_fft)/2);
fmin=0;
fmax=1000;
subplot(2,2,3)
plot(wf,f_fft)
axis([fmin fmax min(f_fft) max(f_fft)*1.2]);
xlabel('Frequency [Hz]')
ylabel('Amplitude')
%-----------------------------------------------------------
dat=load('F:\GORUSME SONRASI_25012019\VERI\E_2A2_2500.txt');
tm=dat(:,1);
acc=dat(:,2);
d=acc;
byt=length(d);
dt=(tm(2)-tm(1))/1000;
fs=1/dt;
 subplot(2,2,2),plot(tm,d)
```

```
xlabel('Time [mS]'),ylabel('Acceleration [G]')
sigmin=min(d);
sigmax=max(d);

%*********************************************************************
display ('=====================================')
p2p=sigmax-sigmin                % peak to peak
rms=sqrt(sum(d.^2)/length(d))      % rms
cf=p2p/rms                       % crest factor
kurtosis=sum((d-mean(d)).^4)/(length(d).*(std(d)^4)) % kurtosis
%*********************************************************************
display
('=========================================================')
f_fft=abs(fft(d,nfft))*dt*2*pi;
wf=(0:(nfft/2-1))/(nfft/2)*(fs/2);
f_fft=f_fft(1:length(f_fft)/2);
fmin=0;
fmax=1000;
subplot(2,2,4)
plot(wf,f_fft)
axis([fmin fmax min(f_fft) max(f_fft)*1.2]);
xlabel('Frequency [Hz]')
ylabel('Amplitude')
```

Filtering of vibration signals.

```
clc;clear
fa=170;
fb=171;
dat=load('F:\DATA\E_1A2_500.txt');  .
tm=dat(:,1);
acc=dat(:,2);
d=acc;
byt=length(d);
dt=(tm(2)-tm(1))/1000;
fs=1/dt;
subplot(2,2,1),plot(tm,d)
xlabel('Time [mS]'),ylabel('Acceleration [G]')
sigmin=min(d);
sigmax=max(d);
%**************************************************************************
display ('=========================')
p2p=sigmax-sigmin                % peak to peak
rms=sqrt(sum(d.^2)/length(d))       % rms
cf=p2p/rms                       % crest factor
kurtosis=sum((d-mean(d)).^4)/(length(d).*(std(d)^4)) % kurtosis
%**************************************************************************
display
('=========================================================')
nfft=256*32;
f_fft=abs(fft(d,nfft))*dt*2*pi;
wf=(0:(nfft/2-1))/(nfft/2)*(fs/2);
f_fft=f_fft(1:length(f_fft)/2);
fmin=160;
fmax=180;
subplot(2,2,3)
plot(wf,f_fft)
axis([fmin fmax min(f_fft) max(f_fft)*1.2]);
xlabel('Frequency [Hz]')
ylabel('Amplitude')
%-------------------------------------------------------------
fs=1514;
[b,a]=butter(4,[fa fb]*2/fs);
[H,w]=freqz(b,a,fs);
sf=filter(b,a,d);
subplot(2,2,2),plot(tm,sf)
xlabel('Time [mS]'),ylabel('Acceleration [G]')
%**************************************************************************
display ('================================')
p2p=max(sf)-min(sf)                % peak to peak value
rms=sqrt(sum(sf.^2)/length(sf))       %rms value
cf=p2p/rms                         %crest factor
```

```
kurtosis=sum((sf-mean(sf)).^4)/(length(sf).*(std(sf)^4)) % kurtosis
%*****************************************************************
display
('============================================================')
f_fft=abs(fft(sf,nfft))*dt*2*pi;
wf=(0:(nfft/2-1))/(nfft/2)*(fs/2);
f_fft=f_fft(1:length(f_fft)/2);
subplot(2,2,4)
plot(wf,f_fft)
axis([fmin fmax min(f_fft) max(f_fft)*1.2]);
xlabel('Frequency [Hz]')
ylabel('Amplitude')
```

Creating graph for statistical indicators.

```
clc;clear
d1=load('F:\DATA\GRAFIK\D2_N.txt');
d2=load('F:\ DATA\GRAFIK\GRAFIK\D2_1A.txt');
d3=load('F:\ DATA\GRAFIK\GRAFIK\D2_2A.txt');
d4=load('F:\ DATA\GRAFIK\GRAFIK\D2_4A.txt');
DF=[500 1000 1500 2000 2500];
p2p_N=d1(1,:);
rms_N=d1(2,:);
cf_N=d1(3,:);
krt_N=d1(4,:);
%1HATALI
p2p_1A=d2(1,:);
rms_1A=d2(2,:);
cf_1A=d2(3,:);
krt_1A=d2(4,:);
%2HATALI
p2p_2A=d3(1,:);
rms_2A=d3(2,:);
cf_2A=d3(3,:);
krt_2A=d3(4,:);
%4HATALI
p2p_4A=d4(1,:);
rms_4A=d4(2,:);
cf_4A=d4(3,:);
krt_4A=d4(4,:);
plot(DF,krt_N,'gs-',DF,krt_1A,'rv-',DF,krt_2A,'m*-',DF,krt_4A,'bo-
','LineWidth',1,'markersize',8),grid on
title('Axial Direction')
xlabel('Shaft Speed (RPM)')
ylabel('Kurtosis Value')
```

Bd : Ball or roller diameter

c : Damping

$C(\tau)$: Cepstrum

f : Frequency of oscillation

F{x(t)} : Fourier transform

k : Stiffness

m : mass

m_{eff} : Effective mass

N : Sample size

Nb : Number of balls or rollers

Pd : Pitch diameter

S : Shaft speed

$S_x(\omega)$: Power spectrum

t : Time

T : Period

V : Velocity

ω : Angular frequency

ω_n : Natural frequency

ω_r : Resonance frequency

x : Displacement at any given instant

$\bar{x}$: Mean value

X_0 : Maximum displacement

σ : Standard deviation

Ø : Phase

ɵ : Contact Angle

CLT : Curve length transform

FFT : Fast Fourier transform

HFRT : High frequency resonance technique

MCSA : Motor current signature analysis

RMS : Root mean square

RPM : Revolution per minute

SPM : Shock pulse method

STFT : Short time Fourier transform